Distribution Agreement

In presenting this thesis or dissertation as a partial fulfillment of the requirements for an advanced degree from Emory University, I hereby grant to Emory University and its agents the non-exclusive license to archive, make accessible, and display my thesis or dissertation in whole or in part in all forms of media, now or hereafter known, including display on the world wide web. I understand that I may select some access restrictions as part of the online submission of this thesis or dissertation. I retain all ownership rights to the copyright of the thesis or dissertation. I also retain the right to use in future works (such as articles or books) all or part of this thesis or dissertation.

Signature:

_____ _____

Ting Zhao Date

Differential Proteolysis of Mutant Huntingtin in Astrocytes and Neurons

By

Ting Zhao
Doctor of Philosophy

Graduate Division of Biological and Biomedical Sciences
Neuroscience

_____
Xiao-Jiang Li, M.D., Ph.D.
Advisor

_____
Gary J. Bassell, Ph.D.
Committee Member

_____
James Q. Zheng, Ph.D.
Committee Member

_____
Lary C. Walker, Ph.D.
Committee Member

_____
Jonathan D. Glass, M.D.
Committee Member

Accepted:

_____
Lisa A. Tedesco, Ph.D.
Dean of the James T. Laney School of Graduate Studies

_____
Date

Differential Proteolysis of Mutant Huntingtin in Astrocytes and Neurons

By

Ting Zhao

M.D., Dalian Medical University, 2005

M.S., Dalian Medical University, 2008

Advisor: Xiao-Jiang Li, M.D., Ph.D.

An abstract of
A dissertation submitted to the Faculty of the
James T. Laney School of Graduate Studies of Emory University
in partial fulfillment of the requirements of the degree of
Doctor of Philosophy

Graduate Division of Biological and Biomedical Sciences
Neuroscience

2017

Abstract

Differential Proteolysis of Mutant Huntingtin in Astrocytes and Neurons

By Ting Zhao

Huntington's disease (HD) is a neurodegenerative disorder caused by the expression of misfolded mutant huntingtin protein (mHtt). HD involves the preferential accumulation of mHtt in neuronal cells and selectively kills neurons. The mechanisms underlying the selective neurodegeneration in HD remain unknown. My study addresses two issues: 1) why mHtt preferentially aggregates in neurites; 2) why astrocytes are more resistant than neurons to mHtt and other misfolded proteins. Given that mHtt aggregates in neurites are prevalent in the HD brains, I hypothesize that the degradation of mHtt is inefficient in neurites. To test this hypothesis, I combined the "optical-pulse chase assay" with brain slice and primary culture models. I found that mHtt is slowly cleared in neurites compared with neuronal cell bodies, indicating compartment-dependent degradation of mHtt in neurons. In contrast, mHtt is rapidly degraded in both the cell bodies and processes of astrocytes.

My live-cell imaging results also show that mHtt is cleared faster by astrocytes than by neurons, which explains a well-known phenomenon that astrocytes are affected to a much lesser extent than neurons in the HD brains. Importantly, I found that C-terminus of Hsp70 interacting protein (CHIP), a co-chaperone of Hsp70, is more active in astrocytes than in neurons, which is evidenced by increased mono-ubiquitinated CHIP in astrocytes. CHIP binds to mHtt selectively in astrocytes, promoting ubiquitination and proteasomal degradation of mHtt. Active CHIP accelerates degradation of various misfolded proteins, in addition to mHtt, in astrocytes. It is known that the heat-shock response is induced in astrocytes, but not in neurons, however the mechanism causing this differential response is poorly understood. I found that differential CHIP activity in astrocytes and neurons leads to a distinct heat-shock response. Moreover, active CHIP also increases basal levels of Hsp70 in astrocytes, which in turn promotes the association of CHIP with mHtt. Furthermore, I found that deficiency of HspBP1 in astrocytes accounts for the high activity of CHIP, and overexpression of HspBP1 inhibits CHIP activation and causes the accumulation of mHtt in astrocytes. Finally, knocking down HspBP1 in neurons with CRISPR/Cas9 in a HD knock-in mouse model reduced mHtt aggregates and ameliorated neuropathology. Collectively, my results provide an explanation for the higher resistance to deleterious effects of misfolded proteins in astrocytes compared to neurons in neurodegenerative diseases, and suggest that HspBP1 is a potential therapeutic target for HD treatment.

Differential Proteolysis of Mutant Huntingtin in Astrocytes and Neurons

By

Ting Zhao

M.D., Dalian Medical University, 2005

M.S., Dalian Medical University, 2008

Advisor: Xiao-Jiang Li, M.D., Ph.D.

A dissertation submitted to the Faculty of the
James T. Laney School of Graduate Studies of Emory University
in partial fulfillment of the requirements of the degree of
Doctor of Philosophy

Graduate Division of Biological and Biomedical Sciences
Neuroscience

2017

ACKNOWLEDGMENTS

I would like to thank my advisor, Xiao-Jiang Li, who introduced me to the filed of Huntington's disease research, and has provided academic guidance as well as financial support over the past years. I feel lucky to have joined Dr. Li's lab in that its specialization in research on glia has given me the opportunity to study and explore the biological differences between glia and neurons. I would also like to thank Dr. Shi-Hua Li, who has offered assistance in technical aspect of the experiments. I cherish the fun time we spent together at Dr. Li's house to celebrate Christmas and the Spring Festival. I would also like to thank my committee members Dr. Gary Bassell, Dr. Lary Walker, Dr. James Zheng, and Dr. Jonathan Glass. They always provided me with valuable suggestions on experiments, which has inspired and helped me to overcome experimental obstacles, and to improve the quality of my research papers. I would like to thank my wife, Yan Hong, who is not only a perfect life partner, but also an amazing research collaborator. I will never forget the fun and hard times that we spent together over the past several years in the lab, which has further tightened our bond. I would also like to thank all the faculty and staff of the Department of Human Genetics and the Division of Animal Resources. Without the environment that they established, my research would never have been undertaken so smoothly. Finally, I must thank my parents, who raised, educated and shaped me to become the man who I am today. Without them, I would never have achieved my current accomplishments. I am tremendously grateful for their love.

Table of Contents

Figures

Chapter 2: Degradation of mHtt is compartment- and cell-type-dependent

Chapter 3: Differential HspBP1 expression accounts for the greater vulnerability of neurons than astrocytes to misfolded proteins

Chapter 1

General Introduction

This Chapter represents part of work published as: T Zhao, Y Hong, XJ Li, SH Li. Subcellular clearance and accumulation of huntington disease protein: A mini-review. Frontiers in molecular neuroscience 9. doi: 10.3389/fnmol.2016.00027.

1.1 Huntington's disease

Huntington's disease (HD) is an autosomal dominant, fatal, neurodegenerative disease that affects 1 in 10,000 Americans (Munoz-Sanjuan and Bates, 2011). Although it is a rare disease, HD is broadly studied as a prototypic neurodegenerative disease due to its clear etiology. HD is caused by the mutation in HTT gene, which results in CAG trinucleotide repeat expansion that encodes an expanded polyglutamine (polyQ) tract in the N-terminus of the huntingtin protein. HD is one of nine polyQ diseases (Shao and Diamond, 2007), and other polyQ diseases include dentatorubropallidoluysian atrophy (DRPLA), spinal and bulbar muscular atrophy (SBMA), spinocerebellar ataxia type 1, 2, 3, 6, 7 and 17.

Typically, the onset of HD occurs between the ages of 30 and 50 years. The length of expanded polyQ tracts carried by HD patients ranges generally from 38 to 55, compared with normal people whose CAG repeats are no longer than 36 (Ross et al., 2014). Long polyQ tracts (> 100) are found in rare, earlier-onset juvenile cases with aggressive progression of disease, which indicates inverse correlation between polyQ length and onset as well as severity of disease. Clinical manifestations of HD include motor abnormality, psychiatric problems and cognitive decline (Munoz-Sanjuan and Bates, 2011). Individuals with the adult-onset form of HD generally live about 15 to 20 years after symptoms begin. To date, there is no disease-modifying treatment available.

HD shares several common features with other types of neurodegenerative diseases: 1) detergent-insoluble aggregates form in the brains; 2) neurodegeneration occurs and progresses in an age-dependent manner; 3) certain brain regions are selectively vulnerable to the disease. For HD, the medium-size spiny neurons (MSN) in striatum are

first and most affected (Margulis and Finkbeiner, 2014), and the loss of these neurons leads to striatal atrophy. As the disease progresses, cortical and hippocampal neurons are affected at later stages of HD. In contrast, degeneration in glia is never seen in the HD brains in spite of the expression of mHtt in these cells (Shin et al., 2005), suggesting unknown cell-type-specific protective mechanisms in astrocytes.

Although a plethora of studies have explored molecular mechanisms underlying the pathogenesis of HD, the exact causal mechanisms are still poorly understood. So far, it is the consensus that an expanded polyQ tract confers toxic gain of function on huntingtin proteins, which consequently impairs normal cell processes and causes neuronal death eventually. Indeed, mHtt aberrantly interacts with a variety of proteins, and disrupts their normal functions (Li and Li, 2004; Shirasaki et al., 2012). For instance, the association between mHtt and peroxisome proliferator-activated receptor delta (PPAR-δ) suppressed PPAR-δ-mediated transactivation, and pharmacological activation of PPAR-δ rescued mHtt-induced neurotoxicity (Dickey et al., 2016). Another example is the abnormal association between mHtt and motor proteins, kinesin and dynein; mHtt impairs microtubule-dependent transport of cargoes, such as BDNF-containing vesicles and mitochondria, along axons, which perturbs the transport network in neurons (Gauthier et al., 2004; Orr et al., 2008; Reddy and Shirendeb, 2012). On the other hand, an alternative explanation for mHtt-mediated neuropathology is a loss-of-function mechanism. Consistent with this perspective, a mouse model, in which the huntingtin gene was inactivated in the forebrain and testis, showed progressive neurodegeneration (Dragatsis et al., 2000). Additional evidence for the loss-of-function theory includes the findings that the expansion mutation abolished the competence of normal huntingtin to bind to

Hip-1, which activated the caspase-8-mediated apoptotic pathway (Gervais et al., 2002); in addition, the removal of endogenous huntingtin leads to neurodegeneration in a *Drosophila* model (Zhang et al., 2009). Taken together, it is proposed that both gain-of-function and loss-of-function mechanisms contribute to the pathogenesis of HD

1.2 Proteolysis of mutant huntingtin

Full-length huntingtin is a large protein composed of 3144 amino acids, and the protein is ubiquitously expressed throughout the body. The polyglutamine (polyQ) tract is located near the N-terminus of huntingtin, flanked by highly conserved first 17 amino acids (N17) and a proline-rich region followed by multiple HECT domains that are involved in protein-protein interaction (Cattaneo et al., 2005). Normal huntingtin is involved in a broad range of cellular processes including transcription, mitosis, trafficking, endocytosis, and signaling (Cattaneo et al., 2005). Its counterpart, mutant huntingtin (mHtt), is recognized and cleaved by a variety of proteases (Gafni and Ellerby, 2002; Gafni et al., 2004; Wellington et al., 1998; Wellington et al., 2000), such as caspase-6 and calpain, to generate shorter, and more toxic N-terminal fragments that are the major constituents of mHtt aggregates. The expanded polyQ tract increases β-sheet structures and renders mHtt prone to misfolding and aggregation. Although the roles of aggregated misfolded proteins are still controversial (protective versus detrimental), it is known that the accumulation of misfolded proteins is a prerequisite for neurodegeneration (Goldberg, 2003; Sherman and Goldberg, 2001). To maintain protein homeostasis and prevent the accumulation of misfolded proteins, eukaryotic cells take advantage of two quality

control systems, the ubiquitin-proteasome system (UPS) and autophagy, to remove misfolded proteins (Chen et al., 2011).

Initially thought to only clear soluble and short-lived proteins, recent studies found that the proteasome is also responsible for degrading long-lived and aggregated proteins, the latter of which are segregated by the hsp70-hsp110 machinery prior to proteasomal degradation (Hjerpe et al., 2016; Zhao et al., 2015). The proteasome consists of 33 subunits that are assembled into two sub-complexes, the 20S core particle flanked at either one or both ends by regulatory 19S particles, to form the 26S proteasome. Protein clearance by the UPS involves two sequential reactions: tagging substrates via ubiquitination and then degradation of tagged substrates by the proteasome. Ubiquitination is a stepwise process coordinated by three enzymes: ubiquitin-activating (E1), ubiquitin-conjugating (E2), and ubiquitin-ligating enzymes (E3) (Ciechanover, 2005), and E3 ligases confer specificity on ubiquitination via recognizing specific substrates (Deshaies and Joazeiro, 2009). Substrates that are tagged by the K48-linked polyubiquitin chain are destined for proteasomal degradation. Following proteasomal degradation, ubiquitin chains are disassembled by deubiquitinating enzymes, and free ubiquitin molecules are released for recycling (Eletr and Wilkinson, 2014).

Proteolysis of mHtt by the proteasome is found in various HD cell and animal models. The first evidence to implicate proteasome-mediated degradation of mHtt is that ubiquitin was localized in mHtt aggregates (DiFiglia et al., 1997; Gutekunst et al., 1999), suggesting that mHtt is ubiquitinated. Subsequent studies showed that proteasomal inhibition leads to the accumulation of both soluble and aggregated mHtt, which provided direct experimental evidences for mHtt clearance by the proteasome (Li et al., 2010;

Waelter et al., 2001). Furthermore, it was found that mHtt is polyubiquitinated by different ubiquitin E3 ligases, such as the C-terminus of Hsp70 interacting protein (CHIP) and Ube3a (Bhat et al., 2014; Jana et al., 2005), suggesting that multiple E3 ligases mediate the ubiquitination of mHtt for proteasomal degradation in a coordinated manner.

Macroautophagy (hereafter, referred to as autophagy) is a bulk degradation system that is activated by starvation and then engulfs and digests a portion of the cytosol to provide nutrients for energy generation (Rabinowitz and White, 2010). In addition to digestion of cytosolic components under starvation, autophagy also clears misfolded-protein aggregates and damaged organelles selectively. In HD cell and animal models, upregulation of autophagy leads to the reduction of mHtt aggregates, confirming the degradation of aggregates by autophagy (Qin et al., 2003; Ravikumar et al., 2002; Tsvetkov et al., 2010). Unlike the nonspecific bulk degradation under starvation, autophagy-mediated clearance of mHtt aggregates is selective since mHtt is K63-polyubiquitinated, and K63-ubiquitinated substrates are recognized by autophagy receptors such as p62 or optineurin, both of which have been shown to bind Htt (Korac et al., 2013; Tan et al., 2008). Autophagy receptor proteins, such as p62 bind to LC3-II (microtubule-associated protein light chain 3), which is located on autphagosome membranes, and therefore presents substrates to the autophagosome (Kirkin et al., 2009; Shaid et al., 2013). Subsequently, the autophagosome fuses with lysosomes to form autolysosome in which substrates are digested by hydrolytic enzymes from lysosomes (Bjorkoy et al., 2005).

Autophagy also plays a role in clearing soluble mHtt. Suppressing autophagy with 3-Methyladenine (MA), which can inhibit autophagosome formation, or with bafilomycin A1, which prevents the fusion of autophagosomes with lysosomes, hinders mHtt clearance and causes accumulation of soluble and aggregated mHtt in HD cell models (Ravikumar et al., 2002). Conversely, activating autophagy with rapamycin, which inhibits mTOR, reduced the levels of both soluble and aggregated mHtt (Ravikumar et al., 2002). Interestingly, autophagy modulators did not influence the clearance of wild-type Htt (Ravikumar et al., 2002), which suggests that autophagy selectively recognizes and clears mHtt. This selective degradation might be caused by the acetylation at lysine residue 444 (K444) specifically on mHtt, a post-translational modification essential for autophagic degradation, and which is absent on wild-type Htt (Jeong et al., 2009). Given the removal of mHtt by the UPS and autophagy, activation of either system has the potential to ameliorate HD neuropathology through promoting the degradation of mHtt.

1.3 Aggregation of mutant huntingtin in the neuropil

mHtt is an aggregation-prone protein that, in disease states, forms detergent-insoluble aggregates in the brains. The mHtt aggregates consist of N-terminal fragment of mHtt, chaperones, ubiquitin, sequestosome1/p62, and proteasomal subunits, some of which are common components also found in the aggregates of other neurodegenerative diseases, such as Parkinson's disease and Alzheimer's disease. mHtt aggregates were recognized by antibodies to the epitopes in the N-terminus of mHtt, indicating that N-terminal fragments constitute these aggregates. In comparison with its full-length counterpart, N-terminal fragments of mHtt are more toxic, which is evidenced by the findings that

transgenic R6/2 mice expressing mHtt exon1 (the shortest N-terminal fragment of mHtt), display extremely aggressive progression of disease and severe phenotypes (Mangiarini et al., 1996).

Although mHtt is ubiquitously expressed in the brain, it preferentially accumulates in neuronal nuclei and the neuropil (DiFiglia et al., 1997; Gutekunst et al., 1999), the latter of which refers to dendrites and axons. However, mHtt aggregates in astrocytes are not as prevalent as in neurons. This cell-type-specific and compartment-specific localization of mHtt aggregates suggests that degradation of mHtt is heterogeneous in different types of brain cells as well as in different compartments of the same cell. A growing body of evidence indicates that mHtt aggregates are toxic. For instance, intranuclear mHtt aggregates disrupt gene expression via binding to a broad range of transcriptional factors, such as SP1 and CREB-binding protein (CBP) (Dunah et al., 2002; Li et al., 2002). Neuropil aggregates are far more prevalent than intranuclear aggregates in patients at the early stage of HD (Gutekunst et al., 1999). Formation of aggregates is recapitulated in a variety of HD animal models. Of these models, a knock-in (KI) HD mouse model, in which full-length mHtt is expressed at the endogenous level, mimics HD patients genetically (Chang et al., 2015). In HD KI mice carrying 140 CAG repeats, abundant neuropil aggregates were seen in the lateral globus pallidus (LGP) and substantia nigra (SN) (Li et al., 2001), the brain regions to which striatal neurons project and where marked degeneration occurs in the early stage of HD patients. Consistently, degeneration of the neuropil was also found in the HD KI mice, probably due to physically blocking axonal transport by the aggregates in the neuropil (Li et al., 2001).

Given the involvement of neuropil aggregates in neuropathology in the HD brain, it is imperative to investigate why mHTT preferentially accumulates in the neuropil. One explanation is that the accumulation of mHtt in the neuropil is caused by defective transport of mHtt. This postulation is based on the fact that huntingtin is a component of a motor protein complex that mediates microtubule-dependent transport. The expanded polyQ tract affects the interaction and binding affinity of huntingtin with other components of the motor protein complex, which compromises the motility of dynein and kinesin, two motor proteins (Gauthier et al., 2004; Orr et al., 2008; Reddy and Shirendeb, 2012). Thus, mHtt aggregation in the neuropil probably is the outcome of the adverse impact of mHtt on transport. An alternative explanation is that the degradation of mHtt in neurites is not as efficient as that in cell bodies. As mentioned previously, mHtt is degraded by the proteasome, whose activity is compartment-dependent in neurons. For example, the proteasome displays higher activity in the cytoplasm than in the nucleus (Tydlacka et al., 2008). Also, the function of proteasome is impaired specifically in synapses of mHtt-expressing neurons, which is probably caused by ATP-deficiency in this subcellular region (Wang et al., 2008b). On the other hand, given the compartment-dependent biogenesis of autophagy in neurons, autophagy may also contribute to the heterogenous degradation of mHtt in neurons (Maday et al., 2012). Maday and colleagues found that the biogenesis of autophagosomes occurs in distal parts of neurites and in cell bodies. After formation, autophagic vesicles in neurites are retrogradely transported to the cell bodies where events of autophagic degradation occur (Maday and Holzbaur, 2016). Therefore, it is likely that autophagy-mediated clearance of mHtt occurs in cell bodies rather than neurites. Collectively, the quality control machinery exhibits

compartment-dependent features, which may contribute to the preferential accumulation of mHtt in neurites.

1.4 Selective neurodegeneration in Huntington's disease

Neurodegenerative diseases are characterized by selective neuronal death in specific brain regions (Przedborski et al., 2003). For HD, striatal projection neurons are the earliest and most severely affected cells in HD. mHtt is also expressed in glial cells, which make up approximately 90% of the cells in the brain, whereas glial cells are affected to a lesser extent than neurons in the HD brains (Shin et al., 2005). Astrocytes are a major type of glial cell. Initially thought to only provide structural support for neurons, astrocytes are now known to play far more active roles (Sofroniew and Vinters, 2010). For instance, astrocytes secrete neurotrophic factors, such as BDNF and GDNF, to nourish neurons (Sofroniew and Vinters, 2010); astrocytes also prune synapses, actively eliminating synapses in the mammalian CNS (Chung et al., 2013). Expression of mHtt in astrocytes was validated in the brains of HD patients and animal models. In addition, selective expression of mHtt in murine astrocytes gave rise to abnormal phenotypes, suggesting involvement of astrocytes in the pathogenesis and progression of HD (Bradford et al., 2009). Conversely, engraftment of normal human glial progenitor cells, which differentiate into astrocytes, in HD mouse brains ameliorates neuropathology of HD (Benraiss et al., 2016). Although mHtt perturbs multiple cellular processes in astrocytes (Hong et al., 2016; Shin et al., 2005; Tong et al., 2014), astrocytes are affected to a lesser extent than neurons, and degeneration is never seen in astrocytes. Lack of degeneration in astrocytes is probably attributable to the proliferation of astrocytes, which

may dilute protein levels of mHtt in daughter cells. An alternative explanation is that astrocytes are capable of tackling mHtt in a more efficient way than are neurons. The latter explanation is supported by previous findings that mHtt aggregates formed in astrocytes are much smaller and less prevalent than those in neurons in the HD KI mice (Shin et al., 2005). Moreover, the proteasome activity is higher in astrocytes, raising the possibility that the UPS is more actively involved in clearing mHtt in astrocytes (Tydlacka et al., 2008). To provide direct experimental evidence for this hypothesis, comparing half-lives of mHtt between neurons and astrocytes is necessary. Moreover, given the higher proteasomal activity, whether activities of certain upstream ubiquitin enzymes in UPS correspondingly increase in astrocytes remains to be studied. Uncovering potential protective mechanisms against mHtt in astrocytes might provide new therapeutic targets for HD.

1.5 "Optical-pulse chase" assay

It was not feasible to study the degradation of mHtt in living neurons at subcellular levels until phototransformable fluorescent proteins were invented. Phototransformable fluorescent proteins can be classified into three types-photoactivating, photoconverting and photoswitching-based on their responses to light. Currently, these proteins are used widely to study the dynamics of molecules and cells in a spatiotemporal manner (Adam et al., 2014). Recently, using Dendra2, one of the photoconvertible fluorescent proteins, the degradation of mHtt-exon1 was examined in cultured striatal neurons (Tsvetkov et al., 2013). Dendra2 is a green-to-red photoconvertible fluorescent protein featuring fast maturation and bright fluorescence (Chudakov et al., 2007). Light irradiation at a 405-nm

wavelength can efficiently activate Dendra2 and consequently switches its fluorescent color irreversibly from green to red. The linkage of Dendra2 to mHtt does not perturb its neurotoxicity or the property of aggregation in neurons. After transient transfection of Htt-exon1-Dendra2 into striatal neurons, Tsvetkov converted green Htt-exon1-Dendra2 into red fluorescence by activating Dendra2 with 405-nm laser light (Tsvetkov et al., 2013). Therefore, after irradiation, the reduction of red Htt-exon1 over time reflects its degradation in live cells. Using this strategy, called the "optical pulse chase" assay, Tsvetkov and colleagues found that mHtt-exon1 was cleared faster than its wild-type counterpart in whole striatal neurons.

Although optical-pulse chase has been used mainly with *in vitro* cultured cells at the whole-cell level, it should also be useful for determining the turnover of mHtt in live cells at subcellular levels, such as neuronal processes and cell bodies. Examining the change of red fluorescence avoids the potential influence of newly synthesized proteins as they are labeled by inactive green dendra2, so that the degradation of mHtt can be quantified. The dendra2 fusion proteins can be expressed via adenoviral-associated vectors (AAV), and stereotaxic injection would allow the delivery of the AAV vectors to specific brain regions, such as the striatum. The injected brain region can then be isolated and sectioned into brain slices, which can be observed in medium under a fluorescence microscope. Photoconversion of dendra2 can then be achieved to measure the clearance of mHtt in neuronal processes or nerve terminals in brain slices. Moreover, using different promoters would confer the expression of dendra-2-mHtt in specific types of cells, making it possible to study the cell type-dependent degradation of mHtt in the brain.

Further, tagging the dendra-2 fusion protein with organelle-targeting sequences would allow us to study mHtt's degradation in specific organelles.

1.6 Roles of C-terminus of Hsp70-interacting protein in clearance of misfolded proteins

Chaperones are a family of proteins that assist newly synthesized proteins with folding into their native structure, and that refold misfolded proteins. Misfolded proteins that fail to be refolded into the proper structure are targeted for proteasomal degradation. C-terminus of Hsp70 interacting protein (CHIP), a co-chaperone with ubiquitin E3 ligase activity, bridges the gap between the chaperone system and UPS via polyubiquitinating chaperone-associated misfolded proteins for proteasomal degradation (McDonough and Patterson, 2003). In this regard, CHIP plays a central role in the protein triage decision.

CHIP is composed of N-terminal tetratricopeptide (TPR) domain, C-terminal U-box domain, and a coiled-coil domain in the middle. The TPR domain is responsible for the association between CHIP and chaperones, such as Hsp/Hsc70 and Hsp90. The U-box domain is evolutionarily conserved and possesses ubiquitin E3 ligase activity that defines CHIP as U-box-type E3 ligase. The coiled-coil domain mediates the formation of the CHIP homodimer, which is proposed to be necessary for exerting CHIP function (McDonough and Patterson, 2003).

The expression and activity of CHIP are tightly regulated at transcriptional and post-translational levels, respectively. The mRNA level of CHIP is upregulated under a variety of stress conditions, such as hyperthermia, oxidative stress and overexpression of misfolded proteins (Dikshit and Jana, 2007; McDonough and Patterson, 2003). The

response of CHIP to the insults of stress suggests its remarkable roles in maintaining cell homeostasis. Indeed, CHIP overexpression in vivo prevented neuronal death induced by ER stress (Cabral Miranda et al., 2014). Moreover, heat-shock stress is lethal for CHIP knockout mice ($CHIP^{-/-}$) (Dai et al., 2003). In addition, CHIP knockout mice display a shorter lifespan, and accumulated toxic oligomeric proteins (Min et al., 2008). On the other hand, the activity of CHIP is modulated by post-translational modification. CHIP undergoes self-ubiquitination, which servers to regulate CHIP E3 ligase activity. This notion is supported by recent findings that mono-ubiquination of CHIP increased CHIP activity since enhancement of mono-ubiquitnated CHIP promoted degradation of misfolded proteins, and conversely, inhibiting CHIP mono-ubiquitination lead to accumulation of misfolded proteins (Scaglione et al., 2011). It is noteworthy that CHIP activity is also regulated by other factors. For instance, Hsp70-binding protein 1 (HspBP1), a co-chaperone of Hsp70, directly binds to CHIP and inhibits CHIP ubiquitin E3 ligase activity. Co-transfection of CHIP and HspBP1 stabilized cystic fibrosis transmembrane conductance regulator (CFTR), a well-established CHIP substrate, via suppressing CHIP-mediated ubiquitination on CFTP (Alberti et al., 2004).

A plethora of evidence demonstrates that CHIP participates in ubiquitination and degradation of a variety of misfolded proteins that are associated with neurodegenerative models in cell lines and fruit flies (Kumar et al., 2007; Tetzlaff et al., 2008). Overexpression of CHIP could accelerate clearance of these misfolded proteins. Although expression of CHIP has been identified in the brain, whether its activity differs in distinct types of brain cells is still unclear. If so, variant activity of CHIP among

different types of brain cells likely contributes to selective neuronal vulnerability in neurodegenerative disorders.

1.7 Dissertation goals

Given the selective accumulation of mHtt in neuronal processes, my project aims to uncover the mechanisms underlying the cell-type-specific and compartment-specific accumulation of mHtt. To this end, I have studied and compared degradation rates of mHtt in different subcellular compartments of neurons and astrocytes, cell bodies and neurites, using the optical-pulse chase assay. I employed not only primary cultures, but also acute brain slices that allow me to dissect the turnover of mHtt in the mouse brain. The results from these experiments should advance the understanding of the proteolysis of mHtt in brain cells. Moreover, by exploring the clearance of mHtt in different types of brain cells, I hope to reveal mechanisms by which astrocytes are more resistant to HD.

Chapter 2

Degradation of mHtt in neurons is compartment- and cell-type-dependent

This Chapter represents the work published as: T Zhao, Y Hong, SH Li, XJ Li. Compartment-Dependent Degradation of Mutant Huntingtin Accounts for Its Preferential Accumulation in Neuronal Processes. J Neurosci. 2016 32:8317-28. doi: 10.1523/JNEUROSCI. T Zhao and Y Hong performed experiments, T Zhao wrote the manuscript, SH Li and XJ Li participated in writing and editing the manuscript

Abstract

In neurodegenerative diseases caused by misfolded proteins, including Huntington's disease (HD), the neuronal processes and terminals are particularly prone to the accumulation of misfolded proteins, leading to axonal and synaptic dysfunction. This compartment-dependent accumulation can result from either the altered transport of misfolded proteins or impaired protein degradation. Mutant huntingtin (mHtt), the HD protein, is known to affect intracellular transport and can be degraded by the proteasome and autophagy, but how mHtt accumulates in the neuronal processes, an early pathological event in the brains of HD patients, still remains unclear. Using an "optical pulse-chase" assay that can quantify protein degradation in specific subcellular regions, we found that neuronal mHtt is removed faster in the cell body than in neurites. Furthermore, mHtt is cleared more rapidly in astrocytes than in neurons. The ubiquitin-proteasome system (UPS) plays a much bigger role than autophagy in degrading soluble mHtt via K48 ubiquitination in both the cytoplasm and processes of neurons and astrocytes. By injecting adenoviral vectors expressing mHtt into the mouse brain, we confirmed that mHtt is removed more slowly in neurites than in the cytoplasm of the cell body of neurons. Our findings provide evidence for the cell type- and compartment-dependent degradation of mHtt and explain why mHtt preferentially accumulates and aggregates in the neurites of vulnerable neurons. In addition, our findings suggest that enhancing proteasomal activity could be an effective way to reduce the preferential accumulation of soluble mHtt in neuronal processes.

Introduction

Huntington's disease (HD) is an autosomal dominant neurodegenerative disease caused by an expanded polyglutamine (polyQ) tract in the N-terminal region of mutant huntingtin (mHtt). Once the full-length mHtt is degraded by proteolysis, the polyQ expansion causes N-terminal Htt fragments to misfold and form aggregates (Ross and Tabrizi, 2011). Transgenic HD mouse models also indicate that it is N-terminal mHtt fragments with expanded polyQ repeats that can become misfolded, aggregated, and pathogenic (Davies et al., 1997; Schilling et al., 1999) Also, HD knock-in mice, which express full-length mHtt at the endogenous level, show that N-terminal mHtt preferentially forms aggregates in the processes of striatal neurons, which are those mostly affected in HD (Li et al., 2000). In fact, in the brains of HD patients, neuropil aggregates appear to be more abundant than nuclear aggregates in the early disease stage (DiFiglia et al., 1997; Gutekunst et al., 1999). Because neuropil aggregates result from the accumulation of misfolded proteins in neuronal process that can affect axonal transport and synaptic function (Millecamps and Julien, 2013; Milnerwood and Raymond, 2010) and suppression of neuropil aggregates can alleviate the neurological symptoms of HD mice (Wang et al., 2008a), it is important that we understand how mHtt accumulates preferentially in the neuronal processes.

The accumulation of misfolded proteins in the neuronal processes could be due to impaired protein clearance. The clearance of misfolded proteins in cells is largely mediated by the ubiquitin-proteasome system (UPS) and autophagy (Ciechanover and Kwon, 2015); however, which of these clearance systems plays a larger role in removing mHtt in neuronal processes remains unclear. In addition, since mHtt can affect

intracellular transport (Gunawardena et al., 2003; Gauthier et al., 2004; Trushina, 2004; Reddy and Shirendeb 2012; Wong and Holzbaur 2014), it is possible that mHtt accumulates in the elongated neuronal processes because of the adverse impact of the expanded polyQ on intracellular transport. Unfortunately, it is difficult to identify the causes for neuropil Htt accumulation using conventional biochemical or microscopic assays.

Recently, an "optical pulse-chase" assay was used to study the degradation of soluble mHtt in cultured neurons (Tsvetkov et al., 2013). This technique uses Dendra2, a photoconvertible fluorescent protein, to fuse to mHtt, so the decline of fluorescence after photoconversion represents degradation of the fused protein. In the present study, we used this technique to further study the degradation of mHtt in different subcellular compartments of neurons and glial cells in the brain. Our findings show that mHtt is cleared more slowly in neuronal processes than in the cell body and is also removed less efficiently from neurons than astrocytes. By inhibiting the UPS and autophagy, we found that the UPS plays a primary role in clearing soluble mHtt in the neuronal processes, suggesting that increasing proteasome activity could be an efficient way to clear soluble mHtt from the neuronal processes in HD brains.

Results

Soluble mHtt is cleared faster than wild-type Htt in the cell body

The photoconvertible fluorescent protein Dendra2 has been conjugated to Htt to examine the turnover of Htt, and this conjugation does not affect the aggregation or toxicity of mHtt (Tsvetkov et al., 2013). Indeed, mHtt with dendra2 conjugation also formed

aggregates in neurites as mHtt without dendra2 and did not cause any obvious morphological difference in cultured neurons, suggesting that dendra2 did not alter toxicity of mHtt (Fig. 2.1*C*). To evaluate the degradation rate of N-terminal Htt in different subcellular regions, we conjugated Dendra2 to the C-terminus of N-terminal Htt (1-230 amino acids) with 23Q or 130Q (Fig. 2.1*A*). We transfected Htt-Dendra2, which is expressed under the CMV promoter, in cultured primary mouse hippocampal neurons and cortical astrocytes. Western blotting with anti-Htt (mEM48) and anti-Dendra2 showed the integrity of Htt-Dendra2 in cultured neurons and astrocytes (Fig. 2.1*B*). Thus, the proteolytic degradation of this fusion protein or decline in Dendra2 fluorescent signal reflects the degradation of Htt or its clearance in cells. Next, we used fluorescence microscopic imaging to evaluate the turnover of Htt-Dendra2. After activating Dendra2 to convert it to a red fluorescent protein within the region of cell bodies, the intensity of red fluorescence was quantified at different time points. We observed that a small fraction of red fluorescence promptly diffused into neurites immediately after photoconversion, and no such diffusion was seen at 10 min after photoconversion. This rapid diffusion may result from the intracellular transport of Htt. Thus, we started to measure red fluorescence intensity at 10 min after photoconversion to avoid diffusion effects on degradation rates. The fluorescence diffusion in astrocytes is negligible since these cells do not have long processes. Comparison of normal and mutant Htt red fluorescence intensities revealed faster degradation of mHtt (Htt-130Q) than wild-type Htt (Htt-23Q) in the cell bodies of neuronal and astrocytic cells (Fig. 2.1*D*-*G*, $*P < 0.05$, $**P < 0.01$).

mHtt is cleared slowly in neuronal processes

The advantage of using Htt-Dendra2 is that we can examine Htt turnover in neuronal processes. Thus, we activated Dendra2 in segments of processes and saw that a considerable amount of red fluorescence was stable in the activated regions, probably due to the association of Htt with microtubules since it interacts with many proteins and organelles (Harjes and Wanker, 2003; Trushina et al., 2004; Hoffner et al., 2002; Klein et al., 2009). Importantly, we found that Htt-130Q was cleared more slowly than Htt-23Q in neurites of cultured neurons (Fig. 2.2*A,C,* $*P < 0.05$, $**P < 0.01$), suggesting the impaired degradation of mHtt in this subcellular region. In contrast, in the processes of cultured astrocytes, mHtt (Htt-130Q) is still removed faster than normal Htt (Htt-23Q) (Fig. 2.2*B,D,* $***P < 0.001$, $****P < 0.0001$). This difference indicates that neuronal cells and astrocytes have intrinsic differences in clearing mHtt in their processes.

Soluble mHtt is more efficiently cleared by the ubiquitin-proteasome system

We know that both proteasome and autophagy can degrade soluble mHtt (Waelter et al., 2001; Li et al., 2010; Sarkar et al., 2008); however, we know little about which quality control mechanism is primary for mHtt's removal in processes. We therefore treated primary neurons or astrocytes with either 5 μM MG132 to inhibit the UPS or 100 nM BFA to inhibit autophagy. After adding these inhibitors to the culture medium, cells were subjected to live imaging. Again, without MG132 or BFA, normal Htt (Htt-23Q) is degraded much faster than mutant Htt (mHtt-130Q). After inhibiting the UPS by MG132, both Htt-23Q and mHtt-130Q were stable over the same period of time. We also used a specific proteasomal inhibitor, epoxomicin, and found that it also markedly suppressed

the turnover of Htt-23Q and mHtt-130Q in neuronal processes. Interestingly, BFA treatment did not stabilize either Htt-23Q or Htt-130Q (Fig. 2.3, *$P < 0.05$, **$P < 0.01$, ***$P < 0.001$, ****$P < 0.0001$, Con vs. MG132; #$P < 0.05$, ##$P < 0.01$, ####$P < 0.0001$, Con vs. epoxomicin). These results suggest that soluble Htt in neuronal processes is degraded primarily by the UPS.

To examine whether Htt in astrocytic processes is degraded by the UPS and autophagy, we treated Htt-130Q transfected astrocytes in culture with MG132, epoxomicin, or BFA. Similarly, MG132 and epoxomicin, but not BFA, blocked the degradation of mHtt in astrocytes (Fig. 2.4, *$P < 0.05$, **$P < 0.01$, ***$P < 0.001$, Con vs. MG132; #$P < 0.05$, ##$P < 0.01$, ###$P < 0.001$, ####$P < 0.0001$, Con vs. epoxomicin). Thus, in the processes of astrocytes, mHtt is also degraded primarily by the UPS.

Degradation of mHtt by the UPS via K-48 ubiquitination

Although live imaging analysis led us to examine the degradation of mHtt in neuronal processes, quantitatively comparing the global effects of proteasomal and autophagic inhibitors on mHtt in neuronal and astrocytic cells is difficult. We thus performed western blot analysis using antibodies to LC3 for detecting the production of LC3-II, an indicator of autophagy activation, since BFA increases LC3-II during its inhibition of autophagy (Myeku and Figueiredo-Pereira, 2011). As expected, BFA treatment markedly elevated the level of LC3-II, indicating the doses and treatment of BFA we used indeed inhibited autophagic function (Fig. 2.5*A,B*); however, this BFA treatment apparently could not significantly increase levels of soluble normal Htt (Htt-23Q). Moreover, BFA treatment led to a small but significant increase in soluble mutant Htt (Htt-130Q) in

neuronal and astrocytic cells. Compared with BFA, MG132 and epoxomicin remarkably increased both Htt-23Q and Htt-130Q in neuronal cells and astrocytes (Fig. 2.5, $*P < 0.05$, $**P < 0.01$, $***P < 0.01$). These results support the live imaging results that soluble Htt is degraded primarily by the UPS.

To further investigate whether the degradation of Htt by the UPS is via K48 ubiquitination, we performed immunoprecipitation of Htt, and then probed the immunoprecipitates with an anti-K48 antibody. We found that in neuronal cells and astrocytes, both Htt-23Q and Htt-130Q are ubiquitinated via K48, but Htt-130Q is ubiquitinated via K48 to a much greater extent than Htt-23Q (Fig. 2.6*A*,*B*). Quantitative analysis of the ratio of ubiquitinated Htt to precipitated Htt verified that more mHtt is K48 ubiquitinated than normal Htt (Fig. 2.6*C,* $*P < 0.05$). Since K48 ubiquitination is important for protein degradation by the UPS (Pickart and Eddins, 2004), the result suggests that differential K48 ubiquitination may account for faster degradation of mHtt in neuronal cell bodies and astrocytes.

Degradation of mHtt is compartment dependent in neurons in the mouse brain

To explore whether mHtt is differentially cleared from the cell body and processes in the brain, we generated AAV-9 viral vectors that express Htt-Dendra2 under the control of the neuronal promoter synapsin-1 (syn-Htt) or the glial promoter GFAP (GFAP-Htt) (Fig. 2.7*A*). Stereotaxic injection of these viral vectors allows for the selective expression of Htt in neurons or astrocytes. We therefore injected syn-wt-Htt or syn-mHtt into the striatum of 2-month-old wild-type mice (Fig. 2.7*B*). Fluorescence imaging demonstrated restricted expression of the injected AAV viruses in the mouse striatum (Fig. 2.7*B*).

Double immunofluorescent staining showed that syn-mHtt is distributed in NeuN-positive cells, but not GFAP-positive glial cells (Fig. 2.7*C*). Also, syn-mHtt is present in the neuronal process or accumulates in the nuclei to form aggregates (Fig. 2.7*D*).

We next sectioned brain slices from the injected mouse striatum and used fluorescence microcopy to examine the degradation of syn-Htt. Compared to normal Htt (syn-wt-Htt), syn-mHtt in the brain slices showed faster degradation in the neuronal cell body and slower degradation in neuronal processes (Fig. 2.8*A-C,* $*P < 0.05$, $**P < 0.01$, $***P < 0.001$). In the cell body of astrocytes in the brain slices, GFAP-mHtt is also degraded faster than GFAP-wt-Htt (Fig. 2.8*D,E,* $**P < 0.01$, $***P < 0.001$). These findings are consistent with what we have observed in cultured cells and demonstrate that mHtt is indeed differentially degraded in the cell body and processes of neurons. Furthermore, we saw faster degradation of mHtt in astrocytes than neurons in the striatum of brain slices (Fig. 2.8*A,D*), suggesting that the ability of cell body and processes to clear polyQ proteins may depend on cell types, in which the UPS and autophagy as well as proteases could function differentially in different types of cells. It is well established that striatal projection neurons are most affected by HD. To compare the degradation rates of mHtt between cortical and striatal neurons, we injected AAV-mHtt-dendra2 into the striatum and motor cortex and found that cortical neurons were able to clear mHtt faster than striatal neurons (Fig. 2.8*F,G,* $*P < 0.05$). This finding suggests that cell-autonomous mechanisms contribute, at least in part, to the vulnerability of striatal neurons in HD. Taken together, our results from brain slices not only support compartment-dependent degradation of mHtt in neurons, but also show distinct capacity of clearing mHtt in different types of brain cells.

Discussion

In this study, we used an "optical pulse-chase" assay with Dendra2 to show for the first time that mHtt is differentially cleared from the somata and processes of neuronal cells. Many previous studies have used GFP-conjugated mHtt to investigate the distribution and toxicity of expanded polyQ proteins. Our results demonstrated that Dendra2, a GFP derivative, did not change the pattern of formation of mHtt aggregates in neurites and did not cause obvious morphological alterations in transfected neurons. Although it requires further studies to determine whether the conjugation of GFP or dendra2 can modify mHtt function or toxicity, dendra2 conjugation allowed us to investigate the turn-over of Htt in live cells. Using dendra2-Htt, we also showed that mHtt is degraded faster in astrocytes than in neuronal cells. These findings explain why mHtt accumulates preferentially in neuronal processes, a subcellular site whose function is important for neuronal interaction and is vulnerable in many neurodegenerative diseases at the early stages (Li et al., 2001; Volpicelli-Daley et al., 2014; Fischer and Glass, 2007).

The accumulation of misfolded proteins in neuronal cells is a prerequisite for their toxicity (Goldberg, 2003; Sherman and Goldberg, 2001). Thus, the clearance of misfolded proteins is key to preventing their neurotoxicity. Although mHtt is ubiquitously expressed in all types of cells and is distributed widely in different subcellular regions, why this disease protein can preferentially accumulate in the neuronal process and form neuropil aggregates, which appear more abundant than nuclear Htt aggregates in HD patient brains at early disease stages, remains unclear (DiFiglia et al., 1997; Gutekunst et al., 1999). We already know that Htt plays roles in a broad range of cellular functions (Zuccato, et al. 2010). One of its important functions is to regulate

intracellular trafficking (Gunawardena et al., 2003; Gauthier et al., 2004; Trushina, 2004; Wong and Holzbaur 2014). Consistent with this function, mHtt can associate with microtubules and affect microtubule-dependent transport (Trushina et al., 2004; Klein et al., 2009; Reddy and Shirendeb 2012;). Because microtubule-dependent transport is essential for maintaining the function and integrity of long neuronal processes, it is possible that mHtt may affect its transport along the processes, leading to its accumulation and aggregation in the neuropil. We also know that mHtt can be cleared by the UPS and autophagy (Li et al., 2010; Sarkar and Rubinsztein et al., 2008). However, sorting out the mechanism for the accumulation of mHtt in neuronal processes is a challenge, as conventional biochemical assays and microcopy cannot distinguish the causes for the accumulation of mHtt in neuronal processes.

Our studies provide evidence for the slow degradation of mHtt in neuronal processes. First, the property of photoconversion of green Dendra2 to red fluorescence allowed us to examine the half-life of mHtt located in a defined region in neuronal processes. By examining this half-life and comparing normal and mutant Htt, we found that the decline in mHtt or its degradation is slower in the neuronal process than in the cell body. Second, we also performed pharmacological experiments to block the function of the UPS and autophagy and found that the UPS plays a more important role in clearing soluble mHtt. Third, we examined the decline of mHtt in the mouse brain by expressing viral Htt-Dendra2. This study also verified that mHtt is cleared slowly in neuronal processes in the context of neuron-glia interactions.

Using “optical pulse-chase,” Tsvetkov and colleagues observed a faster degradation of exon1 mHtt (1-67 amino acids) than its wild-type form in the soma of cultured striatal

and cortical neurons (Tsvetkov et al., 2013). In our study, we examined the degradation of a larger N-terminal Htt fragment (1-230 amino acids), whose toxicity has been confirmed in transgenic HD mice (Bradford et al., 2009; Huang et al., 2015), in the soma and processes of hippocampal neurons and astrocytes. In Tsvetkov's findings, exon1 mHtt is cleared mainly by autophagy (Tsvetkov et al., 2013) whereas our finding show that the larger N-terminal mHtt fragment (1-230 amino acids) is more efficiently degraded by the UPS. These differences suggest that the length of N-terminal htt and protein context can influence the degradation of Htt in cells by different proteolytic machineries. Also, different methodologies, such as differences in types of cultured neurons examined, culturing conditions, and drug treatments used, may lead to different results. For example, we examined healthy cells in culture in which the UPS may play a more important role in removing Htt than autophagy. By comparing the UPS versus autophagy in removing mHtt in neuronal processes under the same experimental conditions, we found that the UPS plays a more important role in removing mHtt in neuronal processes. This finding is consistent with the age-dependent decline in the UPS in the brain (Chondrogianni et al., 2015) and explains why, in the aged HD brain, reduced UPS activity promotes the accumulation of mHtt in neuronal processes or neuropil. In support of this idea, astrocytes, which can clear mHtt more efficiently than neurons, are found to have higher UPS activities than neurons (Tydlacka et al., 2008).

Understanding how mHtt preferentially accumulates in neuronal processes will help us to find effective strategies to treat HD. This is because in many neurodegenerative diseases, including Alzheimer's, Parkinson's and ALS, neuronal process degeneration and dysfunction are the early pathological events (Li et al., 2001; Volpicelli-Daley et al.,

2014; Fischer and Glass, 2007). In HD knock-in mice that express full-length mHtt, neuropil aggregates appear to occur at the earlier HD stage (Li et al., 2001), further underscoring the important role of neuropil mHtt in HD pathology (DiFgila et al., 1997; Gutekunst et al., 1999). The accumulated mHtt in neuronal processes can affect intracellular transport and synaptic function (Xu et al., 2013; Trushina, 2004). Although mHtt does not impair the overall proteasomal function in brain homogenates (Bett et al., 2009), it can locally affect the proteasomal activity in axonal terminals (Wang et al., 2008b). Our findings suggest that improving proteasomal function would be an effective way to alleviate the neuropathology caused by neuropil mHtt. Moreover, we show the feasibility of using "optical pulse-chase" to study protein turnover at subcellular levels, which could be expanded to other neurodegenerative disease proteins, providing new insights into their pathogenesis and neuropathology at subcellular levels.

Materials and Methods

Wild-type mice were maintained at the Emory University Animal facility. Both male and female pups from these mice were used for primary cultures, and both male and female adult mice at the age of 2 months were used for viral injection and brain slice preparation. This study was carried out in strict accordance with the recommendations in the Guidelines for the Care and Use of Laboratory Animals of the National Institutes of Health. The protocol was approved by the Institutional Animal Care and Use Committee of Emory University (Permit Number: 2002557).

Plasmids, antibodies, and reagents. Htt-23Q and -130Q were generated by subcloning N-

terminal fragments of huntingtin (1-230 amino acids) containing 23Q or 130Q into pDendra2-N (Clontech) using SalI and ApaI cloning sites with a CMV promoter. For *in vivo* expression, Htt-Dendra2 fusion genes were subcloned into a pAAV-MCS vector (Cell Biolabs) with a synapsin-1 or GFAP promoter to generate adeno-associated virus (AAV-9). AAV-9 virus was generated by the Emory Viral Vector Core. Antibodies used were anti-huntingtin (rabbit or mouse EM48), anti-NeuN (ABN78, Millipore), anti-GFAP (Millipore, MAB360), anti-Dendra2 (Origene, TA180094), anti-LC3 (Novus, NB100-2220), anti-ubiquitin, K48-specific (Millipore, 05-1307), and anti-β-actin (Sigma, A5060). Secondary antibodies were HRP-labeled donkey anti-mouse, donkey anti-rabbit, donkey anti-mouse Alexa Fluor 488 or 594, and donkey anti-rabbit Alexa Fluor 488 or 594 from Jackson ImmunoResearch. MG132, epoxomicin, and bafilomycin A were purchased from Sigma, as were proteinase inhibitor cocktails.

Primary cell cultures. Brains of postnatal (day 1-3) murine pups were used for culturing cortical astrocytes. Following dissection, the cortex was subjected to 0.3 mg/ml papain digestion. The cell suspension flew through 70-μm nylon cell strainers (Fisher). Cells were plated onto petri dishes; culture medium was replaced 24 h later, and then once every 3 days thereafter. Microglia and oligodendrocytes were removed from cultures by shaking at DIV14. The remaining cells were detached with 0.25% trypsin and plated for the following experiments. For neuronal cultures, neurons were prepared from postnatal day 0 murine pups. Cortex or hippocampus was digested with 0.3 mg/ml papain. Cell suspension was filtered through 40-μm nylon cell strainers (Fisher) to remove debris. Neurons were cultured in Neurobasal-A medium supplemented with B27 and glutamine

(Invitrogen). Half the culture medium was changed with fresh medium every 3 days. To reduce glial proliferation, cytosine was added to the cultures 3 days after plating. Cultured neurons at DIV3 and astrocytes at DIV 21-28 were used for the transfection of Htt-dendra2 and were subjected to live imaging 24 h later or to western blotting 40 h later.

Stereotaxic injection of viral vectors. Two-month-old mice were anesthetized with an i.p. injection of Avertin (0.5 mg/g). Their heads were placed and fixed in a Kopf stereotaxic frame (Model 1900) equipped with a digital manipulator, and a UMP3-1 Ultra pump. Mice were kept deeply anesthetized as assessed by monitoring pinch withdrawal and respiration rate. Viral vector injections were given in the striatum (0.6 mm anterior to bregma, 2.0 mm lateral to the midline, and 3.5 mm ventral to dura), and motor cortex (1.0 mm anterior to bregma, 1.25 mm lateral to the midline, 0.8-1.0 mm ventral to dura). The injections were performed at a rate of 0.2 μl/min. The needle was left in place for 10 min after each injection to minimize upward flow of viral solution after raising the needle.

Photoconversion, imaging system, and data analysis. Photoconversion of Dendra2 was performed with a Nikon A1R confocal live imaging system with a 60X objective lens. Transfected primary neurons and astrocytes, as well as acute brain slices, were placed in a chamber at 37^{o}C, 5% CO_2 during the imaging session. After transfection for 24 h, cultured hippocampal neurons or cortical astrocytes were subjected to live imaging. About 2 weeks after viral injection, the brains were sliced with a vibratome (Leica) in cold artificial cerebral spinal fluid (ACSF). Subsequently, acute brain slices were allowed

to recover for 30 min-1 h in a 37°C and 5% CO_2 incubator, and then subjected to live imaging. During imaging sessions, brain slices were maintained in brain slice culture medium containing 50% MEM/HEPES (Gibco), 25% heat-inactivated horse serum (Gibco), 25% Hank's solution (Gibco), and 6.5 mg/ml glucose (Sigma), pH 7.2. 405-nm UV light was used to activate Dendra2. To avoid UV damage to cells, the power and duration of UV irradiation was optimized. The photoconversion of Dendra2-Htt was performed on selected cell bodies and segments of processes in which no mHtt aggregates were visible and green fluorescence of inactive Dendra2 was seen. After photoconversion of green fluorescence to red fluorescence, images were taken at 10-min intervals. Decays of red fluorescence of active Dendra2 in the region of interest were used to measure degradation rates of Htt. Nikon Element software was used to quantify the red fluorescence in the region of interest. The intensity values were background subtracted. To avoid the influence of red fluorescence diffusion on degradation rates, the intensity value was normalized to that at 10 min after photoconversion, except for measuring degradation rates of Htt in cell bodies of cultured astrocytes, in which no diffusion of fluorescence was observed after photoconversion since target astrocytes did not have long processes.

Immunoprecipitation. Primary cultures were harvested and lysed in ice-cold 0.5% Triton X-100/PBS solution with protease inhibitor cocktail and phosphatase inhibitors on ice. The lysates were centrifuged at 16,000g for 30 min. Protein concentrations were measured with BCA assay (Thermo Scientific). Total 300 μg samples were precleared with protein A agarose beads (Sigma), and huntingtin proteins were immunoprecipitated

by anti-Htt (mEM48) at 4°C overnight. Protein A agarose beads were added to capture the immunoprecipitates for 1 h at 4°C. Ice-cold lysis buffer was used to wash beads 3 times. Proteins from the immunoprecipitates and inputs were subjected to Western blotting.

Immunofluorescence staining. Mice were anesthetized, perfused with fresh 4% paraformaldehyde in PBS, and postfixed overnight in the same fixative. Fixed brains were switched to 30% sucrose at 4°C. Mouse brains were sliced at 15-μm thickness with a cryostat at -20°C, and then mounted onto gelatin-coated slides. The brain slices were blocked with 3% bovine serum albumin in PBS supplemented with 0.2% Triton X-100 for 30 min at room temperature. Slices were incubated with primary antibodies at 4°C overnight and washed. Fluor-conjugated secondary antibodies and nuclear dye Hoechst were added to the samples for staining. Images were acquired with an Imager Z1 microscope equipped with a 63X objective lens.

Western blot analysis. Primary cultures were lysed in ice-cold RIPA buffer (50 mM Tris pH 8.0, 150 mM NaCl, 1 mM EDTA pH 8.0, 1 mM EGTA pH 8.0, 0.1% SDS, 0.5% DOC, and 1% Triton X-100) containing protease inhibitor cocktail and phosphatase inhibitors. The lysates were sonicated and subjected to SDS-PAGE. The proteins on the gel were transferred to a nitrocellulose membrane, which was then blocked with 5% milk/TBST for 1 h at room temperature. The blot was incubated with primary antibodies in 5% milk/TBST overnight at 4°C. After 3 washes in TBST, the blot was incubated with HRP-conjugated secondary antibodies in 5% milk/TBST for 1 h at room temperature.

After 3 washes in TBST, ECL Prime (GE Healthcare) was used to detect immunoreactive bands on the blot

Statistical analyses. Unpaired two-tailed Student's *t*-test and repeated measures (RM) two-way ANOVA followed by Bonferroni *post hoc* test were performed with GraphPad Prism 6. Results are expressed as the means ± SEM. A P-value < 0.05 was considered significant. The statistical significance level was set as follows: * if $P < 0.05$, ** if $P < 0.01$, *** if $P < 0.001$, **** if $P < 0.0001$.

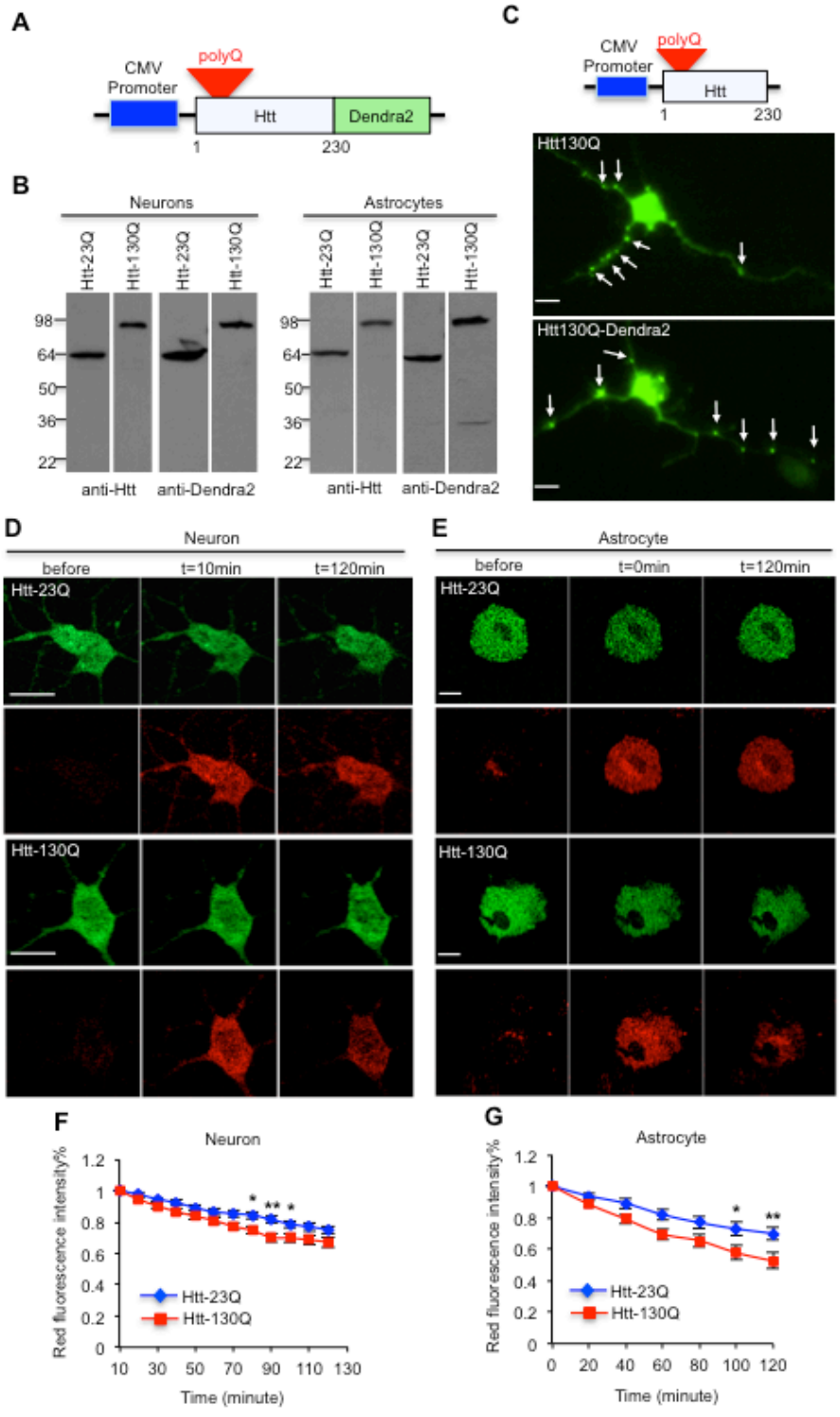
A
CMV Promoter
polyQ
Htt
Dendra2
1
230
B
Neurons
Astrocytes
Htt-23Q
Htt-130Q
98
64
50
36
22
anti-Htt
anti-Dendra2
C
CMV Promoter
polyQ
Htt
1
230
Htt130Q
Htt130Q-Dendra2
D
Neuron
before
t=10min
t=120min
Htt-23Q
Htt-130Q
E
Astrocyte
before
t=0min
t=120min
Htt-23Q
Htt-130Q
F
Neuron
Red fluorescence intensity%
Htt-23Q
Htt-130Q
Time (minute)
G
Astrocyte
Red fluorescence intensity%
Htt-23Q
Htt-130Q
Time (minute)

Figure 2.1. Soluble mHtt is promptly removed from the bodies of both neuronal and astrocytic cells. ***A*****,** Schematic representation of Htt-Dendra2 plasmids. Dendra2 is conjugated to N-terminal (1-230 amino acids) Htt under the control of an exogenous promoter. In this figure, Htt-23Q and Htt-130Q are expressed by the CMV promoter. ***B***, Western blotting analysis of transfected Htt-Dendra2 in cultured primary neurons and astrocytes. Antibodies to Htt (mEM48) and Dendra2 were used. ***C***, Immunostaining with EM48 antibody showed that both mHtt and mHtt-dendra2 fusion protein aggregated in processes of cultured neurons, and neuropil aggregates are indicated by arrow. ***D-E***, mHtt (Htt-130Q) is degraded faster than wild-type Htt (Htt-23Q) in the cytoplasm of neuronal (D) and astrocytic (E) cell bodies (hippocampal neurons in D, and cortical astrocytes in E). ***F-G***, Reduction of red fluorescence intensity in Figure *D-E* is quantified at indicated time points; n = 23 (23Q), 21 (130Q) cells in *F*, n = 10 (23Q), 14 (130Q) cells in *G*. For neurons, the red fluorescence intensity at 10 min was normalized to 1. For astrocytes, the red fluorescence intensity at 0 was normalized to 1. [*$P < 0.05$, **$P < 0.01$, RM two-way ANOVA followed by Bonferroni *post hoc* test (factor 1: time; factor 2:genotype)]. Error bars represent s.e.m. Scale bars = 10 μm.

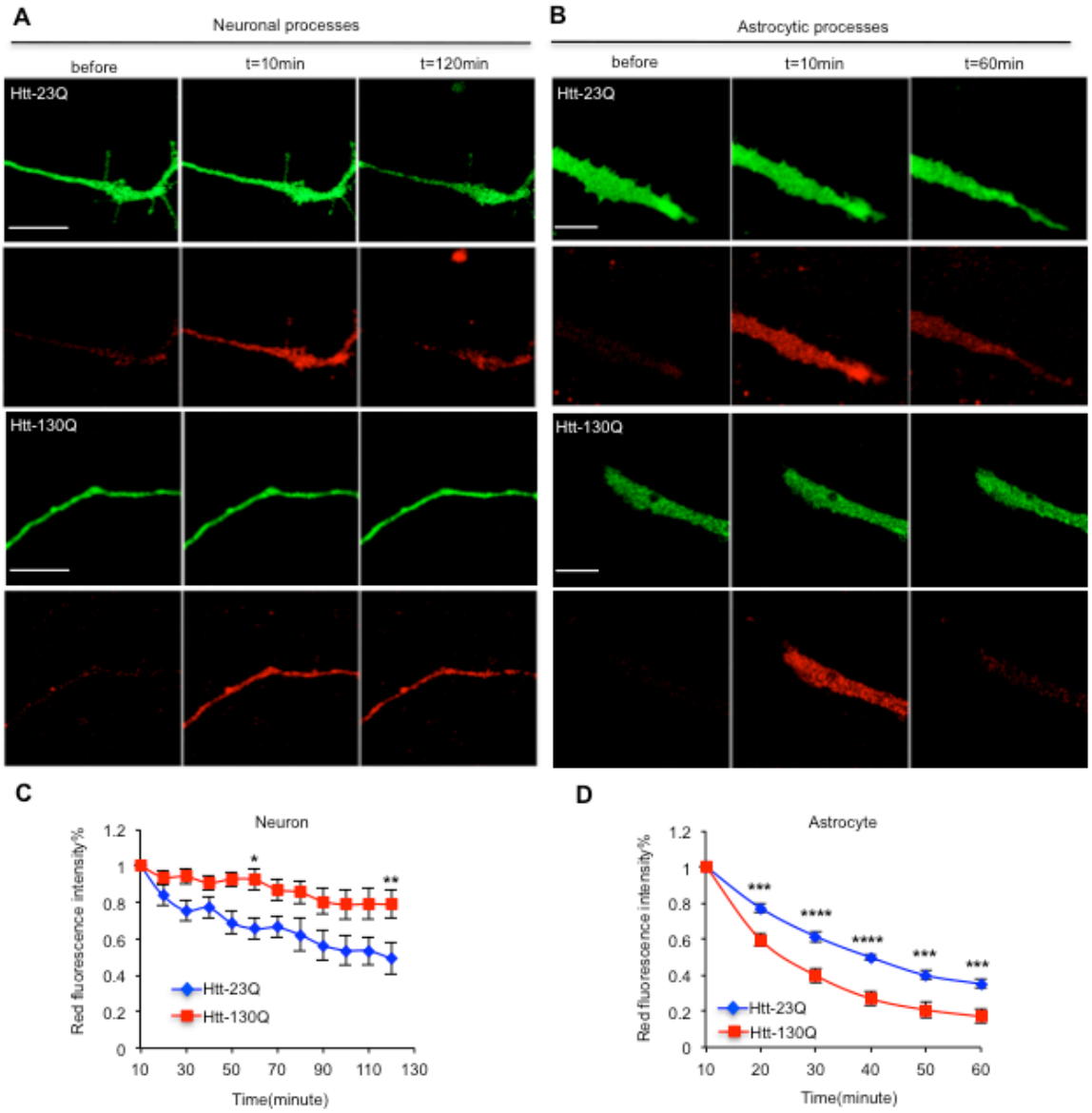
A
Neuronal processes
before
t=10min
t=120min
Htt-23Q
Htt-130Q
B
Astrocytic processes
before
t=10min
t=60min
Htt-23Q
Htt-130Q
C
Neuron
Red fluorescence intensity%
Htt-23Q
Htt-130Q
Time(minute)
D
Astrocyte
Red fluorescence intensity%
Htt-23Q
Htt-130Q
Time(minute)

Figure 2.2. mHtt is slowly cleared from neuronal processes. ***A***, Htt-130Q is degraded slower than Htt-23Q in processes of cultured hippocampal neurons; n = 13 (23Q) and 18 (130Q) cells. ***B***, In the processes of cortical astrocytes, Htt-130Q is cleared more rapidly than Htt-23Q; n = 10 (23Q), 11 (130Q) cells. ***C-D***, Quantitative results for ***A*** and ***B*** showing that the degradation rate of mHtt in neuronal processes is slow. (**P* < 0.05, ***P* < 0.01, ****P* < 0.001, *****P* < 0.0001. RM two-way ANOVA followed by Bonferroni *post hoc* test (factor 1: time; factor 2: genotype)] Error bars represent SEM. Scale bars = 10 μm.

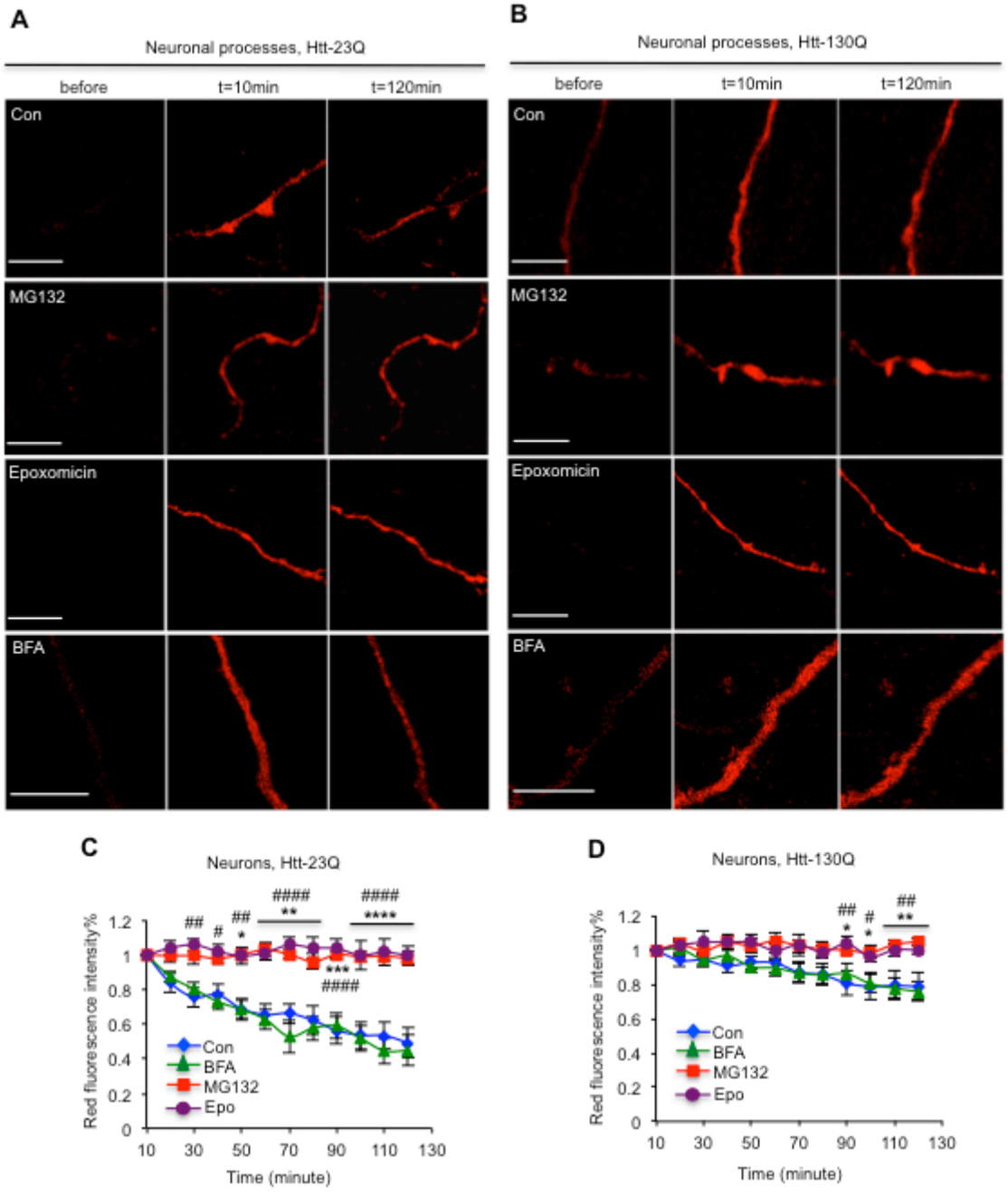
A
Neuronal processes, Htt-23Q
before
t=10min
t=120min
Con
MG132
Epoxomicin
BFA
B
Neuronal processes, Htt-130Q
before
t=10min
t=120min
Con
MG132
Epoxomicin
BFA
C
Neurons, Htt-23Q
Red fluorescence intensity%
Time (minute)
Con
BFA
MG132
Epo
D
Neurons, Htt-130Q
Red fluorescence intensity%
Time (minute)
Con
BFA
MG132
Epo

Figure 2.3. Proteasome plays a major role in clearing Htt from neuronal processes. ***A-B*****,** Fluorescent images show the clearance of Htt-23Q (A) and Htt-130Q (B) in the processes of cultured hippocampal neurons. MG132 or epoxomicin stabilizes the levels of Htt-23Q and Htt-130Q in the neuronal process. n = 13 (Con), 8 (BFA), 5 (MG132), 10 (epoxomicin) cells in *A*; n = 18 (Con), 8 (BFA), 9 (MG132), 12 (epoxomicin) cells in *B*. ***C-D***, Quantitative results of red fluorescent intensity of Htt-Dendra2 at different time points showing that MG132 (5 μM) and epoxomicin (100 nM), but not BFA (100 nM), can stabilize the levels of Htt-23Q and Htt-130Q in the neuronal processes. [**P* < 0.05, ***P* < 0.01, ****P* < 0.001, *****P* < 0.0001, Con vs MG132; #*P* < 0.05, ##*P* < 0.01, ###*P* < 0.001, ####*P* < 0.0001, Con vs epoxomicin, RM two-way ANOVA followed by Bonferroni *post hoc* test (factor 1: time; factor 2: treatment)]. Error bars represent SEM. Scale bars = 10 μm.

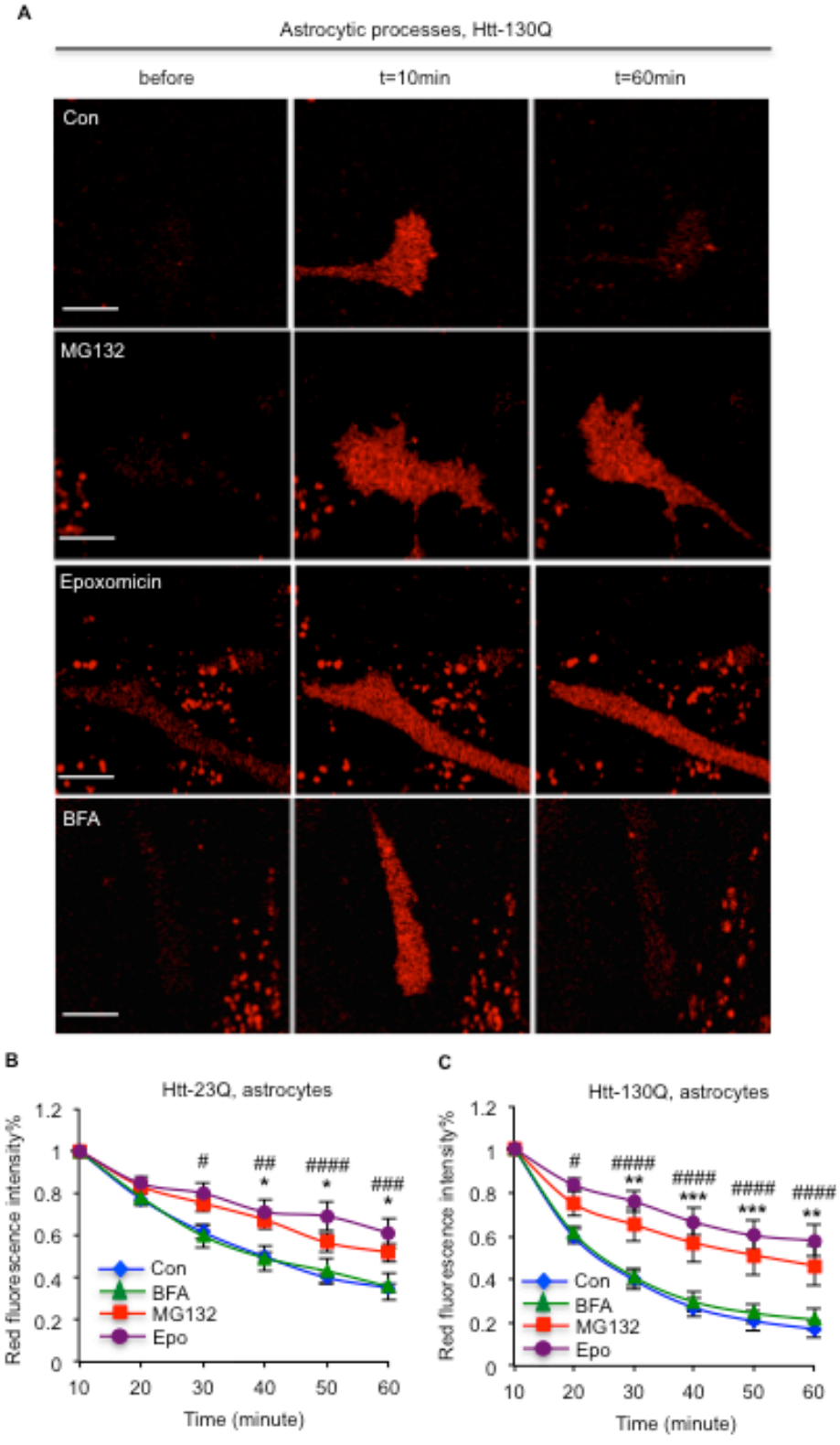
A
Astrocytic processes, Htt-130Q
before
t=10min
t=60min
Con
MG132
Epoxomicin
BFA
B
Htt-23Q, astrocytes
Red fluorescence intensity%
Time (minute)
Con
BFA
MG132
Epo
C
Htt-130Q, astrocytes
Red fluorescence intensity%
Time (minute)
Con
BFA
MG132
Epo

Figure 2.4. Proteasomal inhibitors also stabilize mHtt in the processes of cultured astrocytes. ***A,*** Fluorescent imaging showing that MG132 (5 μM) or epoxomicin (100 nM) treatment blocks the clearance of mHtt in the processes of cultured cortical astrocytes. ***B-C***, Quantitative results of red fluorescence intensity of Htt-Dendra2 at different time points showing that MG132 and epoxomicin, but not BFA (100 nM), can stabilize the levels of Htt-23Q and Htt-130Q in processes of cultured astrocytes. n = 10 (Con), 10 (BFA), 15 (MG132), and 13 (epoxomicin) cells in *B*; n = 11 (Con), 10 (BFA), 12 (MG132), and 11 (epoxomicin) in *C*. [**P* < 0.05, ***P* < 0.01, *** *P* < 0.001, Con vs. MG132; #*P* < 0.05, ##*P* < 0.01, ### *P* < 0.001, #### *P* < 0.0001, Con vs. epoxomicin, RM two-way ANOVA followed by Bonferroni *post hoc* test (factor 1: time; factor 2: treatment)]. Error bars represent SEM. Scale bars = 10 μm.

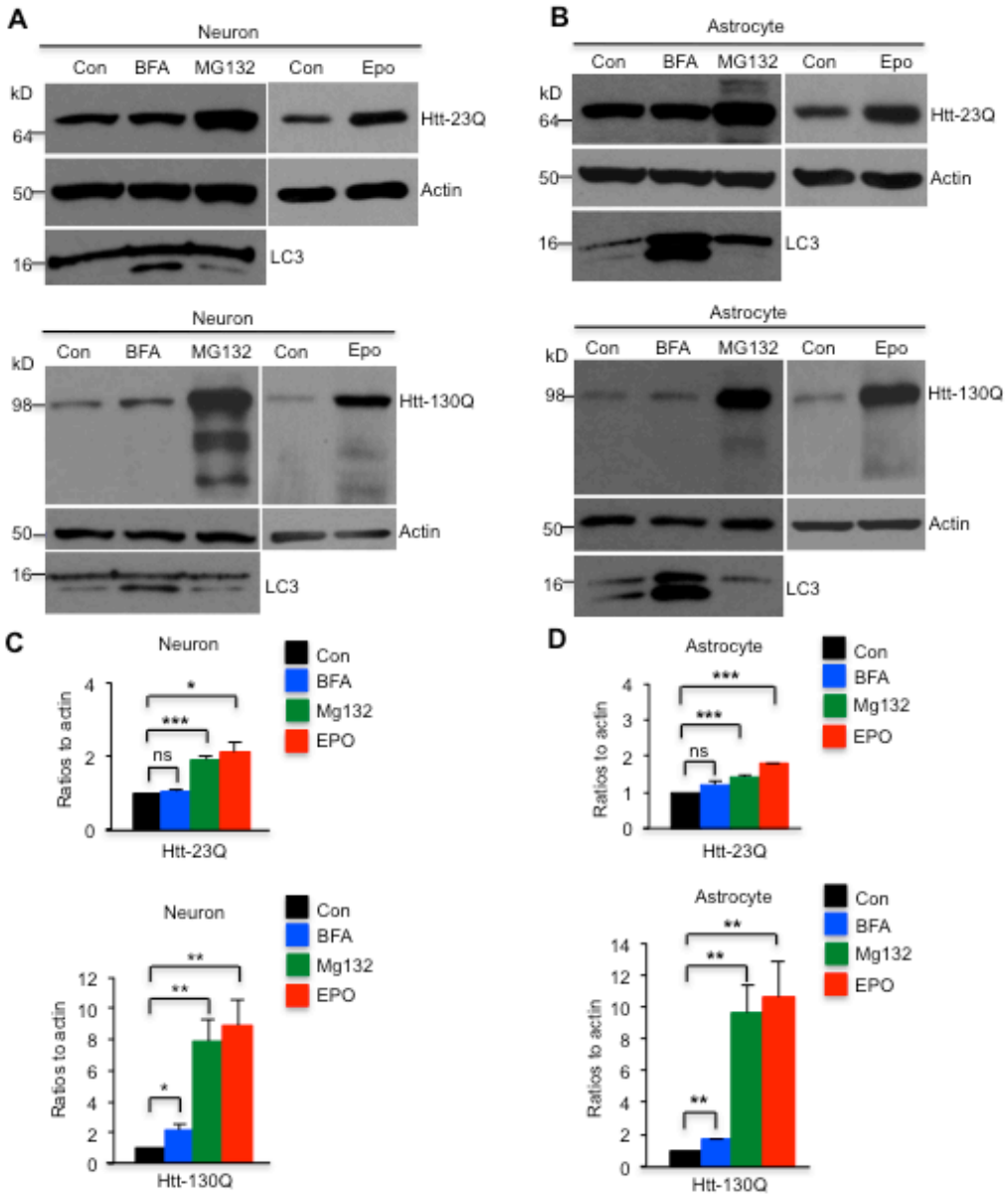
A
Neuron
Con
BFA
MG132
Con
Epo
kD
64
Htt-23Q
50
Actin
16
LC3
Neuron
kD
98
Htt-130Q
50
Actin
16
LC3
B
Astrocyte
Con
BFA
MG132
Con
Epo
kD
64
Htt-23Q
50
Actin
16
LC3
Astrocyte
kD
98
Htt-130Q
50
Actin
16
LC3
C
Neuron
Ratios to actin
Con
BFA
Mg132
EPO
ns
*
***
Htt-23Q
Neuron
**
**
*
Htt-130Q
D
Astrocyte
***
***
ns
Htt-23Q
Astrocyte
**
**
**
Htt-130Q

Figure 2.5. Western blot analysis of Htt-Dendra2 expression. ***A-B,*** Western blot analysis of cultured Htt transfected cortical neurons (A) and astrocytes (B) following treatments with MG132 (5 μM), epoxomicin (100 nM) or BFA (100 nM). MG132 and epoxomicin have stronger effects on inhibiting clearance of Htt-130Q than BFA in neurons and astrocytes. ***C-D***, Ratios of Htt-Dendra2 to actins from three independent experiments are presented. MG132, epoxomicin, or BFA treatment time is 16 h. BFA, bafilomycin A; Epo, epoxomicin. (*$P < 0.05$, **$P < 0.01$, *** $P < 0.001$, unpaired two-tailed Student's *t*-test.) ns, not significant. Error bars represent SEM.

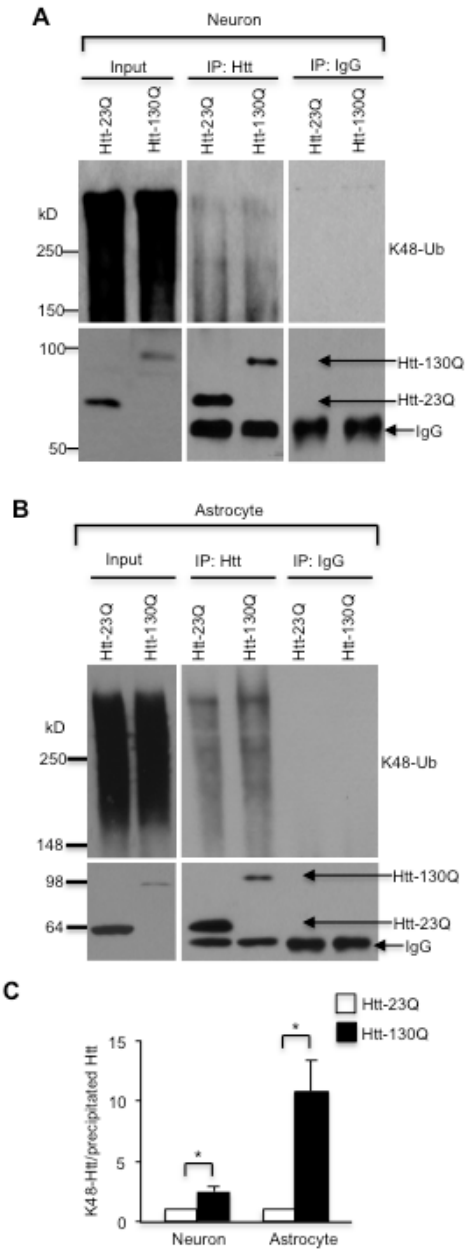
A
Neuron
Input
IP: Htt
IP: IgG
Htt-23Q
Htt-130Q
Htt-23Q
Htt-130Q
Htt-23Q
Htt-130Q
kD
250
150
100
50
K48-Ub
Htt-130Q
Htt-23Q
IgG
B
Astrocyte
Input
IP: Htt
IP: IgG
Htt-23Q
Htt-130Q
Htt-23Q
Htt-130Q
Htt-23Q
Htt-130Q
kD
250
148
98
64
K48-Ub
Htt-130Q
Htt-23Q
IgG
C
Htt-23Q
Htt-130Q
K48-Htt/precipitated Htt
15
10
5
0
*
*
Neuron
Astrocyte

Figure 2.6. Western blot analysis of immunoprecipitated Htt. ***A-B,*** Transfected Htt was immunoprecipitated by anti-Htt antibody (EM48) from cultured cortical neurons (A) and astrocytes (B), and IgG was used as a control. The immunoprecipitates were probed with antibodies to Htt (EM48) or K48 ubiquitination. 5 μM MG132 was used to inhibit proteasomal activity. ***C,*** Ratios of K48 ubiquitinated Htt to the immunoprecipitated Htt from three independent experiments are presented beneath the blots. (*$P < 0.05$, unpaired two-tailed Student's *t*-test.) Error bars represent SEM.

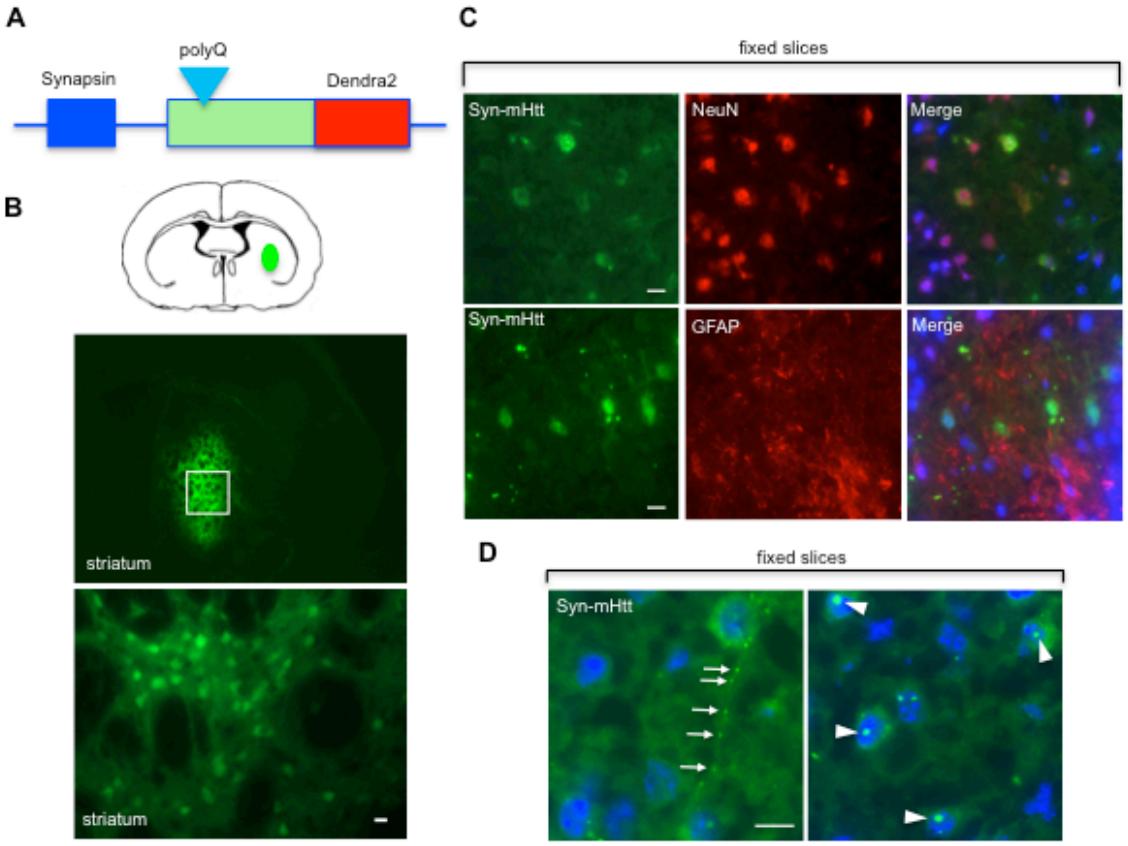
A
polyQ
Synapsin
Dendra2
B
striatum
striatum
C
fixed slices
Syn-mHtt
NeuN
Merge
Syn-mHtt
GFAP
Merge
D
fixed slices
Syn-mHtt

Figure 2.7. Htt-Dendra2 is expressed selectively in neurons and astrocytes in vivo. ***A***, Schematic representation of AAV plasmids. The specific expression of Htt is controlled by the synapsin-1 or GFAP promoter. ***B***, Immunostaining confirms the selective expression of Htt-Dendra2 in neurons and astrocytes in the mouse brain after stereotaxic injection for 1-2 weeks. ***C***, Immunostaining of fixed brain sections of mice injected with AAV-Htt-Dendra2. Double immunostaining with antibodies to Htt, the neuronal marker protein NeuN, and astrocytic marker protein GFAP. The result shows that synapsin promoter-driven mHtt (syn-mHtt) is selectively distributed in NeuN-positive neuronal cells, and GFAP promoter-driven mHtt (GFAP-mHtt) is specifically expressed in GFAP-positive astrocytes. ***D***, mHtt forms aggregates in the neurites (arrow) and nuclei (arrowhead) of striatal neurons in the mouse brain. Scale bar = 20 μm.

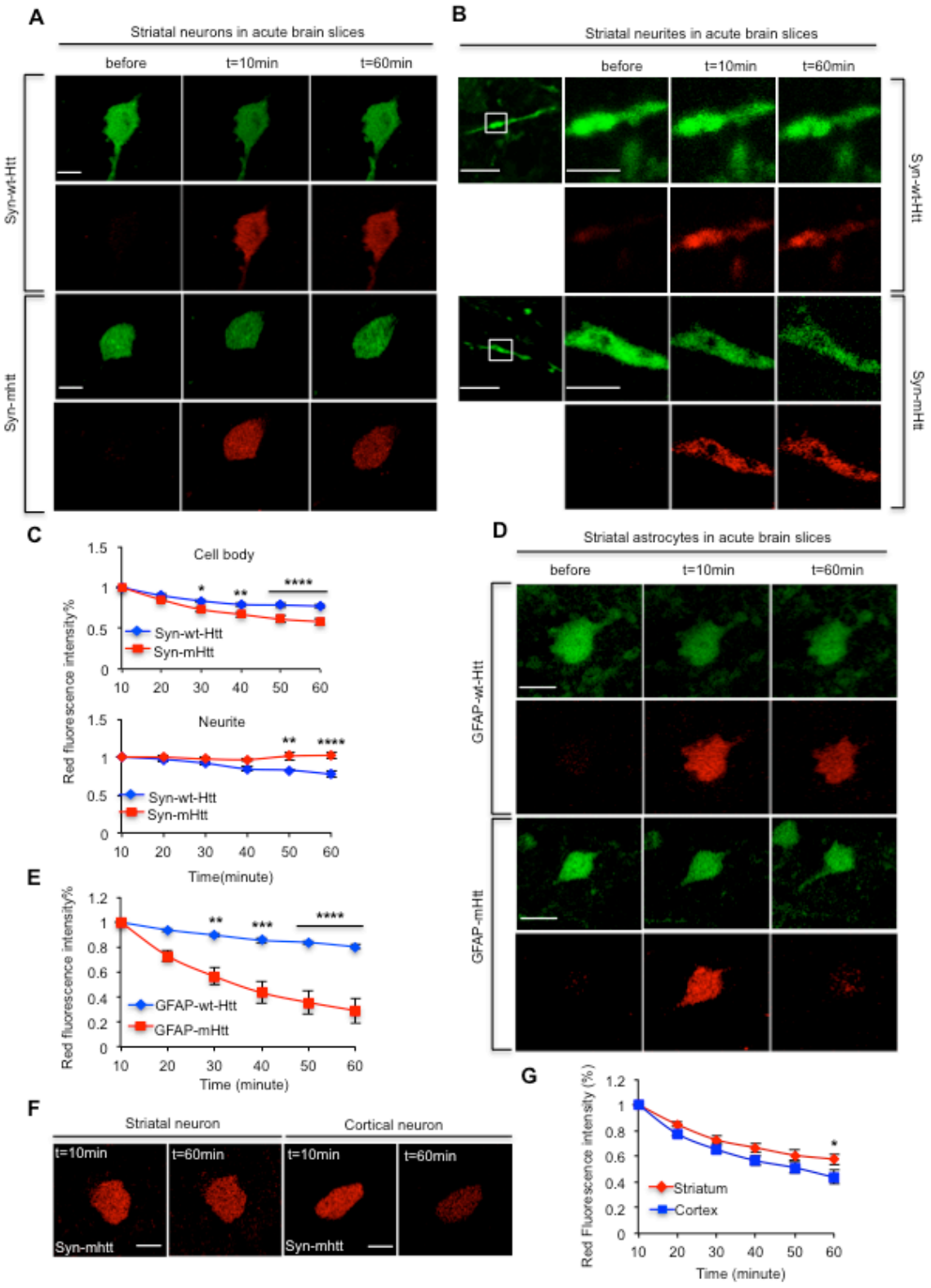
A
Striatal neurons in acute brain slices
before
t=10min
t=60min
Syn-wt-Htt
Syn-mhtt
B
Striatal neurites in acute brain slices
before
t=10min
t=60min
Syn-wt-Htt
Syn-mHtt
C
Cell body
Red fluorescence intensity%
Syn-wt-Htt
Syn-mHtt
Neurite
Time(minute)
D
Striatal astrocytes in acute brain slices
before
t=10min
t=60min
GFAP-wt-Htt
GFAP-mHtt
E
Red fluorescence intensity%
GFAP-wt-Htt
GFAP-mHtt
Time (minute)
F
Striatal neuron
Cortical neuron
t=10min
t=60min
Syn-mhtt
G
Red Fluorescence intensity (%)
Striatum
Cortex
Time (minute)

Figure 2.8. Expanded polyQ promotes the clearance of soluble Htt in the cell bodies, but impairs the clearance of Htt in neurites in the mouse brain. ***A-B***, mHtt expressed under the synapsin promoter is cleared faster than wild-type Htt (wt-Htt) in neuronal cell bodies (A) in brain slices. In B, mHtt is more stable in neuronal process than wt-Htt. ***C,*** Quantitative results of decline in mHtt and wt-Htt. n = 13 (wt-Htt), 15 (mHtt) cells for cell bodies. n = 4 (wt-Htt), 3 (mHtt) cells for neurites. ***D-E***, mHtt is removed more promptly than wt-Htt in astrocytic cells in the mouse brain slices. D shows representative fluorescent images, and E shows quantitative data for the clearance of wt-Htt and mHtt. n = 7 (wt-Htt), 11 (mHtt) cells. ***F-G***, cortical neurons cleared mHtt faster than striatal neurons. F shows representative fluorescent images, and the statistical result is shown in G, n= 15 (striatal neurons), and 13 (cortical motor neurons). [*$P < 0.05$, **$P < 0.01$, ***$P < 0.001$, **** $P < 0.0001$, RM two-way ANOVA followed by Bonferroni *post hoc* test (factor 1: time; factor 2: genotype for C and E; factor 1: time, factor 2: neuronal type for G)]. Error bars represent SEM. Scale bar = 10 μm; scale bar = 3 μm (for amplified figures in B).

Chapter 3

Differential HspBP1 expression accounts for the greater vulnerability of neurons than astrocytes to misfolded proteins

This Chapter represents the unpublished work as: T Zhao, Y Hong, SH Li, XJ Li. Differential CHIP activity mediated by HspBP1 accounts for the greater vulnerability of neurons than astrocytes to misfolded proteins. (submitted)

Abstract

Although mHtt is expressed ubiquitously in the brain, degeneration selectively occurs in neurons. This phenomenon can be explained by our live-cell imaging findings that astrocytes degraded mHtt faster than neurons. To explore the mechanism underlying prompt clearance of mHtt in astrocytes, we compared the expression level of various ubiquitin E3 ligases. We found that neurons and astrocytes show markedly different activities in CHIP, a co-chaperone of Hsp70. CHIP is more actively mono-ubiquitinated and binds to mutant huntingtin (mHtt), the Huntington's disease protein, more avidly in astrocytes than neurons, facilitating its K48-linked polyubiquitination and degradation. Consistently, astrocytes show higher levels and heat-shock induction of Hsp70 and faster CHIP-mediated degradation of various misfolded proteins than do neurons. In astrocytes, the CHIP inhibitory protein (HspBP1) is deficient but its overexpression increases mHtt accumulation. Conversely, silencing HspBP1 expression via CRISPR-Cas9 in neurons ameliorates mHtt aggregation and neuropathology in HD knock-in mouse brains. Our findings indicate a critical role of HspBP1 in differential CHIP/Hsp70 activities in neuronal and glial cells and the greater neuronal vulnerability to misfolded proteins in neurodegenerative diseases.

Introduction

Protein misfolding causes a wide range of neurodegenerative diseases, including Alzheimer's, Parkinson's, and polyglutamine diseases, such as Huntington's disease (HD) (Soto, 2003). Although all of these disease proteins are ubiquitously expressed in different types of cells, they preferentially accumulate in neuronal cells and cause

neurotoxicity (Saxena and Caroni, 2011). In the brain, more than 90% of cells are glial cells, which are affected to a much lesser extent than neurons in neurodegenerative diseases (Maragakis and Rothstein, 2006). A challenging issue in the pathogenesis of neurodegenerative diseases is why misfolded proteins preferentially kill neurons rather than glial cells in the brain. Understanding the mechanism for the selective neurodegeneration is important for developing effective treatments of neurodegenerative diseases.

It is established that the accumulation of misfolded proteins in neuronal cells is a prerequisite for their toxicity (Sherman and Goldberg, 2001; Goldberg, 2003). Preventing the accumulation of misfolded proteins in cells relies highly on molecular chaperones, which refold misfolded proteins, and the ubiquitin-proteasome system (UPS) and autophagy, which degrade misfolded proteins. CHIP, a co-chaperone of Hsp70 with ubiquitin E3 ligase, links chaperones to the UPS and plays a critical role in protein triage decisions. Mice with CHIP deficiency show increased levels of toxic oligomeric proteins and decreased proteasomal activity (Min et al., 2008). CHIP is recruited to chaperone-substrate complexes, and consequently polyubiquitinates the chaperone-bound substrates, which are then degraded by the proteasome (McDonough and Patterson, 2003; McClellan and Frydman, 2001; Scaglione et al., 2011). Hsp70-binding protein 1 (HspBP1), a co-chaperone of Hsp70 that inhibits the activity of Hsp70 ATPase (Raynes and Guerriero, 1998), also associates with CHIP and prevents CHIP-mediated ubiquitination on substrates (Alberti et al., 2004). However, it remains unclear whether CHIP/Hsp70 activities are differentially regulated in neuronal and glial cells and whether differential CHIP/Hsp70 activities account for the preferential neuronal vulnerability to misfolded

proteins in neurodegenerative diseases.

In the current study, we investigated the mechanism underlying the differential vulnerability of neurons and glia to misfolded proteins. We found that the higher CHIP activity in astrocytes than neurons accounts for the higher Hsp70 activity and faster degradation of misfolded proteins in astrocytes. Neurons express much more abundant HspBP1, which inhibits CHIP activity, and knocking down HspBP1 in neurons rescued neuropathology in a HD knock-in mouse model. Our findings provide mechanistic insight into the differential vulnerabilities of neuronal and glial cells to misfolded proteins and also offer a therapeutic target in neurodegenerative diseases.

Results

Increased mono-ubiquitinated CHIP indicates active CHIP in astrocytes

Our recent study showed that astrocytes degraded mutant huntingtin (mHtt), the HD protein, faster than neurons (Zhao et al., 2016). Since CHIP is a co-chaperone of Hsp70 with ubiquitin E3 ligase activity for degradation of misfolded proteins (McDonough and Patterson, 2003; McClellan and Frydman, 2001; Scaglione et al., 2011), we examined its expression in cultured astrocytes and neurons and found more abundant CHIP with a high molecular weight (MW) in astrocytes than neurons (Figure 3.1*A*). This high-MW CHIP is reminiscent of mono-ubiquitinated CHIP (Ub1-CHIP) as reported previously (Scaglione et al., 2011) and consistently, is decreased by CHIP knockdown (Figure 3.1*B*). To provide further evidence for the ubiquitination of the high-MW CHIP, we transfected CHIP-myc in cultured astrocytes and immunoprecipitated CHIP with anti-myc antibody. Immunoblotting with anti-ubiquitin to detect endogenous ubiquitin in

immunoprecipitates clearly showed that the high-MW band represents mono-ubiquitinated CHIP in astrocytes (Figure 3.1*C*).

Because CHIP is mono-ubiquitinated when it polyubiquitinates misfolded proteins (Scaglione et al., 2011), increased Ub1-CHIP suggests that CHIP is more active in astrocytes than neurons tackling misfolded proteins. To test this idea, we transfected N-terminal Htt (1-230 amino acids), which contained normal 23 (Htt-23Q) or expanded 130 (Htt-130Q) glutamine repeats conjugated with the photoswitchable fluorescent protein Dendra2 (Zhao et al., 2016; Tsvetkov et al., 2013), into astrocytes and neurons. Compared with Htt-23Q, Htt-130Q increased the expression of CHIP and Ub1-CHIP in astrocytes but not in neurons (Figures 3.1*D*), suggesting that CHIP plays a specific role in coping with mHtt in astrocytes. Indeed, we found that CHIP co-localizes with transfected Htt-130Q (Figure 3.1*E*), and CHIP knockdown stabilized Htt-130Q in astrocytes (Figure 3.1*F*). Furthermore, we found that in HD 140Q knock-in (KI) mouse model in which full-length mHtt is expressed at endogenous levels, CHIP is co-localized with mHtt aggregates in the corpus callosum where astrocytes are enriched (Figure 3.1*G*). It has been reported that in the brains of HD patients and KI mice, large and round aggregates are localized in neuronal nuclei, and small, bead-like aggregates are localized in neurites (DiFiglia et al., 1997; Li et al., 2001). However, there is absence of CHIP in neuronal aggregates (Figure 3.1*G*), suggesting that CHIP does not associate with mHtt in neurons. By immunoprecipitating endogenous mHtt from cultured neurons and astrocytes of KI mice, we also saw an association of mHtt with both CHIP and Ub1-CHIP in astrocytes, but not in neurons (Figure 3.1*H*). Collectively, these data suggest that CHIP is more active in clearing mHtt in astrocytes.

Active CHIP promotes ubiquitination of mHtt in astrocytes

CHIP has ubiquitin E3 ligase activity and polyubiquitinates substrates for proteasomal degradation (McDonough and Patterson, 2003; McClellan and Frydman, 2001). Indeed, our results indicated that astrocyte-specific association between CHIP and mHtt increased K48-linked polyubiquitinated mHtt in HD KI astrocytes (Figures 3.2*A* and 3.2*B*), which is corroborated by elimination of the enhanced K48-polyubiquitinated mHtt via CHIP knockdown (Figures 3.2*C* and 3.2*D*). Using an *in vitro* proteasome activity assay, we ruled out the possibility that the increased K48-linked polyubiquitination of mHtt in astrocytes is due to mHtt-causing proteasomal dysfunction (Figure 3.2*E*). Given that K48 polyubiquitnation targets substrates for proteasomal degradation, increased K48-linked polyubiquitinated mHtt explains the faster clearance of mHtt in astrocytes (Zhao et al., 2016).

Active CHIP increases Hsp70 and facilitates degradation of various misfolded proteins in astrocytes

Although the binding of CHIP to substrates depends on Hsp70 (Paul et al., 2013; Lee et al., 2013) and CHIP is able to enhance Hsp70 expression in cultured fibroblast cells in response to heat shock (Qian et al., 2006), its relation with Hsp70 in neuronal and glial cells remained elusive. By inducing Hsp70 in HEK293 cells with PU-H71, a compound that up-regulates Hsp70 transcription (Pimienta et al., 2011), we found that increased Hsp70 promoted the association of CHIP with transfected mHtt (Htt-73Q) and that this association was suppressed by Hsp70 knockdown (Figures 3.3*A* and 3.3*B*). Importantly,

we also found that basal Hsp70 was more abundant in cultured astrocytes than neurons (Figure 3.4*A*). To validate this difference in the brain, we isolated the corpus callosum (CC), a brain region enriched in astrocytes, and the cerebral cortex (CTX) with less abundant astrocytes to examine Hsp70 levels. Western blotting also showed a higher level of basal Hsp70 in the astrocyte-enriched corpus callosum (Figure 3.4*B*).

We then compared heat-shock responses in wild-type neurons and astrocytes under hyperthermic conditions and found robustly increased Hsp70 in astrocytes but not in neurons (Figure 3.5*A*). In addition, expression of mHtt did not have an impact on these differential responses (Figures 3.6*A* and 3.6*B*). Strikingly, both CHIP and Ub1-CHIP were increased in wild-type and HD 140Q KI astrocytes, whereas CHIP declined in neurons after heat shock (Figures 3.5*A*, 3.6*A* and 3.6*B*). To verify that the different Hsp70 responses in cultured neurons and astrocytes also occur in brain tissues, we isolated brain slices from wild-type and HD140Q KI mice. The brain slices consisting of the cerebral cortex and corpus callosum were incubated under normal physiological or heat-shock stress conditions. The cortex and corpus callosum were then dissected for western blotting. Consistently, hyperthermia induced Hsp70 in glia-, but not neurons-, enriched regions in both wild-type and HD140Q KI mouse brains (Figure 3.5*B*). The differential heat-shock response found here is consistent with previous findings that heat-shock response is absent in neurons, but robust in astrocytes (Marcuccilli et al., 1996; Batulan et al., 2003; Li et al., 1992).

The exact mechanism underlying distinct heat-shock responses from astrocytes and neurons is unknown. We postulated that differential activities of CHIP in astrocytes and neurons cause different heat-shock responses. Indeed, CHIP knockdown abolished heat-

shock induction of Hsp70 in astrocytes (Figures 3.5*C* and 3.5*E*), confirming that the specific induction of Hsp70 by heat-shock stress in astrocytes is CHIP-mediated. Furthermore, CHIP knockdown also decreases the basal levels of Hsp70/Hsp90 but not Hsc70 in astrocytes (Figures 3.5*D* and 3.5*E*), which is opposite to previous finding that CHIP knockdown enhanced the basal Hsp70 in immortal cell lines (Qian et al., 2006), also suggesting that the CHIP-mediated Hsp70 level is differentially regulated in different cell types. The finding that CHIP is more active in astrocytes also explains why astrocytes have the higher basal levels of Hsp70 than neurons. Together, our results suggest that CHIP-dependent up-regulation of Hsp70 in astrocytes contributes to the preferential and Hsp70-dependent binding of CHIP to mHtt in astrocytes.

To investigate whether CHIP also promotes the clearance of other misfolded proteins in astrocytes, we transfected mutant TDP-43 (M337V), polyQ expanded TATA box binding protein (TBP-105Q), or mutant α-synuclein (A53T), in astrocytes and neurons, as these mutant proteins cause neurodegenerative diseases (Friedman et al., 2007; Jucker and Walker, 2013). The cycloheximide (CHX) half-life assay demonstrated that all of these mutant proteins were removed faster by astrocytes than neurons, which was abolished by CHIP knockdown (Figures 3.8*A*-3.8*C*). These results suggest that astrocytes use CHIP to accelerate the degradation of misfolded proteins, which protects astrocytes from misfolded proteins in neurodegenerative diseases.

We further investigated the role of CHIP in the viability of astrocytes under severe heat-shock stress (45^{o}C for 30 min). Astrocytes were resistant to heat-shock stress, which was indicated by no difference in viability and morphology between untreated and hyperthermia-treated astrocytes (Figures 3.7*A* and 3.7*C*). In contrast, ~86% neurons were

killed by the same hyperthermic condition (Figures 3.7*A* and 3.7*C*). However, the lethality of astrocytes after hyperthermia was increased when CHIP was knocked down (Figures 3.7*B*-3.7*E*), indicating that the high activity of CHIP is involved not only in the prompt clearance of mHtt, but also in protection of cell viability.

Differential HspBP1 expression results in distinct CHIP activity between astrocytes and neurons

Our findings raise a key question of why CHIP is more active in astrocytes than in neurons. Using a RNA-Seq database to compare the profiles of gene expression between neurons and astrocytes (Zhang et al., 2014), we found that HspBP1, a co-chaperone of Hsp70 that inhibits CHIP E3 ligase activity (Alberti et al., 2004), shows approximately a 5-fold increase at the transcriptional level in neurons compared with astrocytes. The different expression level of HspBP1 was first confirmed with western blotting, showing the abundant level of HspBP1 in cultured neurons but the undetectable level in cultured astrocytes (Figure 3.9*A*). In addition, HspBP1 is distributed throughout the neurons, and its cellular localization is well consistent with that of CHIP (Figure 3.9*B*). In contrast, only faint or background staining of HspBP1 was seen in astrocytes (Figure 3.9*B*). Since Bag2 has been reported to be another CHIP inhibitor, we also examined the level of Bag2 and found there was no difference between neurons and astrocytes, suggesting that Bag2 is not the determinant of the high activity of CHIP in astrocytes (data not shown). Furthermore, we performed HspBP1 immunostaining of mouse brains, in which neurons and astrocytes were labeled respectively with antibodies to cell-specific markers, NeuN and GFAP. Indeed, there was more HspBP1 staining in neurons, whereas HspBP1 was

almost undetectable in astrocytes (Figures 3.9*C* and 3.9*E*). Consistently, in the brain section of human basal ganglia, human neurons exhibited a considerable amount of HspBP1, whereas human astrocytes lacked HspBP1 staining (Figures 3.9*D* and 3.9*E*). Together, our results indicate an intrinsic and significant difference of HspBP1 expression in neurons and astrocytes, which may account for differential CHIP activities in astrocytes and neurons.

To investigate whether expression of HspBP1 could inhibit CHIP activation and CHIP-mediated degradation of mHtt in astrocytes, we transfected HspBP1 into cultured astrocytes. Overexpression of HspBP1 reduced Ub1-CHIP and increased the unmodified form of CHIP correspondingly (Figure 3.10*A*). This blockade of conversion of CHIP to Ub1-CHIP suggests an inhibition of CHIP activity by HspBP1 in astrocytes. In addition, increased unmodified CHIP was not caused by alteration in CHIP expression since HspBP1 overexpression did not affect the transcription of CHIP in astrocytes (Figure 3.10*B*). Furthermore, co-transfection of HspBP1 and mHtt (Htt-130Q) into cultured astrocytes stabilized mHtt, suggesting that CHIP-mediated degradation of mHtt was inhibited by HspBP1. In addition, HspBP1 suppressed mHtt-induced increases in CHIP and Ub1-CHIP, which is evidenced by decreased Ub1-CHIP and CHIP in co-transfected astrocytes (Figure 3.10*C*). Given that CHIP is required for heat-shock response in astrocytes (Figure 3.5*C*), we also investigated whether expression of HspBP1 could inhibit heat-shock response via suppressing CHIP activity. Indeed, HspBP1 suppressed heat-shock induction of Hsp70, CHIP, and Ub1-CHIP in astrocytes (Figure 3.10*D*). Moreover, HspBP1 reduced Hsp70, but not Hsc70, under physiological conditions (Figure 3.10*E*). Taken together, the inhibitory effect of HspBP1 on CHIP-mediated

protective cellular processes in astrocytes supports our conclusion that lack of HspBP1 accounts for the high activity of CHIP in astrocytes.

Silencing HspBP1 expression activates CHIP in neurons and ameliorated neuropathology

If the expression of HspBP1 in neuronal cells is responsible for the increased accumulation of misfolded proteins, knocking down HspBP1 in neurons should alleviate misfolded proteins-causing neuropathology. Thus, we used CRISPR/Cas9 to target the HspBP1 gene (Figure 3.11*A*) and silence the expression of HspBP1 in the striatum of HD 140Q knock-in (KI) mice via stereotaxic injection of AAV viruses expressing Cas9 and HspBP1 sgRNA. T7E1 assay and western blotting validated the genome editing of HspBP1 sgRNA/Cas9 and efficient reduction of HspBP1 at the protein level in N2a cells, respectively (Figures 3.11*B* and 3.11*C*). The targeted HspBP1 DNA was also subcloned for sequencing, which verified Cas9/gRNA-mediated mutations in the HspBP1 gene (Figure 3.11*D*). Furthermore, HspBP1 knockdown (KD) induced the expression of Ub1-CHIP in cultured neurons, suggesting increased activity of CHIP (Figure 3.12*A*). In addition, Hsp70/Hsp90 were induced by heat shock in HspBP1-knockdown neurons (Figure 3.12*B*). To knock down HspBP1 in the HD KI mouse brain, both HspBP1 sgRNA and Cas9 were transduced into the mouse brain striatal region via stereotaxic injection (Figure 3.12*C*). Four to six weeks after injection of AAV-HspBP1 sgRNA and AAV-Cas9, HspBP1 was markedly decreased in the striatum of HD KI mice compared with the control injected only with AAV-HspBP1 sgRNA (Figure 3.12*D*). Consequently, Cas9-mediated HspBP1 knockdown markedly reduced mHtt aggregates (Figures 3.12*E*

and 3.12*F*). Astrogliosis is characterized by increased glial fibrillary acidic protein (GFAP) staining and is an early neuropathological event caused by neuronal injury in HD KI mouse brains (Yu et al., 2003). Reducing mHtt accumulation in neuronal cells via knocking down HspBP1 attenuated the extent of reactive astrocytes (Figures 3.12*G* and 3.12*H*). Synaptophysin is a presynaptic marker protein whose loss is also found in HD KI mice (Valencia et al., 2013). HspBP1 knockdown restored the intensity of immunostaining of synaptophysin in the striatum of HD KI mice (Figures 3.12*I* and 3.12*J*). All of these results suggest that knocking down HspBP1 in neuronal cells could increase CHIP activity, enhance the clearance of mHtt, and subsequently reduce mHtt-mediated neuropathology. Based on our findings, we propose that the high level expression of HspBP1 in neurons accounts for the preferential accumulation of misfolded proteins in neurons and their greater vulnerability than astrocytes to misfolded proteins (Figure 3.13).

Discussion

Although misfolded proteins are ubiquitously expressed in neuronal and glial cells in the brain, they are more prone to accumulation in neurons and kill neuronal cells (Saxena and Caroni, 2011). This differential vulnerability to misfolded proteins is likely due to distinct capacities of maintaining protein homeostasis between neuronal and glial cells. However, whether and how neuronal and glial cells have differential capacities to maintain protein folding and to prevent protein misfolding have not been rigorously investigated. Our findings demonstrate for the first time that the higher activity of CHIP in astrocytes than neurons is related to monoubiquitinated CHIP. An additional new

finding is that the differential HspBP1 expression accounts for different CHIP/Hsp70 activities in neurons and astrocytes.

Our results also revealed two major functional consequences of increased CHIP activity in astrocytes, both of which account for their faster degradation of misfolded proteins. First, CHIP associates with mHtt specifically in astrocytes, resulting in polyubiquitination and subsequent proteasomal degradation of mHtt. The increased mHtt ubiquitination in astrocytes explains why astrocytes clear mHtt more efficiently than do neurons (Zhao et al., 2016). In support of this idea, clearance of several other neurodegeneration-related misfolded proteins is also CHIP-dependent in astrocytes. Second, active CHIP enhances both basal and inducible levels of Hsp70 in astrocytes, and increased Hsp70 prevents aggregation of misfolded proteins and facilitates the binding of CHIP to misfolded proteins.

The heat-shock response plays a vital role in maintaining cellular homeostasis. The chaperone network is extremely sophisticated and well-coordinated. For example, CHIP activates HSF1 (Dai et al., 2003) but is inhibited by HspBP1 (Alberti et al., 2004). Our findings provide compelling evidence that HspBP1 is differentially expressed in neurons and astrocytes, which accounts for the cell-type dependent regulation of CHIP and Hsp70 activities. Consistent with this idea, expression of HspBP1 attenuates CHIP-dependent protective effects in astrocytes. Conversely, silencing HspBP1 expression with CRISPR/Cas9 in neurons activated CHIP and alleviated neuropathology in the HD knock-in mouse model.

Our findings offer a mechanistic insight into the phenomenon that astrocytes, the largest cell population in the brains, are able to clear misfolded protein more efficiently

so that they are affected to a much lesser extent than neurons in a variety of neurodegenerative diseases (Maragakis and Rothstein, 2006). Since CHIP is an ubiquitin E3 ligase that bridges the chaperone system and the UPS (McDonough and Patterson, 2003; McClellan and Frydman, 2001), the increased CHIP activity may also contribute to the higher proteasomal activity in astrocytes than neurons (Tydlacka et al., 2008). The finding that inhibition of HspBP1 in HD140Q KI mouse brain can diminish mHtt aggregation and neuropathology also suggests the therapeutic benefits by removing endogenous inhibition of CHIP activity in neuronal cells, which can be an alternative approach to treat a wide range of neurodegenerative diseases that are caused by the accumulation of misfolded proteins in neuronal cells.

Materials and Methods

Animals. Full-length mHtt CAG140Q (HD KI) mice were kindly provided by Dr. Michael Levine of UCLA (Hickey et al., 2008) and were maintained at the Emory University Animal facility. This study was carried out in strict accordance with the recommendations in the Guidelines for the Care and Use of Laboratory Animals of the National Institutes of Health. The protocol was approved by the Institutional Animal Care and Use Committee of Emory University (Permit Number: 2003631).

Plasmids, antibodies and reagents. Htt-23Q, -73Q, and-130Q were generated by subcloning N-terminal fragments of huntingtin (1-230 amino acids) containing 23Q, 73Q or 130Q into pDendra2-N (Clontech) using SalI and ApaI cloning sites. Murine HspBP1 was cloned into a pRK5 vector using BamH1 and EcoR1 cloning sites. sgRNA backbone

vector and Cas9 plasmids were purchased from Addgene. Synthetic HspBP1 target site sequence (20bp) was cloned into the sgRNA backbone vector using Sap1 sites to generate HspBP1 sgRNA plasmid. TDP-43 (M334V), TBP-105Q, and α-synuclein (A53T)-CFP plasmids were generated in our previous studies (Friedman et al., 2007; Yan et al., 2014). Mouse CHIP-myc vector was obtained from Origene (MR204258). Antibodies used were anti-CHIP (Thermo, PA5-32046), anti-expanded polyQ (1C2) (Millipore, MAB1574), anti-ubiquitin (abcam, 7780; Dako, z0458), anti-ubiquitin, K48-specific (Millipore, 05-1307), anti-huntingtin (mEM48), anti-Hsp70 (Cell Signaling, 4872S), anti-Hsc70 (Santa Cruz, sc-7298), anti-Hsp90 (Cell Signaling, 4874S), anti-TDP-43 (Abnova, H00023435-M01), anti-TBP (QED Bioscience, 70102), anti-CFP (Clontech, 632381), anti-HspBP1 (Santa Cruz, sc-390467), anti-Cas9 (Millipore, MAC133), anti-GFAP (Thermo, RB-087-A1), anti-NeuN (ABN78, Millipore), anti-synaptophysin (Sigma, SVP38), anti-MBP (AB980, Millipore), anti-Bag2 (29-709, ProSci), anti-NeuN (ABN78, Millipore), anti-Beta III tubulin (AB9354, Millipore), anti-GAPDH (Thermo, MA1-10036), anti-Myc (Cell Signaling, 2276S, 2272S), and anti-β-actin (Sigma, A5060). Secondary antibodies were HRP-labeled donkey anti-mouse, donkey anti-rabbit, donkey anti-mouse Alexa Fluor 488 or 594, and donkey anti-rabbit Alexa Fluor 488 or 594 from Jackson ImmunoResearch. Lactacystin, PU-H71, PYR-41 and cycloheximide (CHX) were purchased from Sigma. Proteinase inhibitor cocktails were purchased from *Sigma.*

Knockdown assay. The Hsp70 siRNA duplexes and negative control siRNA were purchased from Origene (SR418598). The following combination of oligonucleotides

was used to target the Hsp70 gene: rGrUrCrUrUrArArArCrArArArCrGrUrCrUrUrGrGrCrArCT G, rGrGrCrArCrCrGrArUrUrArCrUrGrUrCrArArGrGrUrUrATT, andrUrGrGrGrAr ArGrArCrArUrArUrArGrUrCrUrArGrCrUrGCC. The shRNA of CHIP and negative control shRNA were products of Origene (TL503190). The combination of plasmids carrying the following oligonucleotides were transfected into cells: GCCTGCTACGGCCGCGCCATCACTCGGAA, GCTAAGAAGAAGCGCTGGA ACAGTATCGA, ATCCACCAGGAGAGTGAGCTGCATTCATA, and CATTGA CGCTTTCATCTCTGAGAACGGCT.

Cell cultures. Brains of postnatal (day 1-3) murine pups were used for culturing cortical astrocytes. Following dissection, cortex was subjected to 0.3 mg/ml papain digestion. Cell suspension flew through 70-μm nylon cell strainers (Fisher). Cells were plated onto petri dishes, and culture medium was replaced 24 h later and once every 3 days thereafter. Microglia and oligodendrocytes were removed from cultures by shaking at DIV14. Remaining cells were detached with 0.25% trypsin and plated for the following experiments. For cortical neuron cultures, cortical neurons were prepared from postnatal day 0 murine pups. Cortex was digested with 0.3 mg/ml papain. The cell suspension was filtered through 40-μm nylon cell strainers (Fisher) to remove debris. Neurons were plated at 1×10^6 on poly-D-lysine-coated 6-well plate, and cultured in Neurobasal-A medium supplemented with B27 and glutamine (Invitrogen). Half of the culture medium was exchanged with fresh medium every 3 days. To reduce glial proliferation, cytosine was added to the cultures 3 days after plating. N2a cells were cultured in Dulbecco's

modified Eagle's medium (DMEM), containing 10% FBS (Invitrogen) and penicillin/streptomycin at 37^{o}C and 5%CO2.

Cycloheximide chase assay. DIV 2-3 cortical neurons and DIV 21-30 cortical astrocytes were transfected with plasmids encoding misfolded proteins. Transfected cells were treated with 100 μM cycloheximide at various time points from 0 to 24 hours. After CHX treatment, cells were harvested and lysed in ice-cold 0.5% Triton-X100 in PBS with protease inhibitor mixture and PMSF on ice. Following this, the lysates were sonicated, and protein concentrations were determined by BCA assay (Thermo Scientific). Samples were loaded into SDS-PAGE gels and subjected to western blotting.

Heat shock. Heat shock was performed on cortical astrocytes and neurons, which were seeded on 6-well plates. To study effects of CHIP knockdown on heat-shock response, CHIP shRNA was transfected into cortical astrocytes. Prior to heat shock, the medium was replaced with fresh medium pre-warmed to 42°C. Primary cultures were incubated at 42°C for 1 h in a water bath. For HD140Q KI neurons that were less tolerable to heat shock, they were treated with heat shock for 30 min. The plates were sealed with parafilm. Control cells were maintained in a 37°C incubator. After heat shock, cells were allowed to recover in the same medium at 37°C for various time periods. For heat shock on brain slices, we cut the brains of 3-month-old mice into 1-mm coronal slices with a vibratome (Leica) in chilled artificial cerebral spinal fluid (ACSF). Prior to heat shock, slices were plated on transwells (Costar), maintained with culture medium containing 50% MEM/HEPES (Gibco), 25% heat-inactivated horse serum (Gibco), 25% Hank’s solution

(Gibco), 6.5 mg/ml glucose (Sigma), pH 7.2, and allowed to recover in a 37°C, 5% CO_2 incubator for 1 h. Heat shock was performed on slices from one hemisphere, and those from the other hemisphere were used as controls. For heat shock, slices on transwells were incubated at 42°C for 1.5 h in the water bath. Following heat shock, slices recovered for 6 h in a 37°C, 5% CO_2 incubator, and then the cortex and corpus callosum were dissected and prepared for western blotting.

Stereotaxic injection of viral vectors. Mice were anesthetized with an i.p. injection of Avertin (0.5 mg/g). Their heads were placed and fixed in a Kopf stereotaxic frame (Model 1900) equipped with a digital manipulator, and a UMP3-1 Ultra pump. Mice were kept deeply anesthetized as assessed by monitoring pinch withdrawal and respiration rate. Viral vector injections were given in the striatum (0.6 mm anterior to bregma, 2.0 mm lateral to the midline, and 3.5 mm ventral to dura). The injections were performed at a rate of 0.2 μl/min. The needle was left in place for 10 min after each injection to minimize upward flow of viral solution after raising the needle

Western blot analysis. Cells or brain tissues were lysed in ice-cold RIPA buffer (50 mM Tris pH 8.0, 150 mM NaCl, 1 mM EDTA pH 8.0, 1 mM EGTA pH 8.0, 0.1% SDS, 0.5% DOC, and 1% Triton X-100) containing protease inhibitor cocktail and phosphatase inhibitors. The lysates were sonicated and subjected to SDS-PAGE. The proteins on the gel were transferred to a nitrocellulose membrane, which was then blocked with 5% milk/TBST for 1 h at room temperature. The blot was incubated with primary antibodies in 5% milk/TBST overnight at 4°C. After 3 washes in TBST, the blot was incubated with

HRP-conjugated secondary antibodies in 5% milk/TBST for 1 h at room temperature. After 3 washes in TBST, ECL Prime (GE Healthcare) was used to detect immunoreactive bands on the blot.

Immunoprecipitation. Cells were harvested and lysed in ice-cold 0.5% Triton X-100/PBS solution with protease inhibitor cocktail and 100 μM PMSF on ice. The lysates were centrifuged at 16,000g for 30 min. Protein concentrations were measured with BCA assay (Thermo Scientific). Total 300 μg samples were precleared with protein A agarose beads (Sigma), and huntingtin proteins were immunoprecipitated by anti-Htt (mEM48) or 1C2 at 4^{o}C overnight. Protein A agarose beads were added to capture the immunoprecipitates for 1 h at 4^{o}C. Ice-cold lysis buffer was used to wash beads 3 times. Proteins from the immunoprecipitates and inputs were subjected to Western blotting. For immunoprecipitation of ubiquitinated CHIP, CHIP-myc was transfected into cultured astrocytes. Anti-myc antibody was used to pull down CHIP-myc, and the immunoprecipitates were probed with anti-ubiquitin antibody to detect the ubiquitinated form of CHIP.

Immunofluorescence staining. Mice were anesthetized, perfused with fresh 4% paraformaldehyde in PBS, and postfixed overnight in the same fixative. Fixed brains were switched to 30% sucrose at 4^{o}C. Mouse brains were sliced at 15 μm thickness with a cryostat at -20^{o}C, and then mounted onto gelatin-coated slides. The brain slices were blocked with 3% bovine serum albumin in PBS supplemented with 0.2% Triton X-100 for 30 min at room temperature. For immunostaining cultured cells, cells were fixed with

4% paraformaldehyde for 8-10 min, followed by blocking with 3% BSA/0.2% Triton X-100 for 30 min at room temperature. Following incubation of fixed cells or brain slices with primary antibodies at 4^{o}C overnight and washes, fluor-conjugated secondary antibodies and nuclear dye Hoechst were added to the samples for staining. Images were taken using a microscope (Axiovert 200 MOT; Carl Zeiss) and a 63X lens (LD-Achroplan 63X/0.75 NA) with a digital camera (ORCA-100; Hamamatsu Photonics). The Openlab software (PerkinElmer) was used for imaging acquisition.

Proteasomal activity assay. For determining proteasome activity, clear whole-cell extracts or cell fractions were adjusted to 0.5 mg/ml total protein by dilution with homogenization buffer. All assays were done in triplicate. Chymotrypsin-like activity of 20S β5 was determined using the substrate Suc-LLVY-aminomethylcoumarin (AMC) (40 μM; Bilmol), trypsin-like activity of 20S β2 was determined using the substrate Boc-LRR-AMC (Bilmol; 100 μM). Equal amounts (10 μg) of the extracts were incubated with corresponding substrates in 100-μl proteasome activity assay buffer (0.05 M Tris-HCl, pH 8.0, 0.5 mM EDTA, 1 mM ATP, and 1 mM DTT) for 30–60 min at 37°C. The reactions were stopped by adding 0.8 ml of cold water and placing the reaction mixtures on ice for at least 10 min. The free AMC fluorescence was quantified by using the CytoFluor multi-well plate reader (FLUOstar; BMG Labtech) with excitation and emission wavelengths at 380 and 460 nm, respectively. All readings were standardized using the fluorescence intensity of an equal volume of free 7-amino-4-methyl-coumarin (AMC) solution (40 mM), normalized by the protein concentrations.

qRT-PCR. Reverse transcription reactions were performed with 1.5 μg of total RNA using the Superscript III First-Strand Synthesis System (Invitrogen). One microliter of cDNA was combined with 10 μl SYBR Select Master Mix (Applied Biosystems) and 1 μl of each primer in a 20 μl reaction. The reaction was performed in a thermal cycler (Eppendorf, RealPlex Mastercycler).

T7 endonuclease 1 assay. N2a cells pre-cultured in a 6-well plate were co-transfected with HspBP1 sgRNA and Cas9 plasmids, or transfected only with HspBP1 sgRNA as control using Lipofectamine 2000 (Invitrogen). 72 h after transfection, the genomic DNA was extracted from transfected N2a cells. The target genomic region was amplified with PCR. The sequences of the PCR primers are as follows: forward, 5' ATAGTCTATCTTTAGGCGTGGTG 3', and reverse, 5' ACCCAACTACGTTGTGTACGAGT 3'. The PCR products were denatured and reannealed, and then incubated with T7 Endonuclease I (New England BioLabs) for 20 min at 37^{o}C. The reaction products were subjected to 2% agarose gel electrophoresis.

Statistical analyses. Unpaired two-tailed Student's t-test was performed with GraphPad Prism 6. Results are expressed as the means ± SEM. A P value < 0.05 was considered significant. Statistical significance level was set as follows: * if $P < 0.05$, ** if $P < 0.01$, *** if $P < 0.001$, **** if $P < 0.0001$.

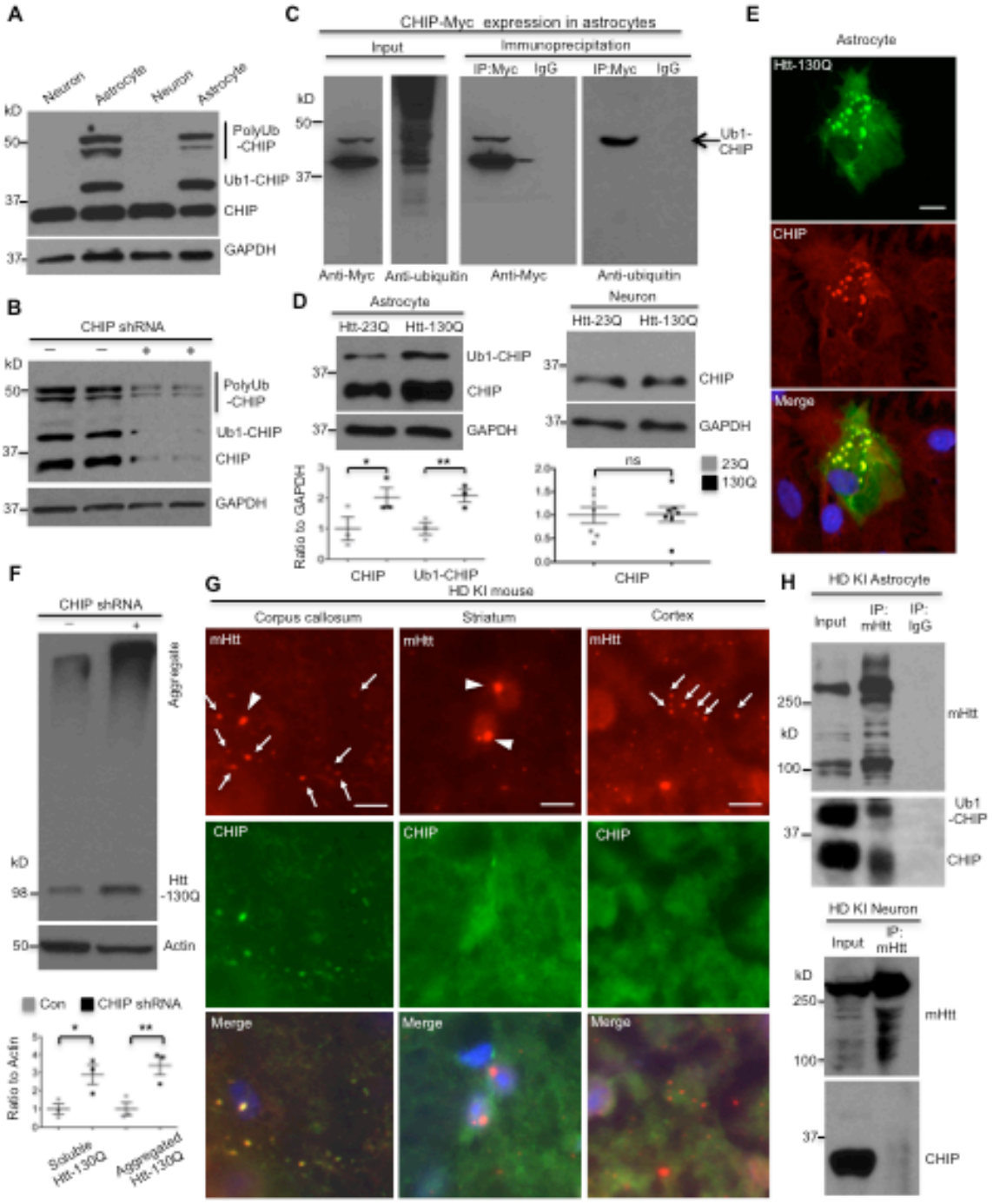
A
Neuron
Astrocyte
Neuron
Astrocyte
kD
50
37
PolyUb -CHIP
Ub1-CHIP
CHIP
GAPDH
37
B
CHIP shRNA
– – + +
kD
50
37
PolyUb -CHIP
Ub1-CHIP
CHIP
GAPDH
37
C
CHIP-Myc expression in astrocytes
Input
Immunoprecipitation
IP:Myc IgG IP:Myc IgG
kD
50
37
Ub1-CHIP
Anti-Myc Anti-ubiquitin Anti-Myc Anti-ubiquitin
D
Astrocyte
Htt-23Q Htt-130Q
Ub1-CHIP
CHIP
GAPDH
37
37
Neuron
Htt-23Q Htt-130Q
CHIP
GAPDH
37
37
Ratio to GAPDH
*
**
CHIP Ub1-CHIP
ns
CHIP
23Q
130Q
E
Astrocyte
Htt-130Q
CHIP
Merge
F
CHIP shRNA
– +
Aggregate
kD
98
Htt -130Q
50
Actin
Con CHIP shRNA
Ratio to Actin
*
**
Soluble Htt-130Q
Aggregated Htt-130Q
G
HD KI mouse
Corpus callosum
Striatum
Cortex
mHtt
mHtt
mHtt
CHIP
CHIP
CHIP
Merge
Merge
Merge
H
HD KI Astrocyte
Input
IP: mHtt
IP: IgG
250
kD
100
mHtt
37
Ub1 -CHIP
CHIP
HD KI Neuron
Input
IP: mHtt
kD
250
100
mHtt
37
CHIP

Figure 3.1 CHIP is more actively involved in mHtt degradation in astrocytes. ***A***, More abundant mono-ubiquitinated CHIP (Ub1-CHIP) is present in cultured astrocytes than in neurons. ***B***, CHIP knockdown decreased Ub1-CHIP in astrocytes (n=3 independent experiments). ***C***, Immunoprecipitation indicated mono-ubiquitination of CHIP-Myc in cultured astrocytes. ***D***, Expression of transfected mHtt (Htt-130Q) selectively increases the levels of CHIP and Ub1-CHIP in astrocytes but not in neurons [n=3 independent experiments (astrocytes), =5 independent experiments (neurons)]. ***E***, Immunofluorescent staining shows the colocalization of transfected mHtt (Htt-130Q) with endogenous CHIP in cultured astrocytes. Scale bar = 5 μm. ***F***, CHIP knockdown increases both soluble and aggregated mHtt (Htt-130Q) in astrocytes (n=3 independent experiments). ***G***, Colocalization of CHIP with mHtt aggregates was detected in glial cells in the corpus callosum, but not in neuronal cells in the striatum and cortex, in HD140Q KI mice at the age of 12 months. Arrowheads indicate nuclear mHtt aggregates; arrows indicate cytoplasmic aggregates in glial cells or neuropil mHtt aggregates in neurons. Scale bar = 15 μm. ***H***, Association of mHtt with CHIP and Ub1-CHIP was detected in HD140Q KI astrocytes but not in KI neurons. Quantitative data beneath the blots are represented as mean ± SEM (Error bar). *, $P < 0.05$, **, $P < 0.01$ (unpaired two-tailed Student's *t*-test); ns, not significant.

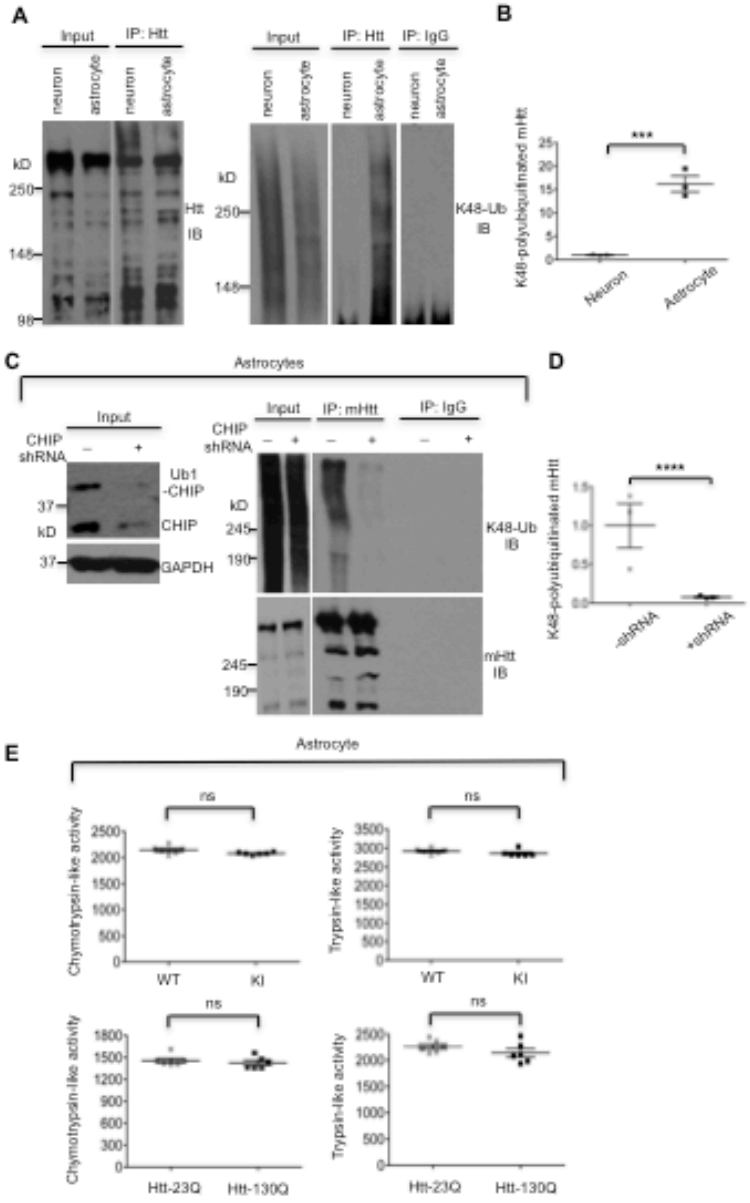
A
Input
IP: Htt
IP: IgG
neuron
astrocyte
kD
250
148
98
Htt IB
K48-Ub IB
B
K48-polyubiquitinated mHtt
***
Neuron
Astrocyte
C
Astrocytes
CHIP shRNA
Ub1-CHIP
CHIP
GAPDH
IP: mHtt
245
190
mHtt IB
D
****
-shRNA
+shRNA
E
Astrocyte
Chymotrypsin-like activity
Trypsin-like activity
ns
WT
KI
Htt-23Q
Htt-130Q

Figure 3.2 CHIP enhances K48-linked polyubiquitination on mHtt in astrocytes. ***A-B***, There are more K48-polyubiquitinated mHtt in KI cortical astrocytes than KI neurons. Ratios of K48-polyubiquitinated mHtt to total immunoprecipitated mHtt are from three independent experiments. ***C-D***, CHIP knockdown suppressed K48-linked polyubiquitination on endogenous mHtt in HD140Q KI cortical astrocytes. Ratios of K48-polyubiquitinated mHtt to total immunoprecipitated mHtt are from three independent experiments. ***E***, Expression of mHtt in Htt-130Q transfected astrocytes and HD140Q KI astrocytes did not affect proteasomal function when compared with Htt-23Q transfected or wild-type (WT) astrocytes (n=3 independent experiments). In figures a-d, cultured cells were treated with lactacystin (10 μM for 6 h) to inhibit proteasomal degradation. ***, $P < 0.001$, ****, $P < 0.0001$. ns, not significant. Data are represented as mean ± SEM. Error bars indicate SEM.

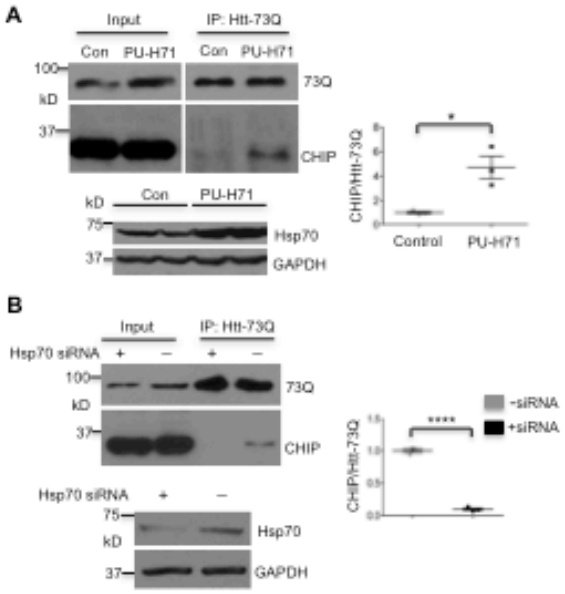
A
Input
IP: Htt-73Q
Con
PU-H71
Con
PU-H71
100
kD
37
73Q
CHIP
kD
Con
PU-H71
75
37
Hsp70
GAPDH
CHIP/Htt-73Q
Control
PU-H71
B
Input
IP: Htt-73Q
Hsp70 siRNA
+
–
+
–
100
kD
37
73Q
CHIP
-siRNA
+siRNA
****
CHIP/Htt-73Q
Hsp70 siRNA
+
–
75
kD
37
Hsp70
GAPDH

Figure 3.3 Hsp70 promotes the association of CHIP with mHtt. ***A***, PU-H71 induction promoted the association of transfected Htt-73Q with CHIP (upper panel) and also increased the expression of Hsp70 (lower panel). The ratios of immunoprecipitated CHIP to Htt-73Q in transfected HEK293 cells untreated (Control) or treated with PU-H71 from three independent experiments are also shown. ***B***, Knocking down Hsp70 via siRNA abolished the co-immunoprecipitation of Htt-73Q with CHIP (upper panel) and diminished the level of Hsp70 in transfected HEK293 cells (lower panel). Right panel shows the ratios of CHIP to Htt-73Q in co-immunoprecipitation from three independent experiments. $*P < 0.05$, $****P < 0.0001$ (unpaired two-tailed Student's *t*-test). Data are represented as mean ± SEM. Error bars indicate SEM.

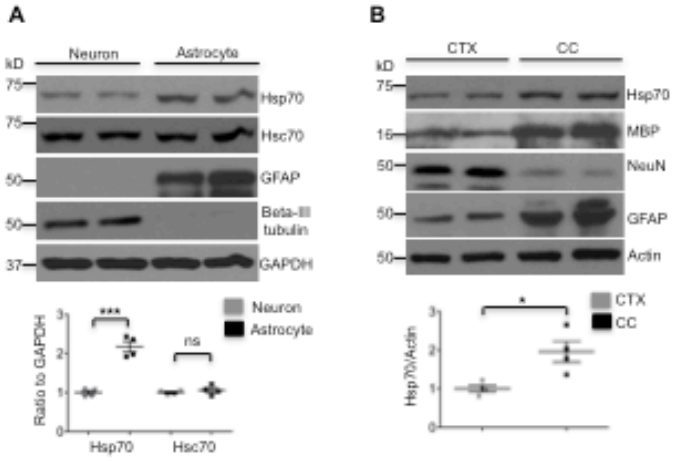
A
kD
Neuron
Astrocyte
75
Hsp70
75
Hsc70
50
GFAP
50
Beta-III tubulin
37
GAPDH
***
ns
Neuron
Astrocyte
Ratio to GAPDH
Hsp70
Hsc70
B
CTX
CC
kD
75
Hsp70
16
MBP
50
NeuN
50
GFAP
50
Actin
*
CTX
CC
Hsp70/Actin

Figure 3.4 There is more abundant Hsp70 in astrocytes than in neurons. ***A***, Hsp70 is expressed at a higher level in wild-type cultured cortical astrocytes than neurons (n=4 independent experiments). ***B***, The higher level of Hsp70 in the corpus callosum (CC) than in the cortex (CTX) of 3-month-old wild-type mouse (n=4 independent experiments). *, $P < 0.05$, ***, $P < 0.001$, (unpaired two-tailed Student's *t*-test); ns, not significant. Data are represented as mean ± SEM (Error bar).

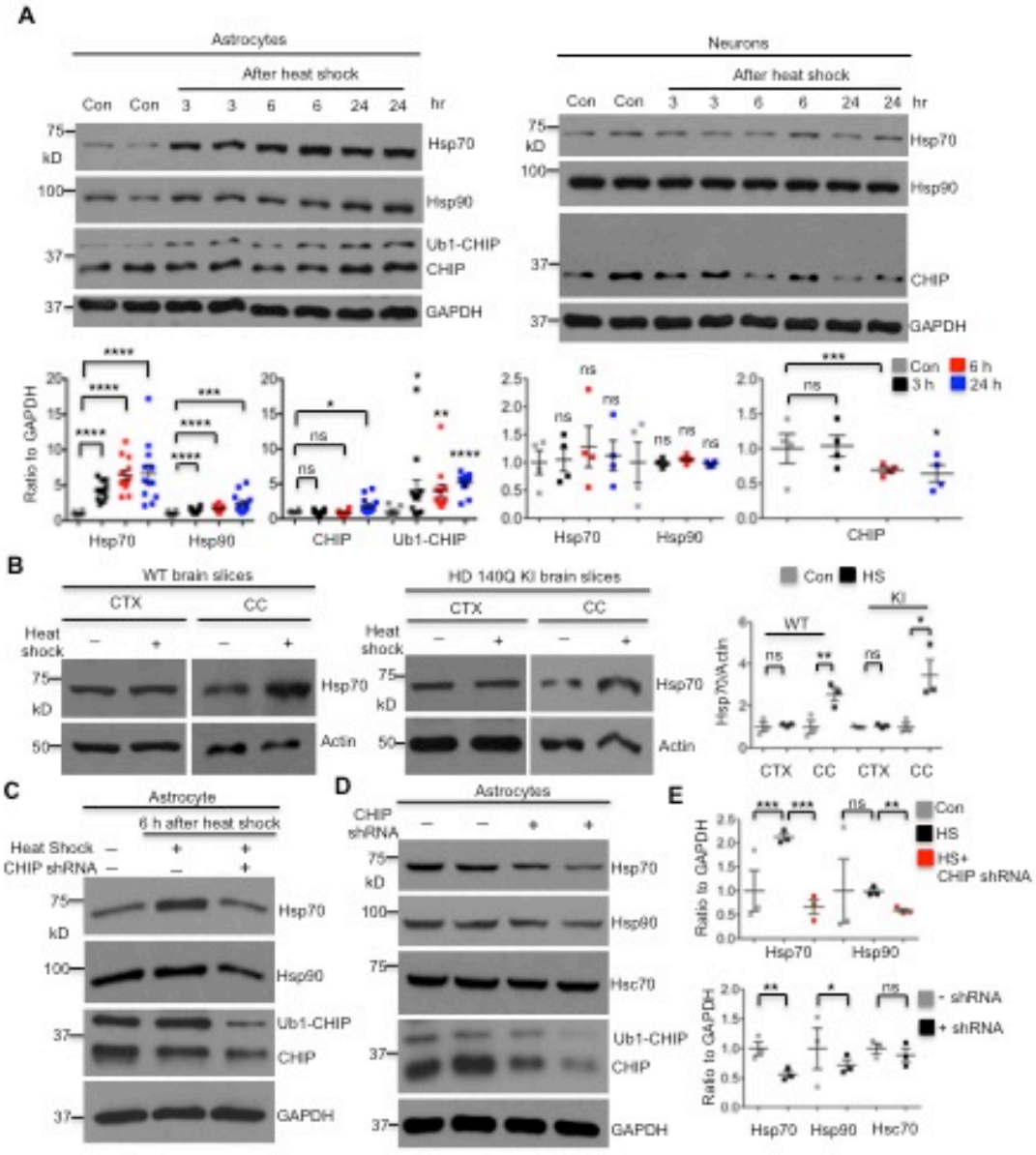
A
Astrocytes
After heat shock
Con Con 3 3 6 6 24 24 hr
75 kD
Hsp70
100
Hsp90
37
Ub1-CHIP
CHIP
37
GAPDH
Neurons
After heat shock
Con Con 3 3 6 6 24 24 hr
75 kD
Hsp70
100
Hsp90
37
CHIP
37
GAPDH
Ratio to GAPDH
Hsp70 Hsp90 CHIP Ub1-CHIP
Hsp70 Hsp90
CHIP
Con 6 h
3 h 24 h
B
WT brain slices
CTX CC
Heat shock
75 kD
Hsp70
50
Actin
HD 140Q KI brain slices
CTX CC
Heat shock
75 kD
Hsp70
50
Actin
Con HS
WT KI
Hsp70/Actin
CTX CC CTX CC
C
Astrocyte
6 h after heat shock
Heat Shock
CHIP shRNA
75 kD
Hsp70
100
Hsp90
37
Ub1-CHIP
CHIP
37
GAPDH
D
Astrocytes
CHIP shRNA
75 kD
Hsp70
100
Hsp90
75
Hsc70
37
Ub1-CHIP
CHIP
37
GAPDH
E
Ratio to GAPDH
Hsp70 Hsp90
Con
HS
HS+ CHIP shRNA
Ratio to GAPDH
Hsp70 Hsp90 Hsc70
- shRNA
+ shRNA

Figure 3.5 Differential CHIP activity causes distinct heat-shock responses in astrocytes and neurons. ***A***, Typical heat shock for 1 h induced Hsp70, Hsp90, CHIP and Ub1-CHIP specifically in wild-type cortical astrocytes at DIV 21-30 (left panels), but not in wild-type cortical neurons at DIV 10-14 (right panels). Ratios of indicated proteins to GAPDH are from 4 independent experiments. ***B***, Heat shock stress increased Hsp70 in the corpus callosum, but not in the cortex, of brain slices from wild-type (WT) and HD140Q KI mice at the age of 3 months. Quantitative results are from 3 independent experiments. CTX, cortex; CC, corpus callosum; HS, heat shock. ***C***, Induction of Hsp70 by 1 h heat shock was completely inhibited by CHIP knockdown, and no Hsp90 was induced in wild-type astrocytes at DIV 40-50. ***D***, CHIP knockdown decreased the expression of Hsp70 and Hsp90, but did not affect levels of Hsc70 in DIV 40-50 wild-type astrocytes. ***E***, Ratios of indicated proteins to GAPDH are from three (for c) and four (for d) independent experiments [upper panel for (c) and lower panel for (d)]. *, $P < 0.05$, **, $P < 0.01$, ***, $P < 0.001$ (unpaired two-tailed Student's *t*-test). ns, not significant. Data are represented as mean ± SEM (Error bar).

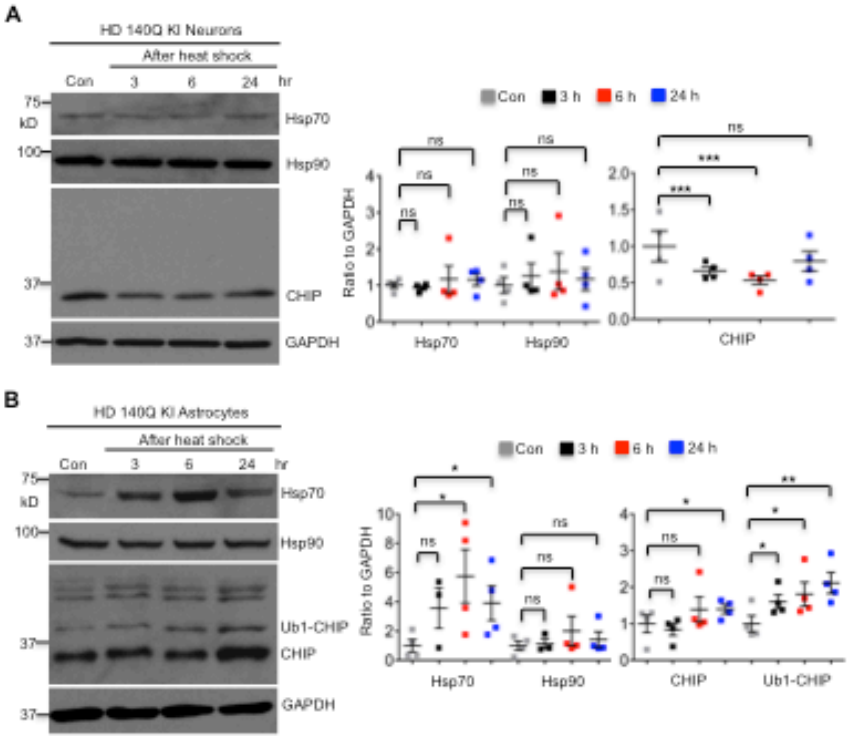
A
HD 140Q KI Neurons
After heat shock
Con
3
6
24
hr
75
kD
100
37
37
Hsp70
Hsp90
CHIP
GAPDH
Con
3 h
6 h
24 h
Ratio to GAPDH
ns
***
Hsp70
Hsp90
CHIP
B
HD 140Q KI Astrocytes
After heat shock
Con
3
6
24
hr
75
kD
100
37
37
Hsp70
Hsp90
Ub1-CHIP
CHIP
GAPDH
Con
3 h
6 h
24 h
Ratio to GAPDH
ns
*
**
Hsp70
Hsp90
CHIP
Ub1-CHIP

Figure 3.6 Increased mono-ubiquitinated CHIP and Hsp70 responses in HD140Q KI astrocytes. ***A***, Hsp70 and Hsp90 were not inducible in cultured KI neurons at DIV 10-14 by 30 min of heat shock stress, and CHIP decreased after heat shock. Quantitative results are from four independent experiments. ***B***, Heat shock for 30 min was able to induce Hsp70, CHIP, and Ub1-CHIP, but not Hsp90, in cultured KI astrocytes at DIV 21-30. Relative levels of proteins (ratios to GAPDH) on western blots were from four independent experiments. $*P < 0.05$, $**P < 0.01$, $***P < 0.001$ (unpaired two-tailed Student's *t*-test); ns, not significant. Data are represented as mean ± SEM. Error bars indicate SEM.

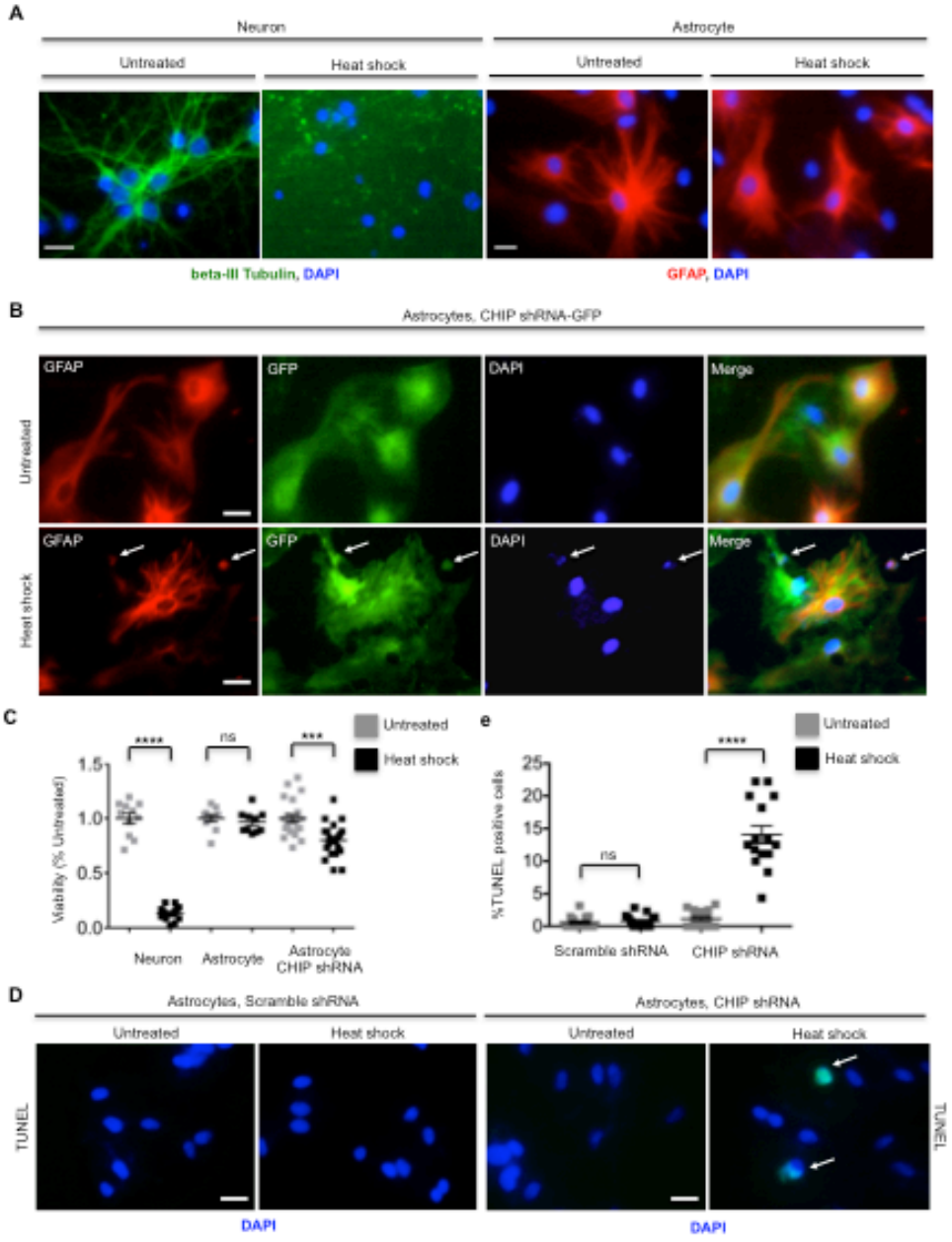
A
Neuron
Astrocyte
Untreated
Heat shock
Untreated
Heat shock
beta-III Tubulin, DAPI
GFAP, DAPI
B
Astrocytes, CHIP shRNA-GFP
GFAP
GFP
DAPI
Merge
Untreated
Heat shock
C
Viability (% Untreated)
1.5
1.0
0.5
0.0
****
ns
***
Untreated
Heat shock
Neuron
Astrocyte
Astrocyte CHIP shRNA
e
%TUNEL positive cells
25
20
15
10
5
0
****
ns
Untreated
Heat shock
Scramble shRNA
CHIP shRNA
D
Astrocytes, Scramble shRNA
Astrocytes, CHIP shRNA
Untreated
Heat shock
Untreated
Heat shock
TUNEL
TUNEL
DAPI
DAPI

Figure 3.7 High activity of CHIP contributes to astrocytic resistance to hyperthermia. ***A***, Apparent demise of cultured cortical neurons at DIV 10-12 after heat-shock stress (45^{o}C, 30min). The same heat-shock stress (45^{o}C, 30min) did not affect viability of cultured cortical astrocytes at DIV 40-45. Neurons and astrocytes were fixed and immunostained at 24 h after heat shock. ***B***, CHIP knockdown caused the death of a portion of CHIP shRNA-transfected astrocytes, which was characterized by shrunken nuclei, at 24 h after heat shock (45^{o}C, 30min). Arrows indicate corpse of astrocytes. ***C***, Quantitative results of Figures 4a,b. At least ten visual fields were randomly picked up for each group, and the live cells in each visual field were quantified. ***D-E***, TUNEL assay showing increased susceptibility of CHIP-knockdown astrocytes to heat shock stress (45^{o}C, 30 min). Arrows indicate apoptotic astrocytes (TUNEL-positive cells indicated by green fluorescence). ***$P < 0.001$, ****$P < 0.0001$ (unpaired two-tailed Student's *t*-test); ns, not significant. Data are represented as mean ± SEM. Error bars indicate SEM. Scale bars: 10 μm.

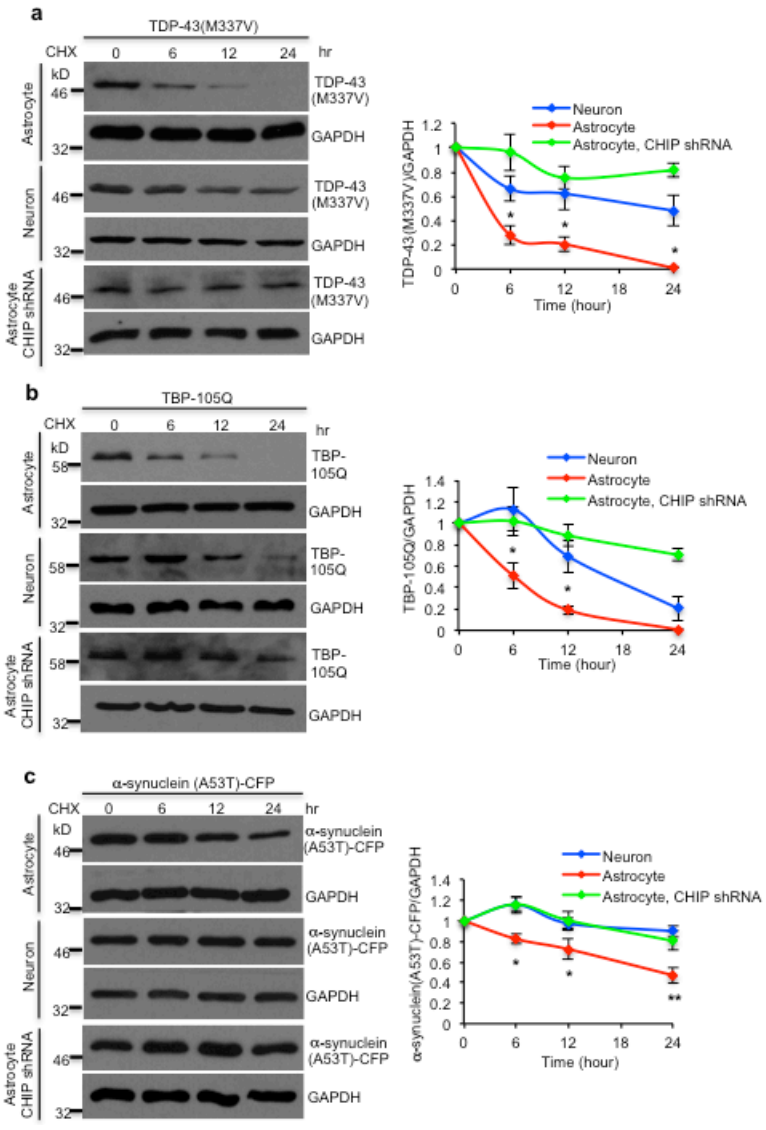
a
TDP-43(M337V)
CHX 0 6 12 24 hr
kD
Astrocyte
46
TDP-43 (M337V)
32
GAPDH
Neuron
46
TDP-43 (M337V)
32
GAPDH
Astrocyte CHIP shRNA
46
TDP-43 (M337V)
32
GAPDH
Neuron
Astrocyte
Astrocyte, CHIP shRNA
TDP-43(M337V)/GAPDH
Time (hour)
b
TBP-105Q
CHX 0 6 12 24 hr
kD
Astrocyte
58
TBP-105Q
32
GAPDH
Neuron
58
TBP-105Q
32
GAPDH
Astrocyte CHIP shRNA
58
TBP-105Q
32
GAPDH
Neuron
Astrocyte
Astrocyte, CHIP shRNA
TBP-105Q/GAPDH
Time (hour)
c
α-synuclein (A53T)-CFP
CHX 0 6 12 24 hr
kD
Astrocyte
46
α-synuclein (A53T)-CFP
32
GAPDH
Neuron
46
α-synuclein (A53T)-CFP
32
GAPDH
Astrocyte CHIP shRNA
46
α-synuclein (A53T)-CFP
32
GAPDH
Neuron
Astrocyte
Astrocyte, CHIP shRNA
α-synuclein(A53T)-CFP/GAPDH
Time (hour)

Figure 3.8 CHIP is required for prompt degradation of misfolded proteins in astrocytes. ***A-C***, Mutant proteins TDP-43 (M337V), TBP-105Q, and α-synuclein (A53T)-CFP were transfected in cultured neurons and astrocytes untreated or treated with CHIP shRNA. The cells were than treated with cycloheximide (CHX, 0.1 mM) for different time periods (0-24 h). The half-lives of mutant proteins in neurons and astrocytes showed that astrocytes degraded mutant proteins faster than neurons, which is inhibited by CHIP knockdown. Quantitative results are from three independent experiments. Asterisks indicate significant difference between astrocytes (without CHIP shRNA treatment) and neurons. *, $P < 0.05$, **, $P < 0.01$ (unpaired two-tailed Student's *t*-test). Data are represented as mean ± SEM (Error bar).

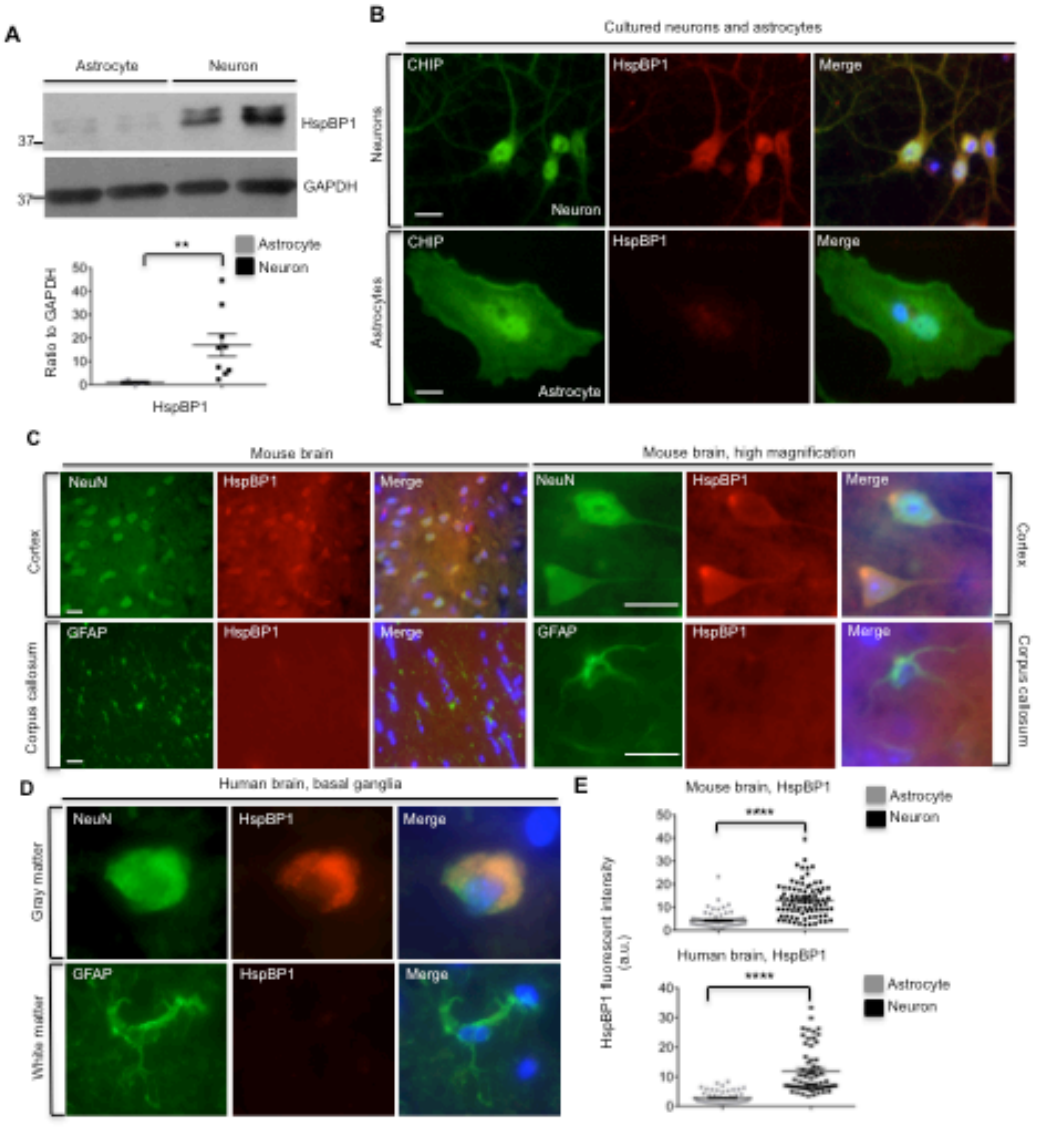
A
Astrocyte
Neuron
HspBP1
GAPDH
37
37
**
Astrocyte
Neuron
Ratio to GAPDH
HspBP1
B
Cultured neurons and astrocytes
Neurons
CHIP
HspBP1
Merge
Neuron
Astrocytes
CHIP
HspBP1
Merge
Astrocyte
C
Mouse brain
Mouse brain, high magnification
Cortex
NeuN
HspBP1
Merge
Corpus callosum
GFAP
HspBP1
Merge
D
Human brain, basal ganglia
Gray matter
NeuN
HspBP1
Merge
White matter
GFAP
HspBP1
Merge
E
Mouse brain, HspBP1
****
Astrocyte
Neuron
HspBP1 fluorescent intensity (a.u.)
Human brain, HspBP1
****
Astrocyte
Neuron

Figure 3.9 Neurons have more abundant HspBP1 than astrocytes in vitro and in vivo. ***A***, Higher levels of HspBP1 in cultured cortical neurons than astrocytes were shown by western blotting, and quantitative results from three independent experiments are beneath blots. ***B***, Representative images of immunostaining showed differential expression levels of HspBP1 between cultured neurons and astrocytes. ***C***, Greater abundance of HspBP1 in neurons than astrocytes in the mouse brains was exhibited by fluorescent immunostaining. ***D***, Immunostaining demonstrated more HspBP1 expression in neurons in the gray matter of human basal ganglia than that in astrocytes in the white matter of basal ganglia. Two brain samples from the people at the ages of 57 years were used (one male and one female). ***E***, Statistical results for figure C from three mice, and figure D from two human brains. **, $P < 0.01$, ****, $P < 0.0001$ (unpaired two-tailed Student's *t*-test). Scale bar = 5 um (Fig. b), = 20 um (Fig. C). Data are represented as mean ± SEM (Error bar).

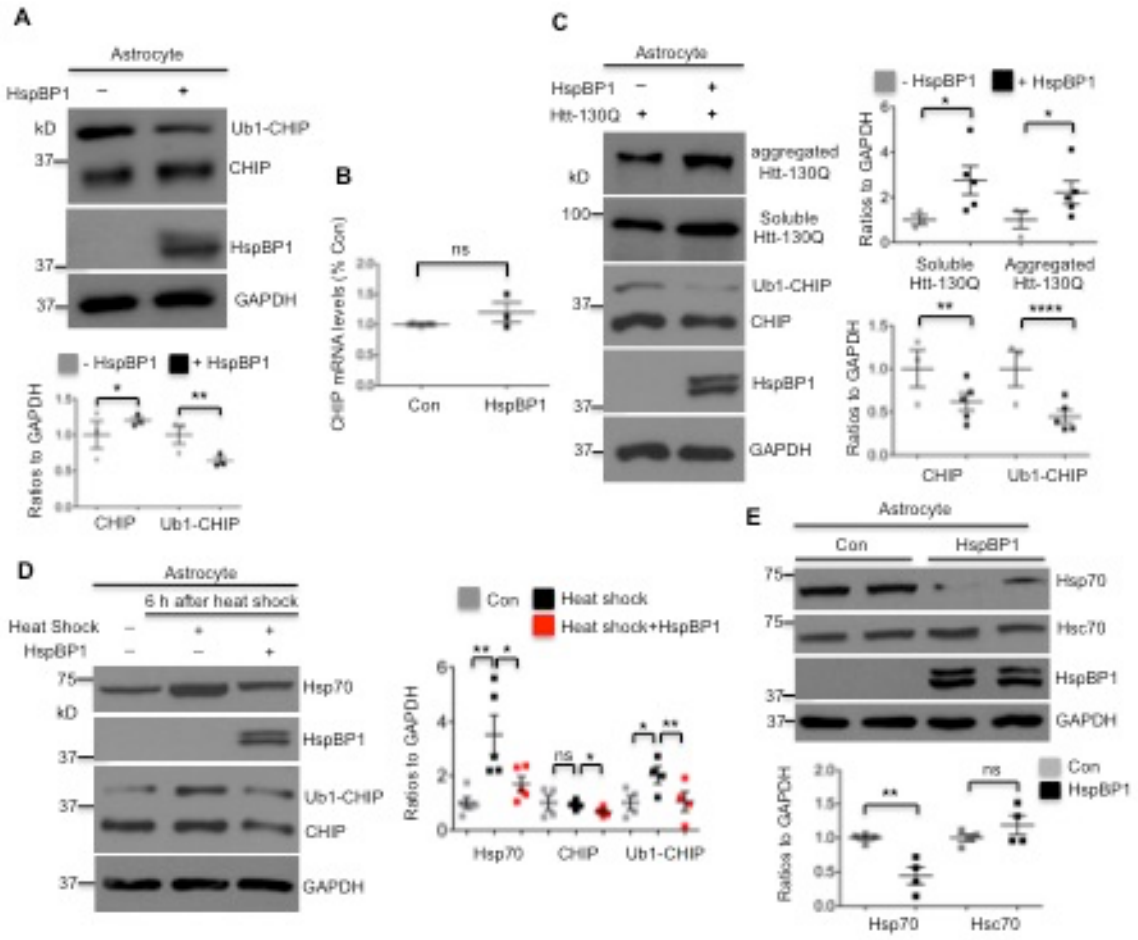
A
Astrocyte
HspBP1 – +
kD
37
Ub1-CHIP
CHIP
HspBP1
GAPDH
- HspBP1 + HspBP1
Ratios to GAPDH
CHIP
Ub1-CHIP
B
CHIP mRNA levels (% Con)
ns
Con
HspBP1
C
Astrocyte
HspBP1 – +
Htt-130Q + +
kD
100
37
aggregated Htt-130Q
Soluble Htt-130Q
Ub1-CHIP
CHIP
HspBP1
GAPDH
- HspBP1 + HspBP1
Ratios to GAPDH
Soluble Htt-130Q
Aggregated Htt-130Q
CHIP
Ub1-CHIP
D
Astrocyte
6 h after heat shock
Heat Shock – + +
HspBP1 – – +
75
kD
37
Hsp70
HspBP1
Ub1-CHIP
CHIP
GAPDH
Con
Heat shock
Heat shock+HspBP1
Ratios to GAPDH
Hsp70
CHIP
Ub1-CHIP
E
Astrocyte
Con
HspBP1
75
37
Hsp70
Hsc70
HspBP1
GAPDH
Con
HspBP1
Ratios to GAPDH
Hsp70
Hsc70

Figure 3.10 Deficient expression of HspBP1 in astrocytes contributes to high activity of CHIP in astrocytes. ***A***, Expression of HspBP1 in cultured astrocytes reduced the level of Ub1-CHIP, and major form of CHIP increased correspondingly (n=3 independent experiments). ***B***, qRT-PCR showed that overexpression of HspBP1 did not affect transcription of CHIP in cultured astrocytes (n=3 independent experiments). ***C***, HspBP1 expression in cultured astrocytes stabilized aggregated and soluble mHtt, and suppressed induction of CHIP and Ub1-CHIP by mHtt, which was seen in Figure 1c (n=3 independent experiments). ***D***, Induction of Hsp70, CHIP, and Ub1-CHIP by heat-shock stress at 42 ^{o}C for 1 h was significantly inhibited by HspBP1 expression in DIV 30-50 astrocytes (n=4 independent experiments). ***E***, Expression of HspBP1 decreased basal levels of Hsp70 in astrocytes (n=3 independent experiments). Scale bar = 5 μm. *, $P < 0.05$, **, $P < 0.01$, ****, $P < 0.0001$ (unpaired two-tailed Student's *t*-test). Data are represented as mean ± SEM (Error bar).

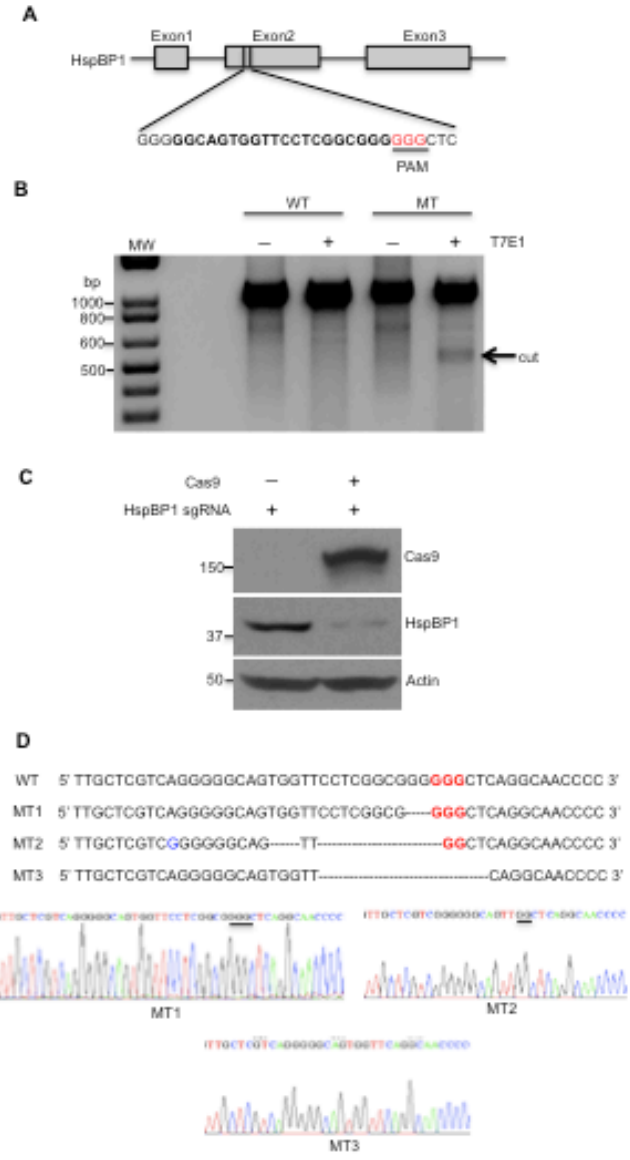
A
Exon1
Exon2
Exon3
HspBP1
GGGGGCAGTGGTTCCTCGGCGGGGGGCTC
PAM
B
WT
MT
MW
–
+
–
+
T7E1
bp
1000
800
600
500
cut
C
Cas9
–
+
HspBP1 sgRNA
+
+
150
Cas9
37
HspBP1
50
Actin
D
WT 5' TTGCTCGTCAGGGGGGCAGTGGTTCCTCGGCGGGGGGCTCAGGCAACCCC 3'
MT1 5' TTGCTCGTCAGGGGGGCAGTGGTTCCTCGGCG-----GGGCTCAGGCAACCCC 3'
MT2 5' TTGCTCGTCGGGGGGCAG------TT----------GGCTCAGGCAACCCC 3'
MT3 5' TTGCTCGTCAGGGGGCAGTGGTT----------CAGGCAACCCC 3'
MT1
MT2
MT3

Figure 3.11 Genome-editing activity of HspBP1 sgRNA. ***A***, For increasing specificity and decreasing off-target binding, we used Target Finder that is generated by Feng Zhang's lab to design gRNA. The chosen target sites of sgRNA are shown in bold font, and the PAM sequence is highlighted in red. ***B***, Genome-editing activity of HspBP1 sgRNA was tested using T7E1 assay. N2a cells were co-transfected with HspBP1 sgRNA and Cas9 plasmids, or transfected only with HspBP1 sgRNA plasmid as control. The T7E1 assay was carried out using PCR products of genome DNA from transfected N2a cells. The arrow indicates cleaved PCR products by T7E1 enzyme. WT, wild-type; MT, mutant. ***C***, Western blotting assay showed knockdown of HspBP1 at the protein level in N2a cells that were co-transfected with HspBP1 sgRNA and Cas9 plasmids. ***D***, Mutations in target HspBP1 gene were identified by TA cloning and subsequent sequencing.

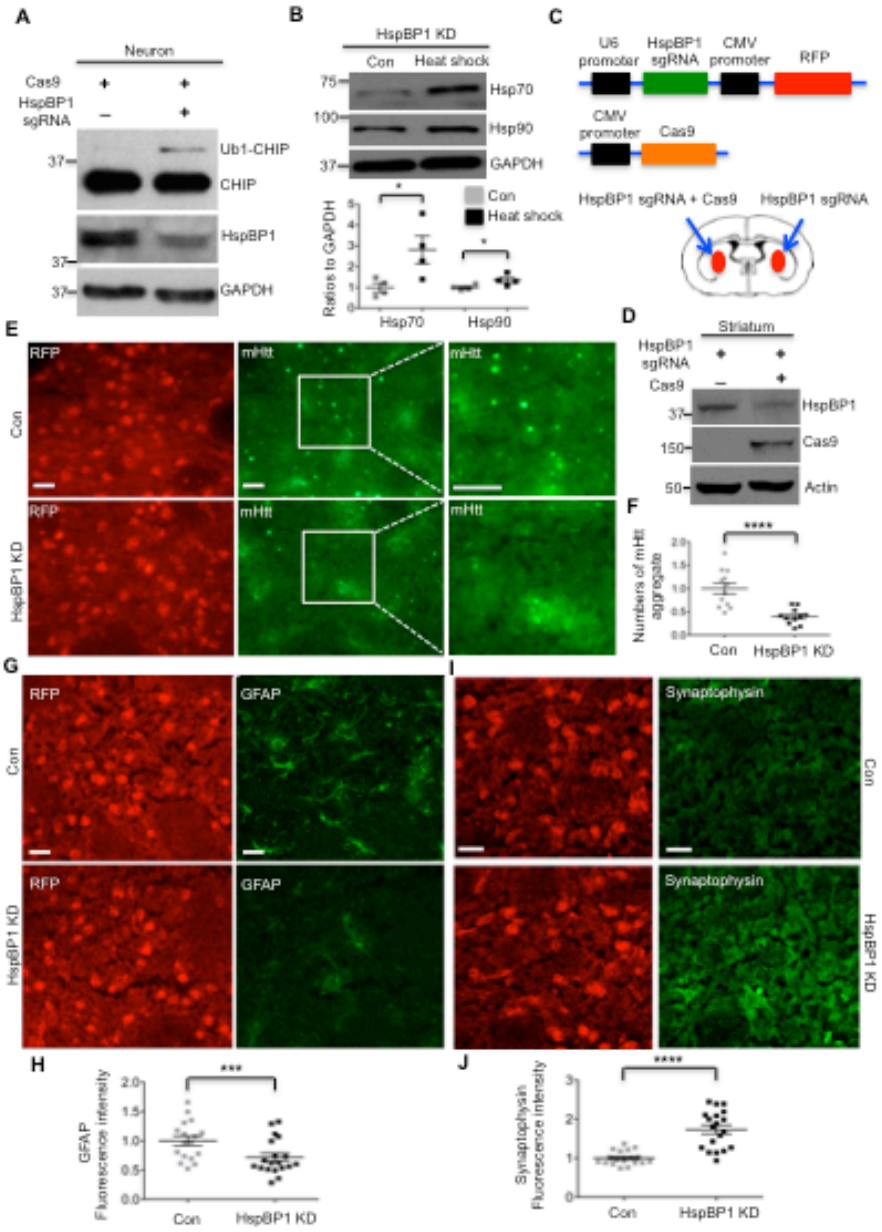
A
Neuron
Cas9
HspBP1 sgRNA
Ub1-CHIP
CHIP
HspBP1
GAPDH
37
B
HspBP1 KD
Con
Heat shock
75
100
Hsp70
Hsp90
GAPDH
Con
Heat shock
Ratios to GAPDH
Hsp70
Hsp90
C
U6 promoter
HspBP1 sgRNA
CMV promoter
RFP
CMV promoter
Cas9
HspBP1 sgRNA + Cas9
HspBP1 sgRNA
D
Striatum
HspBP1 sgRNA
Cas9
HspBP1
Cas9
Actin
37
150
50
E
RFP
mHtt
Con
HspBP1 KD
F
Numbers of mHtt aggregate
****
Con
HspBP1 KD
G
RFP
GFAP
Con
HspBP1 KD
H
GFAP Fluorescence intensity
***
Con
HspBP1 KD
I
Synaptophysin
Con
HspBP1 KD
J
Synaptophysin Fluorescence intensity
****
Con
HspBP1 KD

Figure 3.12 Knocking down HspBP1 is neuroprotective in HD 140Q KI mice. ***A***, HspBP1 knockdown in cultured neurons induced Ub1-CHIP expression. ***B***, Hsp70/90 were induced 6 hr after heat shock (42^{o}C for 1 h) in HspBP1-knockdown neurons (n=3 independent experiment). ***C***, Schematic representation of DNA constructs of HspBP1 sgRNA and Cas9. Viral injection of HspBP1 sgRNA and Cas9 into one striatum of HD 140Q KI mice was performed to knock down endogenous HspBP1, and injection of HspBP1 sgRNA alone into the striatum of the other hemisphere served as a control. ***D***, In the striatum of HD140Q KI mice, HspBP1 knockdown by CRISPR/Cas9 was validated by western blotting. ***E-J***, HspBP1 knockdown (KD) decreased mHtt aggregates and reactive astrocytes, rescued the loss of synaptophysin in the striatum of HD140Q KI mice at the age of 13-14 months as compared with the injection with HspBP1 sgRNA alone (Con). Results were collected from three HD140Q KI mice. *** $P < 0.001$, ****, $P < 0.0001$ (unpaired two-tailed Student's *t*-test). Scale bars = 20 μm. Data are represented as mean ± SEM (Error bar).

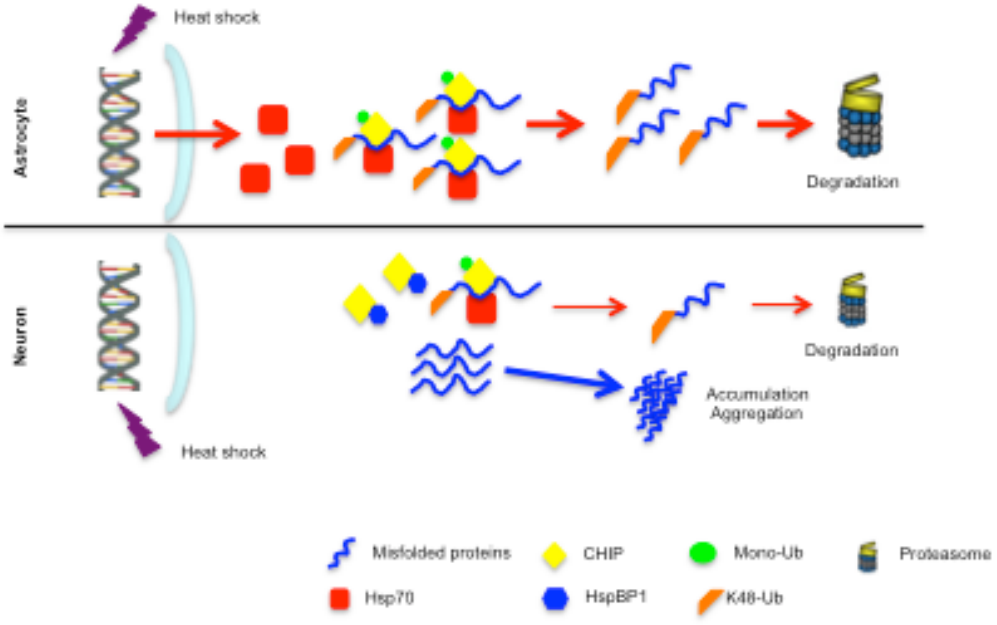
Heat shock
Astrocyte
Degradation
Neuron
Degradation
Accumulation
Aggregation
Heat shock
Misfolded proteins
CHIP
Mono-Ub
Proteasome
Hsp70
HspBP1
K48-Ub

Figure 3.13 Proposed model for the differential accumulation and toxicity of misfolded proteins in neurons and astrocytes. CHIP is more active in astrocytes due to deficient HspBP1 expression. CHIP preferentially binds to and polyubiquitinates misfolded proteins for prompt proteasomal degradation in astrocytes, a process in which CHIP itself is also monoubiquitinated. In addition, the high activity of CHIP confers the robust heat-shock response and the higher basal levels of Hsp70 in astrocytes, which in turn promotes the association between CHIP and misfolded proteins.

Chapter 4

General conclusions and future directions

General conclusions

My study addresses two key issues about HD pathogenesis: 1) why mHtt is prone to aggregation in neuronal processes; 2) why astrocytes are less susceptible to mHtt than neurons. The findings advance our understanding of the pathogenesis of HD, and also reveal cell-type-specific protective mechanisms, offering the promise of developing new molecular targets for therapies against HD. Using the optical-pulse chase assay, I was able to investigate the degradation rates of soluble mHtt in the cell body and process. Faster degradation of mHtt than its wild-type counterpart in cell bodies explains why mHtt is not prone to aggregation in the cell body. In contrast, the expanded polyQ tract stabilizes soluble mHtt in neuronal processes but not in astrocytic processes. This finding suggests not only impairment of mHtt turnover in neurites, but also distinct proteolysis of mHtt in astrocytic processes. It thus seems likely that the proteasome or certain proteinase is more active in astrocytic processes to clear mHtt. HD is characterized by the loss of neurons in striatum. If mHtt is cleared efficiently in the neuronal cell body, why do neurons die? Our findings support the "dying back" model: degeneration that is induced by the accumulation and aggregation of mHtt occurs first in neurites, and then moves retrogradely to the cell body. Indeed, mHtt aggregate-associated axonal degeneration is an early pathological event in the HD mouse model (Li et al., 2001). We also found that the proteasome plays a more important role than autophagy in mHtt degradation in both neurons and astrocytes, which conflicts with a previous report that autophagy plays a primary role in removing exon1-mHtt (Tsvetkov, 2013). We speculate that the length of the N-terminal Htt fragment may influence the degradation of mHtt. Exon1-mHtt, the shortest N-terminal fragment that can aggregate more rapidly than other

longer Htt fragments, may not be the proper substrate for the proteasome, and therefore, this fragment is preferentially degraded by autophagy. On the other hand, our study also demonstrates the feasibility of using optical-pulse chase to study Htt turnover at subcellular levels. This methodology can be extended to other types of misfolded proteins to further reveal their detrimental roles in neuropathology.

Remarkably, our live-cell imaging revealed that astrocytes degraded mHtt more efficiently than did neurons. This observation explains why mHtt aggregates are less prevalent in astrocytes, and why astrocytes are affected to a lesser extent than neurons in the HD brains. This finding is also consistent with the fact that astrocytes have greater proteasomal activity (Tydlacka et al., 2008). To further investigate the mechanisms causing faster clearance of mHtt, we focus on the UPS in astrocytes. Intriguingly, we found greater abundance of mono-ubiquitinated CHIP (Ub1-CHIP) in astrocytes, which is indicative of high activity of CHIP in these cells. There are several lines of evidence to further support this conclusion: 1) the expression of mHtt causes astrocyte-specific induction of CHIP and Ub1-CHIP; 2) both CHIIP and Ub1-CHIP bind to mHtt selectively in astrocytes, which increases K48 polyubiquitinated mHtt; 3) astrocyte-specific robust heat shock response is mediated by CHIP. Given the ubiquitination of misfolded proteins by CHIP for proteasomal degradation, we postulate that active CHIP in astrocytes results in prompt clearing of misfolded proteins. Indeed, in addition to mHtt, a variety of misfolded proteins are cleared faster in astrocytes than in neurons, which was halted by CHIP knockdown. These findings suggest that active CHIP is a common protective mechanism preventing the aggregation of misfolded proteins in astrocytes. It is noteworthy that the expression of mHtt specifically in astrocytes is sufficient to cause

abnormal behavioral phenotypes in mice older than 13 months (Bradford et al., 2009), which is proposed to be due to the reduction of proteasomal activities with aging in these cells.

Next, we sought factors that activate CHIP in astrocytes. We found differential expression of HspBP1, an inhibitor of CHIP, between neurons and astrocytes. Expression of HspBP1 is more abundant in neurons than in astrocytes, which leads to the lower activity of CHIP in neurons. In support of this notion, overexpression of HspBP1 suppressed CHIP activation, which is evidenced by decreased Ub1-CHIP. HspBP1 expression also caused aggregation of mHtt, and eliminated differential Hsp70 expression between neurons and astrocytes under either physiological or heat-shock conditions. Recently, the CRISPR/Cas9 system has been widely used to edit the genome to manipulate the expression of proteins of interest. We took advantage of CRISPR/Cas9 to knock down HspBP1 in neurons, which activates CHIP in primary neurons. In vivo, we found that HspBP1 knockdown in striatal neurons of HD KI mice reduced mHtt aggregates, ameliorated astrogliosis, and rescued loss of synaptophysin, suggesting that silencing HspBP1 expression is neuroprotective.

Collectively, using the optical-pulse chase assay to investigate mHtt degradation in processes and cell bodies, our live-cell imaging results provide clues for the resistance of astrocytes to HD. Importantly, we found that HspBP1-mediated differential CHIP activity accounts for the distinct vulnerability of neurons and astrocytes to misfolded proteins. These findings reveal intrinsic differences in the UPS between neuronal and glial cells, and suggest that activating CHIP via eliminating its molecular inhibitor is a potential therapeutic strategy against misfolded proteins.

Future directions

Several questions remain to be studied, and I list and discuss them as follows:

First, in addition to neuronal processes, mHtt also preferentially aggregates in neuronal nuclei. The nuclear accumulation of mHtt disturbs a broad range of gene expression via binding to various transcriptional factors, such as Sp1. It is proposed that mHtt degradation in the nucleus is not as efficient as in the cytoplasm, owing to lack of autophagy and lower proteasomal activity in the nuclei than that in the cytoplasm. Although we had compared the proteolysis of mHtt in the processes and cell bodies with the optical-pulse chase assay, we did not investigate mHtt degradation in the nucleus. This is because the majority of transfected mHtt was localized in the cytoplasm, and the intensity of red fluorescence of activated dendra2 after photoconversion in the nucleus is too low to evaluate the half-life of mHtt. To overcome this problem, future studies should fuse nuclear localization sequence (NLS) to the Htt-dendra2 to increase translocation of mHtt into the nucleus for the photoconversion experiment.

Second, our results demonstrate the impaired clearance of mHtt in neuronal processes compared with neuronal cell bodies, which raises a question of what causes this compartment-dependent degradation of mHtt in neurons. Given that proteasomal activity is compromised in the synapses of mHtt-expressing neurons (Wang et al., 2008), we postulate that activities of certain chaperones required for refolding misfolded proteins and ubiquitin enzymes of the ubiquitin-proteasome system (UPS) may be correspondingly downregulated in the processes of HD neurons. Considering that normal functions of the UPS and chaperone network in neuronal processes highly rely on microtubule-dependent transport of mRNA and proteins as well as local protein synthesis

(Deglincerti and Jaffrey, 2012; Hsu et al., 2015; Campbell and Holt, 2001), mHtt expression may impair the microtubule-dependent transport along neurites, which leads to insufficient components of the chaperone network and UPS, and as a result, reduced competence of the quality control system in neurites. To test this hypothesis, we need to extract fractions of neuronal processes and somata, and then subject the samples to RNA-sequencing analysis that could provide comparatively quantitative data of mRNA between neuronal processes and cell bodies.

Third, the results of RNA-sequencing indicate differential expression of HspBP1 between neurons and astrocytes at the transcriptional level, but the factors causing this difference are elusive. Gene expression is a sophisticated process that is finely regulated by a variety of transcriptional factors. Given that promoters play essential roles in gene expression, it is imperative to compare the activity of the HspBP1 promoter in cultured neurons and astrocytes, which can be achieved by a luciferase promoter activity assay. If different activities of the promoter in neurons and astrocytes are indeed identified, specific transcriptional factors in astrocytes that bind to the promoter of the HspBP1 gene need to be identified. In addition, the putative differential activity of certain transcriptional factors may cause differential expression of HspBP1 between neurons and astrocytes. On the other hand, although the CRISPR/Cas9 is a convenient tool for gene editing, off-target effects need to be considered. And, whether CRISPR/Cas9 causes unwanted and unexpected mutations remains to be studied (Schaefer et al., 2017). Therefore, to further study the effects of HspBP1 levels on mHtt aggregation in neurons in vivo, we need to generate germline or conditional HspBP1 knockout mice, either of

which could be used to cross with the HD KI mouse to investigate whether the loss of HspBP1 in neuronal cells is protective against mHtt accumulation and its neurotoxicity.

References

Adam, V., Berardozzi, R., Byrdin, M., and Bourgeois, D. (2014). Phototransformable fluorescent proteins: Future challenges. *Curr Opin Chem Biol.* 20, 92-102.

Alberti, S., Bohse, K., Arndt, V., Schmitz, A., and Hohfeld, J. (2004). The cochaperone HspBP1 inhibits the CHIP ubiquitin ligase and stimulates the maturation of the cystic fibrosis transmembrane conductance regulator. *Mol Biol Cell.* 15, 4003-4010.

Batulan, Z., Shinder, G.A., Minotti, S., He, B.P., Doroudchi, M.M., Nalbantoglu, J., Strong, M.J., Durham, H.D. (2003). High threshold for induction of the stress response in motor neurons is associated with failure to activate HSF1. *J Neurosci. 23*, 5789-5798

Benraiss, A., Wang, S., Herrlinger, S., Li, X., Chandler-Militello, D., Mauceri, J., Burm, H.B., Toner, M., Osipovitch, M., Jim Xu, Q.*, et al.* (2016). Human glia can both induce and rescue aspects of disease phenotype in Huntington disease. *Nat Commun.* 7, 11758.

Bett, J.S., Cook, C., Petrucelli, L., Bates, G.P. (2009) The ubiquitin-proteasome reporter GFPu does not accumulate in neurons of the R6/2 transgenic mouse model of Huntington's disease. *PLoS One* **4**:e5128.

Bhat, K.P., Yan, S., Wang, C.E., Li, S., and Li, X.J. (2014). Differential ubiquitination and degradation of huntingtin fragments modulated by ubiquitin-protein ligase E3A. *Proc Natl Acad Sci U S A.* 111, 5706-5711.

Bjorkoy, G., Lamark, T., Brech, A., Outzen, H., Perander, M., Overvatn, A., Stenmark, H., and Johansen, T. (2005). p62/SQSTM1 forms protein aggregates degraded by autophagy and has a protective effect on huntingtin-induced cell death. *J Cell Biol.* 171, 603-614.

Bradford, J., Shin, J.Y., Roberts, M., Wang, C.E., Li, X.J., and Li, S. (2009). Expression of mutant huntingtin in mouse brain astrocytes causes age-dependent neurological symptoms. . *Proc Natl Acad Sci U S A.* 106, 22480-22485.

Cabral Miranda, F., Adao-Novaes, J., Hauswirth, W.W., Linden, R., Petrs-Silva, H., and Chiarini, L.B. (2014). CHIP, a carboxy terminus HSP-70 interacting protein, prevents cell death induced by endoplasmic reticulum stress in the central nervous system. *Front Cell Neurosci.* 8, 438.

Cattaneo, E., Zuccato, C., and Tartari, M. (2005). Normal huntingtin function: an alternative approach to Huntington's disease. *Nat Rev Neurosci.* 6, 919-930.

Chang, R., Liu, X., Li, S., and Li, X.J. (2015). Transgenic animal models for study of the pathogenesis of Huntington's disease and therapy. *Drug Des Devel Ther.* 9, 2179-2188.

Chen, B., Retzlaff, M., Roos, T., and Frydman, J. (2011). Cellular strategies of protein quality control. *Cold Spring Harb Perspect Biol.* 3, a004374.

Chudakov, D.M., Lukyanov, S., and Lukyanov, K.A. (2007). Tracking intracellular protein movements using photoswitchable fluorescent proteins PS-CFP2 and Dendra2. *Nat Protoc*. 2, 2024-2032.

Chung, W.S., Clarke, L.E., Wang, G.X., Stafford, B.K., Sher, A., Chakraborty, C., Joung, J., Foo, L.C., Thompson, A., Chen, C.*, et al.* (2013). Astrocytes mediate synapse elimination through MEGF10 and MERTK pathways. *Nature* 504, 394-400.

Ciechanover, A. (2005). Proteolysis: from the lysosome to ubiquitin and the proteasome. *Nat Rev Mol Cell Biol*. 6, 79-87.

Ciechanover, A., and Kwon, Y.T. (2015). Degradation of misfolded proteins in neurodegenerative diseases: therapeutic targets and strategies. *Exp Mol Med.* 47, e147.

Chondrogianni, N., Voutetakis, K., Kapetanou, M., Delitsikou, V., Papaevgeniou, N., Sakellari, M., Lefaki, M., Filippopoulou, K., Gonos, E.S. (2015) Proteasome activation: An innovative promising approach for delaying aging and retarding age-related diseases.

Ageing Res Rev. **23**:37-55.

Dai, Q., Zhang, C., Wu, Y., McDonough, H., Whaley, R.A., Godfrey, V., Li, H.H., Madamanchi, N., Xu, W., Neckers, L.*, et al.* (2003). CHIP activates HSF1 and confers protection against apoptosis and cellular stress. *EMBO J.* 22, 5446-5458.

Davies, S.W., Turmaine, M., Cozens, B.A., DiFiglia, M., Sharp, A.H., Ross, C.A., Scherzinger, E., Wanker, E.E., Mangiarini, L., and Bates, G.P. (1997). Formation of neuronal intranuclear inclusions underlies the neurological dysfunction in mice transgenic for the HD mutation. *Cell* 90, 537-548.

Deshaies, R.J., and Joazeiro, C.A. (2009). RING domain E3 ubiquitin ligases. *Annu Rev Biochem*. 78, 399-434.

Dickey, A.S., Pineda, V.V., Tsunemi, T., Liu, P.P., Miranda, H.C., Gilmore-Hall, S.K., Lomas, N., Sampat, K.R., Buttgereit, A., Torres, M.J.*, et al.* (2016). PPAR-delta is repressed in Huntington's disease, is required for normal neuronal function and can be targeted therapeutically. *Nat Med.* 22, 37-45.

DiFiglia, M., Sapp, E., Chase, K.O., Davies, S.W., Bates, G.P., Vonsattel, J.P., and Aronin, N. (1997). Aggregation of huntingtin in neuronal intranuclear inclusions and dystrophic neurites in brain. *Science* 277, 1990-1993.

Dikshit, P., and Jana, N.R. (2007). The co-chaperone CHIP is induced in various stresses and confers protection to cells. *Biochem Biophys Res Commun*. 357, 761-765.

Dragatsis, I., Levine, M.S., and Zeitlin, S. (2000). Inactivation of Hdh in the brain and testis results in progressive neurodegeneration and sterility in mice. *Nat Genet.* 26, 300-306.

Dunah, A.W., Jeong, H., Griffin, A., Kim, Y.M., Standaert, D.G., Hersch, S.M., Mouradian, M.M., Young, A.B., Tanese, N., and Krainc, D. (2002). Sp1 and TAFII130 transcriptional activity disrupted in early Huntington's disease. *Science* 296, 2238-2243.

Eletr, Z.M., and Wilkinson, K.D. (2014). Regulation of proteolysis by human deubiquitinating enzymes. *Biochim Biophys Acta.* 1843, 114-128.

Fischer, L.R., Glass, J.D. (2007) Axonal degeneration in motor neuron disease. *Neurodegener Dis.* **4**:431-442.

Friedman, M.J., Shah, A.G., Fang, Z.H., Ward, E.G., Warren, S.T., Li, S., Li, X.J. (2007). Polyglutamine domain modulates the TBP-TFIIB interaction: implications for its normal function and neurodegeneration. *Nat Neurosci. 10*, 1519-1528

Gafni, J., and Ellerby, L.M. (2002). Calpain activation in Huntington's disease. *J Neurosci*. 22, 4842-4849.

Gafni, J., Hermel, E., Young, J.E., Wellington, C.L., Hayden, M.R., and Ellerby, L.M. (2004). Inhibition of calpain cleavage of huntingtin reduces toxicity: accumulation of calpain/caspase fragments in the nucleus. *J Biol Chem*. 279, 20211-20220.

Gauthier, L.R., Charrin, B.C., Borrell-Pages, M., Dompierre, J.P., Rangone, H., Cordelieres, F.P., De Mey, J., MacDonald, M.E., Lessmann, V., Humbert, S., and Saudou, F. (2004). Huntingtin controls neurotrophic support and survival of neurons by enhancing BDNF vesicular transport along microtubules. *Cell* 118, 127-138.

Gervais, F.G., Singaraja, R., Xanthoudakis, S., Gutekunst, C.A., Leavitt, B.R., Metzler, M., Hackam, A.S., Tam, J., Vaillancourt, J.P., Houtzager, V.*, et al.* (2002). Recruitment and activation of caspase-8 by the Huntingtin-interacting protein Hip-1 and a novel partner Hippi. *Nat Cell Biol*. 4, 95-105.

Goldberg, A.L. (2003). Protein degradation and protection against misfolded or damaged proteins. *Nature* 426, 895-899.

Gunawardena, S., Her, L.S., Brusch, R.G., Laymon, R.A., Niesman, I.R., Gordesky-Gold, B., Sintasath, L., Bonini, N.M., Goldstein, L.S. (2003) Disruption of axonal transport by loss of huntingtin or expression of pathogenic polyQ proteins in Drosophila. *Neuron.* **40**:25-40.

Gutekunst, C.A., Li, S.H., Yi, H., Mulroy, J.S., Kuemmerle, S., Jones, R., Rye, D., Ferrante, R.J., Hersch, S.M., and Li, X.J. (1999). Nuclear and neuropil aggregates in Huntington's disease: relationship to neuropathology. *J Neurosci.* 19, 2522-2534.

Harjes, P., Wanker, E.E. (2003) The hunt for huntingtin function: interaction partners tell many different stories. *Trends Biochem Sci* **28**:425-433.

Hickey, M.A., Kosmalska, A., Enayati, J., Cohen, R., Zeitlin, S., Levine, MS., Chesselet, M.F. (2008) Extensive early motor and non-motor behavioral deficits are followed by striatal neuronal loss in knock-in Huntington's disease mice. *Neuroscience.* **157**:280-295.

Hjerpe, R., Bett, J.S., Keuss, M.J., Solovyova, A., McWilliams, T.G., Johnson, C., Sahu, I., Varghese, J., Wood, N., Wightman, M.*, et al.* (2016). UBQLN2 Mediates Autophagy-Independent Protein Aggregate Clearance by the Proteasome. *Cell* 166, 935-949.

Hoffner, G., Kahlem, P., Djian, P. (2002) Perinuclear localization of huntingtin as a consequence of its binding to microtubules through an interaction with beta-tubulin: relevance to Huntington's disease. *J Cell Sci.* **115**:941-948.

Hong, Y., Zhao, T., Li, X.J., and Li, S. (2016). Mutant Huntingtin Impairs BDNF Release from Astrocytes by Disrupting Conversion of Rab3a-GTP into Rab3a-GDP. *J Neurosci.* 36, 8790-8801.

Huang, B., Wei, W., Wang, G., Gaertig, M.A., Feng, Y., Wang, W., Li, X.J., Li, S. (2015) Mutant huntingtin downregulates myelin regulatory factor-mediated myelin gene expression and affects mature oligodendrocytes. *Neuron*. 85:1212-1226.

Jana, N.R., Dikshit, P., Goswami, A., Kotliarova, S., Murata, S., Tanaka, K., and Nukina, N. (2005). Co-chaperone CHIP associates with expanded polyglutamine protein and promotes their degradation by proteasomes. *J Biol Chem.* 280, 11635-11640.

Jeong, H., Then, F., Melia, T.J., Jr., Mazzulli, J.R., Cui, L., Savas, J.N., Voisine, C., Paganetti, P., Tanese, N., Hart, A.C.*, et al.* (2009). Acetylation targets mutant huntingtin to autophagosomes for degradation. *Cell* 137, 60-72.

Jucker, M. & Walker, L.C. (2013). Self-propagation of pathogenic protein aggregates in neurodegenerative diseases. *Nature 501*, 45-51

Klein, P., Onnerfjord, P., Brundin, P., Mulder, H., Li, J.Y. (2009) Mutant huntingtin interacts with beta-tubulin and disrupts vesicular transport and insulin secretion. *Hum Mol Genet* **18**:3942-3954.

Kirkin, V., McEwan, D.G., Novak, I., and Dikic, I. (2009). A role for ubiquitin in selective autophagy. *Mol Cell.* 34, 259-269.

Korac, J., Schaeffer, V., Kovacevic, I., Clement, A.M., Jungblut, B., Behl, C., Terzic, J., and Dikic, I. (2013). Ubiquitin-independent function of optineurin in autophagic clearance of protein aggregates. *J Cell Sci*. 126, 580-592.

Kumar, P., Ambasta, R.K., Veereshwarayya, V., Rosen, K.M., Kosik, K.S., Band, H., Mestril, R., Patterson, C., and Querfurth, H.W. (2007). CHIP and HSPs interact with beta-APP in a proteasome-dependent manner and influence Abeta metabolism. *Hum Mol Genet*. 16, 848-864.

Lee, J.S., Seo, T.W., Yi, J.H., Shin, K.S. & Yoo, S.J. (2013). CHIP has a protective role against oxidative stress-induced cell death through specific regulation of endonuclease G. *Cell Death Dis. 4*, e666

Li, H., Li, S.H., Johnston, H., Shelbourne, P.F., and Li, X.J. (2000). Amino-terminal fragments of mutant huntingtin show selective accumulation in striatal neurons and synaptic toxicity. *Nat Genet.* 25, 385-389.

Li, H., Li, S.H., Yu, Z.X., Shelbourne, P., and Li, X.J. (2001). Huntingtin aggregate-associated axonal degeneration is an early pathological event in Huntington's disease mice. *J Neurosci*. 21, 8473-8481.

Li, S.H., Cheng, A.L., Zhou, H., Lam, S., Rao, M., Li, H., and Li, X.J. (2002). Interaction of Huntington disease protein with transcriptional activator Sp1. *Mol Cell Biol*. 22, 1277-1287.

Li, S.H., and Li, X.J. (2004). Huntingtin-protein interactions and the pathogenesis of Huntington's disease. *Trends Genet.* 20, 146-154.

Li, X., Wang, C.E., Huang, S., Xu, X., Li, X.J., Li, H., and Li, S. (2010). Inhibiting the ubiquitin-proteasome system leads to preferential accumulation of toxic N-terminal mutant huntingtin fragments. *Hum Mol Genet*. 19, 2445-2455.

Li, Y., Chopp, M., Yoshida, Y. & Levine, S.R. (1992). Distribution of 72-kDa heat-shock protein in rat brain after hyperthermia. *Acta Neuropathol. 84*, 94-99

Maday, S., and Holzbaur, E.L. (2016). Compartment-Specific Regulation of Autophagy in Primary Neurons. *J Neurosci*. 36, 5933-5945.

Maday, S., Wallace, K.E., and Holzbaur, E.L. (2012). Autophagosomes initiate distally and mature during transport toward the cell soma in primary neurons. *J Cell Biol*. 196, 407-417.

Mangiarini, L., Sathasivam, K., Seller, M., Cozens, B., Harper, A., Hetherington, C., Lawton, M., Trottier, Y., Lehrach, H., Davies, S.W., and Bates, G.P. (1996). Exon 1 of

the HD gene with an expanded CAG repeat is sufficient to cause a progressive neurological phenotype in transgenic mice. *Cell* 87, 493-506.

Maragakis, N.J. & Rothstein, J.D. (2006). Mechanisms of Disease: astrocytes in neurodegenerative disease. *Nat Clin Pract Neurol. 2*, 679-689

Marcuccilli, C.J., Mathur, S.K., Morimoto, R.I. & Miller, R.J. (1996). Regulatory differences in the stress response of hippocampal neurons and glial cells after heat shock. *J Neurosci*. *16*, 478-485

Margulis, J., and Finkbeiner, S. (2014). Proteostasis in striatal cells and selective neurodegeneration in Huntington's disease. *Front Cell Neurosci*. 8, 218.

McClellan, A.J. & Frydman, J. (2001). Molecular chaperones and the art of recognizing a lost cause. *Nat Cell Biol. 3*, E51-53

McDonough, H., and Patterson, C. (2003). CHIP: a link between the chaperone and proteasome systems. *Cell Stress Chaperones.* 8, 303-308.

Millecamps, S., and Julien, J.P. (2013). Axonal transport deficits and neurodegenerative diseases. *Nat Rev Neurosci*. 14, 161-176.

Milnerwood, A.J., and Raymond, L.A. (2010). Early synaptic pathophysiology in neurodegeneration: insights from Huntington's disease. *Trends Neurosci.* 33, 513-523.

Min, J.N., Whaley, R.A., Sharpless, N.E., Lockyer, P., Portbury, A.L., and Patterson, C. (2008). CHIP deficiency decreases longevity, with accelerated aging phenotypes accompanied by altered protein quality control. *Mol Cell Biol*. 28, 4018-4025.

Munoz-Sanjuan, I., and Bates, G.P. (2011). The importance of integrating basic and clinical research toward the development of new therapies for Huntington disease. *J Clin Invest*. 121, 476-483.

Myeku, N., Figueiredo-Pereira, M.E. (2011) Dynamics of the degradation of ubiquitinated proteins by proteasomes and autophagy: association with sequestosome 1/p62. *J Biol Chem.* **286**:22426-22440

Orr, A.L., Li, S., Wang, C.E., Li, H., Wang, J., Rong, J., Xu, X., Mastroberardino, P.G., Greenamyre, J.T., and Li, X.J. (2008). N-terminal mutant huntingtin associates with mitochondria and impairs mitochondrial trafficking. *J Neurosci*. 28, 2783-2792.

Paul, I., Ahmed, S.F., Bhowmik, A., Deb, S. & Ghosh, M.K. (2013). The ubiquitin ligase CHIP regulates c-Myc stability and transcriptional activity. *Oncogene 32*, 1284-1295

Pimienta, G., Herbert, K.M. & Regan, L. (2011). A compound that inhibits the HOP-Hsp90 complex formation and has unique killing effects in breast cancer cell lines. *Mol Pharm. 8*, 2252-2261

Pickart, C.M., Eddins, M.J. (2004) Ubiquitin: structures, functions, mechanisms. *Biochim Biophys Acta.* **1695**:55-72.

Przedborski, S., Vila, M., and Jackson-Lewis, V. (2003). Neurodegeneration: what is it and where are we? *J Clin Invest*. 111, 3-10.

Qian, S.B., McDonough, H., Boellmann, F., Cyr, D.M. & Patterson, C. (2006). CHIP-mediated stress recovery by sequential ubiquitination of substrates and Hsp70. *Nature 440*, 551-555

Qin, Z.H., Wang, Y., Kegel, K.B., Kazantsev, A., Apostol, B.L., Thompson, L.M., Yoder, J., Aronin, N., and DiFiglia, M. (2003). Autophagy regulates the processing of amino terminal huntingtin fragments. *Hum Mol Genet*. 12, 3231-3244.

Rabinowitz, J.D., and White, E. (2010). Autophagy and metabolism. *Science* 330, 1344-1348.

Ravikumar, B., Duden, R., and Rubinsztein, D.C. (2002). Aggregate-prone proteins with polyglutamine and polyalanine expansions are degraded by autophagy. *Hum Mol Genet.* 11, 1107-1117.

Raynes, D.A. & Guerriero, V., Jr. (1998). Inhibition of Hsp70 ATPase activity and protein renaturation by a novel Hsp70-binding protein. *J Biol Chem. 273*, 32883-32888

Reddy, P.H., and Shirendeb, U.P. (2012). Mutant huntingtin, abnormal mitochondrial dynamics, defective axonal transport of mitochondria, and selective synaptic degeneration in Huntington's disease. *Biochim Biophys Acta* 1822, 101-110.

Ross, C.A., Aylward, E.H., Wild, E.J., Langbehn, D.R., Long, J.D., Warner, J.H., Scahill, R.I., Leavitt, B.R., Stout, J.C., Paulsen, J.S.*, et al.* (2014). Huntington disease: natural history, biomarkers and prospects for therapeutics. *Nat Rev Neurol.* 10, 204-216.

Ross, C.A., and Tabrizi, S.J. (2011). Huntington's disease: from molecular pathogenesis to clinical treatment. *Lancet Neurol*. 10, 83-98.

Saxena, S. & Caroni, P. (2011). Selective neuronal vulnerability in neurodegenerative diseases: from stressor thresholds to degeneration. *Neuron 71*, 35-48

Sarkar, S., Rubinsztein, D.C. (2008) Huntington's disease: degradation of mutant huntingtin by autophagy. *FEBS J.* **275**:4263-4270.

Scaglione, K.M., Zavodszky, E., Todi, S.V., Patury, S., Xu, P., Rodriguez-Lebron, E., Fischer, S., Konen, J., Djarmati, A., Peng, J.*, et al.* (2011). Ube2w and ataxin-3 coordinately regulate the ubiquitin ligase CHIP. *Mol Cell*. 43, 599-612.

Schaefer, K.A., Wu, W.H., Colgan, D.F., Tsang, S.H., Bassuk, A.G., Mahajan, V.B., *et al*. (2017). Unexpected mutations after CRISPR-Cas9 editing in vivo. *Nat Methods* 14, 547-548.

Schilling, G., Becher, M.W., Sharp, A.H., Jinnah, H.A., Duan, K., Kotzuk, J.A., Slunt, H.H., Ratovitski, T., Cooper, J.K., Jenkins, N.A.*, et al.* (1999). Intranuclear inclusions and neuritic aggregates in transgenic mice expressing a mutant N-terminal fragment of huntingtin. *Hum Mol Genet*. 8, 397-407.

Shaid, S., Brandts, C.H., Serve, H., and Dikic, I. (2013). Ubiquitination and selective autophagy. *Cell Death Differ*. 20, 21-30.

Shao, J., and Diamond, M.I. (2007). Polyglutamine diseases: emerging concepts in pathogenesis and therapy. *Hum Mol Genet*. 16 Spec No. 2, R115-123.

Sherman, M.Y., and Goldberg, A.L. (2001). Cellular defenses against unfolded proteins: a cell biologist thinks about neurodegenerative diseases. *Neuron* 29, 15-32.

Shin, J.Y., Fang, Z.H., Yu, Z.X., Wang, C.E., Li, S.H., and Li, X.J. (2005). Expression of mutant huntingtin in glial cells contributes to neuronal excitotoxicity. *J Cell Biol*. 171, 1001-1012.

Shirasaki, D.I., Greiner, E.R., Al-Ramahi, I., Gray, M., Boontheung, P., Geschwind, D.H., Botas, J., Coppola, G., Horvath, S., Loo, J.A., and Yang, X.W. (2012). Network organization of the huntingtin proteomic interactome in mammalian brain. *Neuron* 75, 41-57.

Sofroniew, M.V., and Vinters, H.V. (2010). Astrocytes: biology and pathology. *Acta Neuropathol*. 119, 7-35.

Soto, C. (2003). Unfolding the role of protein misfolding in neurodegenerative diseases. *Nat Rev Neurosci. 4*, 49-60

Tan, J.M., Wong, E.S., Kirkpatrick, D.S., Pletnikova, O., Ko, H.S., Tay, S.P., Ho, M.W., Troncoso, J., Gygi, S.P., Lee, M.K.*, et al.* (2008). Lysine 63-linked ubiquitination promotes the formation and autophagic clearance of protein inclusions associated with neurodegenerative diseases. *Hum Mol Genet*. 17, 431-439.

Tetzlaff, J.E., Putcha, P., Outeiro, T.F., Ivanov, A., Berezovska, O., Hyman, B.T., and McLean, P.J. (2008). CHIP targets toxic alpha-Synuclein oligomers for degradation. *J Biol Chem*. 283, 17962-17968.

Tong, X., Ao, Y., Faas, G.C., Nwaobi, S.E., Xu, J., Haustein, M.D., Anderson, M.A., Mody, I., Olsen, M.L., Sofroniew, M.V., and Khakh, B.S. (2014). Astrocyte Kir4.1 ion channel deficits contribute to neuronal dysfunction in Huntington's disease model mice. *Nat Neurosci.* 17, 694-703.

Trushina, E., Dyer, R.B., Badger, J.D., Ure, D., Eide, L., Tran, D.D., Vrieze, B.T., Legendre-Guillemin, V., McPherson, P.S., Mandavilli, B.S., Van Houten, B., Zeitlin, S., McNiven, M., Aebersold, R., Hayden, M., Parisi, J.E., Seeberg, E., Dragatsis, I., Doyle, K., Bender, A., et al. (2004) Mutant huntingtin impairs axonal trafficking in mammalian neurons in vivo and in vitro. *Mol Cell Biol* **24**:8195-8209.

Tsvetkov, A.S., Arrasate, M., Barmada, S., Ando, D.M., Sharma, P., Shaby, B.A., and Finkbeiner, S. (2013). Proteostasis of polyglutamine varies among neurons and predicts neurodegeneration. *Nat Chem Biol*. 9, 586-592.

Tsvetkov, A.S., Miller, J., Arrasate, M., Wong, J.S., Pleiss, M.A., and Finkbeiner, S. (2010). A small-molecule scaffold induces autophagy in primary neurons and protects against toxicity in a Huntington disease model. *Proc Natl Acad Sci U S A*. 107, 16982-16987.

Tydlacka, S., Wang, C.E., Wang, X., Li, S., and Li, X.J. (2008). Differential activities of the ubiquitin-proteasome system in neurons versus glia may account for the preferential accumulation of misfolded proteins in neurons. *J Neurosci.* 28, 13285-13295.

Valencia, A., Sapp, E., Kimm, J.S., McClory, H., Ansong, K.A., Yohrling, G., Kwak, S., Kegel, K.B., Green, K.M., Shaffer, S.A. et al. (2013). Striatal synaptosomes from Hdh140Q/140Q knock-in mice have altered protein levels, novel sites of methionine oxidation, and excess glutamate release after stimulation. *J Huntingtons Dis. 2*, 459-475

Volpicelli-Daley, L.A., Gamble, K.L., Schultheiss, C.E., Riddle, D.M., West, A.B., Lee, V.M. (2014) Formation of α-synuclein Lewy neurite-like aggregates in axons impedes the transport of distinct endosomes. *Mol Biol Cell.* **25**:4010-4023.

Waelter, S., Boeddrich, A., Lurz, R., Scherzinger, E., Lueder, G., Lehrach, H., and Wanker, E.E. (2001). Accumulation of mutant huntingtin fragments in aggresome-like inclusion bodies as a result of insufficient protein degradation. *Mol Biol Cell*. 12, 1393-1407.

Wang, C.E., Zhou, H., McGuire, J.R., Cerullo, V., Lee, B., Li, S.H., and Li, X.J. (2008a). Suppression of neuropil aggregates and neurological symptoms by an intracellular antibody implicates the cytoplasmic toxicity of mutant huntingtin. *J Cell Biol*. 181, 803-816.

Wang, J., Wang, C.E., Orr, A., Tydlacka, S., Li, S.H., and Li, X.J. (2008b). Impaired ubiquitin-proteasome system activity in the synapses of Huntington's disease mice. *J Cell Biol*. 180, 1177-1189.

Wellington, C.L., Ellerby, L.M., Hackam, A.S., Margolis, R.L., Trifiro, M.A., Singaraja, R., McCutcheon, K., Salvesen, G.S., Propp, S.S., Bromm, M.*, et al.* (1998). Caspase cleavage of gene products associated with triplet expansion disorders generates truncated fragments containing the polyglutamine tract. *J Biol Chem*. 273, 9158-9167.

Wellington, C.L., Singaraja, R., Ellerby, L., Savill, J., Roy, S., Leavitt, B., Cattaneo, E., Hackam, A., Sharp, A., Thornberry, N.*, et al.* (2000). Inhibiting caspase cleavage of huntingtin reduces toxicity and aggregate formation in neuronal and nonneuronal cells. *J Biol Chem*. 275, 19831-19838.

Wong, Y.C., Holzbaur, E.L. (2014) The regulation of autophagosome dynamics by huntingtin and HAP1 is disrupted by expression of mutant huntingtin, leading to defective cargo degradation. *J Neurosci*. **34**:1293-1305

Xu Q, Huang S, Song M, Wang CE, Yan S, Liu X, Gaertig MA, Yu SP, Li H, Li S, Li XJ (2013) Synaptic mutant huntingtin inhibits synapsin-1 phosphorylation and causes neurological symptoms. *J Cell Biol.* **202**:1123-1138.

Yan, S., Wang, C.E., Wei, W., Gaertig, M.A., Lai, L., Li, S., Li, X.J. (2014). TDP-43 causes differential pathology in neuronal versus glial cells in the mouse brain. *Hum Mol Genet. 23*, 2678-2693

Yu, Z.X., Li, S.H., Evans, J., Pillarisetti, A., Li, H., Li, X.J. (2003). Mutant huntingtin causes context-dependent neurodegeneration in mice with Huntington's disease. *J Neurosci*. *23*, 2193-2202

Zhang, S., Feany, M.B., Saraswati, S., Littleton, J.T., and Perrimon, N. (2009). Inactivation of Drosophila Huntingtin affects long-term adult functioning and the pathogenesis of a Huntington's disease model. *Dis Models Mech*. 2, 247-266.

Zhao, J., Zhai, B., Gygi, S.P., and Goldberg, A.L. (2015). mTOR inhibition activates overall protein degradation by the ubiquitin proteasome system as well as by autophagy. *Proc Natl Acad Sci U S A*. 112, 15790-15797.

Zhao, T., Hong, Y., Li, S.H., and Li, X.J. (2016). Compartment-Dependent Degradation of Mutant Huntingtin Accounts for Its Preferential Accumulation in Neuronal Processes. *J Neurosci*. 36, 8317-8328.

Zhang, Y., Chen, K., Sloan, S.A., Bennett, M.L., Scholze, A.R., O'Keeffe, S., Phatnani, H.P., Guarnieri, P., Caneda, C., Ruderisch, N. et al. (2014). An RNA-sequencing

transcriptome and splicing database of glia, neurons, and vascular cells of the cerebral cortex. *J Neurosci. 34*, 11929-11947

Zuccato, C., Valenza, M., Cattaneo, E. (2010) Molecular mechanisms and potential therapeutical targets in Huntington's disease. *Physiol Rev.* **90**:905-981.